Red/NIR-absorbing Oligothiophenes for Organic Solar Cells

Dissertation

Zur Erlangung des Doktorgrades Dr. rer. nat.

der Fakultät für Naturwissenschaften

der Universität Ulm

von

Simon Steinberger

Ulm, 2011

Amtierender Dekan:	Prof. Dr. Peter Bäuerle
1. Gutachter:	Prof. Dr. Peter Bäuerle
2. Gutachter:	Prof. Dr. Volkhard Austel
Tag der Promotionsprüfung:	16. November 2011

Universität Ulm, Fakultät für Naturwissenschaften, 2011

An expert is a man who has made all the mistakes which can be made, in a narrow field.

Niels Bohr (1885-1962)

This work was undertaken between Mai 2006 and March 2010 at the Institute for Organic Chemistry II and Advanced Materials, University of Ulm, Germany.

Acknowledgement – Danksagung

Herrn Prof. Dr. Peter Bäuerle danke ich sehr herzlich für die interessante und praxisbezogene Themenstellung, die exzellenten Arbeitsbedingungen und die vielseitigen Möglichkeiten zur Weiterbildung, die mich weit über das Themengebiet hinaus gefordert und inspiriert haben.
Prof. Dr. Volkhard Austel danke ich herzlich für die freundliche Übernahme des zweiten Gutachtens, sowie Prof. Dr. Kerstin Leopold, Prof. Dr. Welf Alfred Kreiner und Prof. Dr. Thorsten Bernhardt für das Interesse an dieser Arbeit und die Teilnahme am Dissertationskolloquium.
Ich bedanke mich beim Bundesministerium für Bildung und Forschung (BMBF), das im Rahmen des OPEG-Programms diese Arbeit finanziell gestützt hat. Ein weiteres Dankeschön geht an meine Kooperationspartner am IAPP Dresden und der heliatek GmbH, insbesondere an Dr. Martin Pfeiffer, Dr. Jordan Levichkov und Dr. Christian Uhrich, für die Herstellung der Solarzellen und für zahllose Vorschläge und theoretische Rechnungen zu neuen Verbindungen.
Allen Arbeitskreismitgliedern möchte ich für die gute Atmosphäre und Unterstützung während dieser Zeit herzlich danken. Mein besonderer Dank gilt dabei Dr. Egon Reinold und Frau Astrid Vogt, deren herausragende Forschungsergebnisse den Grundstein für diese Arbeit darstellten. Weiterhin danke ich Dr. Günther Götz, Dr. Fan Zhang und ganz besonders meinem Gruppenleiter Dr. Amaresh Mishra, die mir häufig mit Rat und Tat während meiner Arbeit beiseite standen. Bei Frau Dr. Elena Mena-Osteritz bedanke ich mich für ihre Unterstützung bei der Interpretation von Spektren und der theoretischen Berechung von Strukturen. Herrn Dr. Markus Wunderlin danke ich für die Aufnahme der Massenspektren und Fr. Dr. Sylvia Schmid für die vielen NMR-Messungen. Dr. Chang-Qi Ma danke ich für die Herstellung und Charakterisierung der aus Lösung hergestellten Solarzellen.
Ein ganz liebes Dankeschön geht an Dr. Markus Fischer für zahllose Tipps, seine Unterstützung und ganz besonders seine Freundschaft, die weit über den universitären Alltag hinaus reicht.
Meiner Freundin Sylvi sage ich von ganzem Herzen Danke, für ihre Liebe, für all die aufmunternden Worte und für jeden Moment, der mir gezeigt hat, worum es im Leben wirklich geht.
Ein Riesendankeschön gebührt meinen Eltern für ihre emotionale und finanzielle Unterstützung während der gesamten Zeit meines Studiums und darüber hinaus.

Table of Contents

1 Introduction **1**

References 3

2 Organic Solar Cells **5**

2.1 Introduction 6

2.2 Working Principle of Organic Solar Cells 8

2.2.1 Device Architecture 8

2.2.2 Solar Cell Operation and Processes 9

2.2.3 Loss Mechanisms 9

2.3 Optimized Device Architecture 11

2.3.1 Bulk Heterojunction Solar Cells 11

2.3.2 M-i-p Layer Sequence 12

2.4 Characterization of Photovoltaic Devices 13

2.4.1 Background 13

2.4.2 *I-V*-Characteristics 13

2.4.3 Open Circuit Voltage (V_{OC}) 14

2.4.4 Short-Circuit Current (I_{SC}) 14

2.4.5 Fill Factor (*FF*) 15

2.4.6 Power Conversion Efficiency (η) 15

2.4.7 External Quantum Efficiency (EQE) 16

2.5 Multi-Parameter Optimization 16

2.6 Band Gap Engineering of π-conjugated Systems 17

2.7 Applied Materials in “Small Molecule” Solar Cells 20

2.7.1 Solution-processed Photovoltaic Devices 20

2.7.2 Vacuum-processed Photovoltaic Devices 23

2.8 References 26

3 Thienothiadiazole and Thienopyrazine as Core Acceptor in A-D-A-D-A-type Oligothiophenes **31**

3.1 Introduction 32

3.2 Synthesis 33

3.3 Physical Properties 36

3.3.1 Steady-State Spectroscopy 37

3.3.2 Light induced decomposition of thienopyrazines 39

3.3.3 Theoretical calculations 41

3.3.4 Electrochemical Studies 42

3.3.5 Thermal properties 45

3.4 Photovoltaic Performance 46

3.5 Experimental Section 48

3.6 References 58

4 Benzothiadiazole as Core Acceptor in A-D-A-D-A-type Oligothiophenes 61
4.1 Introduction 62
4.2 Synthesis 63
4.3 Physical Properties 65
4.3.1 Steady-State Spectroscopy 65
4.3.2 Electrochemical Studies 67
4.3.3 Thermal Properties 69
4.4 Photovoltaic Performance 70
4.5 Experimental Section 72
4.6 References 80

5 Benzothiadiazole and Thiadiazolo pyridine as Terminal Acceptors in A-D-A-type Oligothiophenes 83
5.1 Introduction 84
5.2 Synthesis 85
5.3 Physical Properties 88
5.3.1 Steady-State Spectroscopy 88
5.3.2 Theoretical calculations 90
5.3.3 Electrochemical Studies 92
5.3.4 Thermal Properties 92
5.4 Photovoltaic Performance 94
5.4.1 Vacuum-processed Solar Cells 94
5.4.2 Solution-processed Solar Cells 97
5.5 Experimental Section 99
5.6 References 105

Summary 108

Zusammenfassung 112

List of Publications 116

Presentations and Posters 117

Curriculum Vitae 118

Abbreviations

A	Acceptor
Abs	Absorption
ads	Adsorbed
AM1	Austin Model 1
AM1.5G	Air Mass 1.5 global
BHJSC	Bulk heterojunction solar cell
BLA	Bond Length Alternation
BPAPF	9,9-bis{4-[di-(p-biphenyl)aminophenyl]}fluorine
BTDA	Benzothiadiazole
BTDAPy	Benzothiadiazolo pyridine
Calc.	Calculated
CI	Chemical ionization
CT	Charge transfer
CuPC	Copper-phthalocyanine
CV	Cyclic voltammetry
D	Donor
dba	Dibenzylideneacetone
DCE	Dichloroethane
DCM	Dichloromethane
DCV	Dicyanovinyl
Di-NPB	N,N′-di(naphthalen-1-yl)-N,N′-diphenyl-benzidine
DMF	*N,N*-Dimethylformamide
DMSO	Dimethyl sulfoxide
DO	Dioxolane
dppp	1,3-Bis(diphenylphosphino)propane
DPV	Differential pulse voltammetry
DSSC	Dye-sensitized solar cell
EI	Electron impact
em	Emission
Et	Ethyl

F4-TCNQ	Tetrafluoro-tetracyanoquinodimethane
Fc/Fc^+	Ferrocene/ferrocenium couple
FF	Fill factor
GC	Gas chromatography
HOMO	Highest occupied molecular orbital
HPLC	High performance liquid chromatography
HTL	Hole transport layer
IPCE	Incident photon to current conversion efficiency
I_{SC}	Short-circuit current
ITDB	2-Isopropoxy-4,4,5,5-tetramethyl-1,3,2-dioxaborolane
ITO	Indium tin oxide
J_{SC}	Short-circuit current density
L_D	Exciton diffusion length
LUMO	Lowest unoccupied molecular orbital
m-MTDATA	4,4',4''-Tris(3-methylphenylphenylamino)triphenylamine
MALDI	Matrix assisted laser desorption/ionization
M.p.	Melting point
MS	Mass spectrometry
NBS	*N*-Bromo succinimide
NMR	Nuclear magnetic resonance
*n*BuLi	*n*-Butyllithium
OFET	Organic field effect transistor
OLED	Organic light emitting diode
OPV	Organic Photovoltaics
OSC	Organic solar cell
OT	Oligothiophene
Ox	Oxidation
P3HT	Poly(3-hexylthiophene)
PCBM	Phenyl-fullerene-butyric acid methyl ester
PEDOT	Poly(3,4-ethylenedioxythiophene)
Ph	Phenyl
Red	Reduction
ss	Solid-state

SubPc	Chloro[subphthalocyanine]boron(III)
T	Thiophene
$TBAPF_6$	Tetra-*n*-butylammonium hexafluorophosphate
TCE	Tetrachloroethane
^{t}Bu	1,1-Dimethylethyl
TFA	Trifluoroacetic acid
TFAA	Trifluoroacetic acid anhydride
TFP	Trifurylphosphine
Th	Thiophene
THF	Tetrahydrofurane
TLC	Thin layer chromatography
TOF	Time of flight
TP	Thienopyrazine
TTDA	Thienothiadiazole
UV	Ultra-violet
V_{OC}	Open-circuit voltage
Vis	Visible
ZnPc	Zinc-phtalocyanine

Chapter 1

Introduction

Abstract

Low band gap oligothiophenes are currently being extensively investigated as active materials for organic photovoltaic devices. Molecular properties of the compounds are tuned with respect to the envisaged applications, in particular by functionalizing the conjugated, semiconducting oligomers with various donor and acceptor moieties to obtain red/NIR absorbers for “small molecule” solar cells. Morphology control, charge carrier mobility, absorption properties, long term stability, etc. makes the development of such materials for organic solar cells a complex multi-parameter problem.

During the last decade, the field of organic electronics has seen a remarkable development in syntheses and device architecture. Organic solar cells (OSC) have the potential to become a low cost alternative to their inorganic counterparts. In particular semiconducting π-conjugated oligomers are being extensively investigated as active materials in photovoltaic devices.[1-5] Currently, both "small molecule" and polymer organic solar cells have already achieved power conversion efficiencies of more than 8%.[6-11] In this respect, donor-acceptor-functionalized oligothiophenes received considerable attention as light-harvesting p-type semiconductors in "small molecule" solar cells.[2, 5, 11] In the case of oligomers, evaporation technique can be used to effectively control the nano-morphology of photoactive layers, which is a significant advantage compared to solution-processed polymers. However, there is still a need to improve the cell efficiency and stability in order to develop large area low-cost solar cells.

Our group presented the first example of a dicyanovinyl-functionalized (DCV) quinquethiophene (Figure 1): DCV5T has an absorption maximum at 513 nm (E_g = 2.01 eV) in solution and 573 nm (E_g = 1.77 eV) in thin films.[12-14] In a p/n-planar heterojunction solar cell, the compound gave an efficiency of 3.4% and an open circuit voltage (V_{OC}) of 1.0 V.[15] Applied in a fully optimized tandem cell, DCV-substituted oligothiophenes just recently gave a certified record power conversion efficiency of 8.3%.[6]

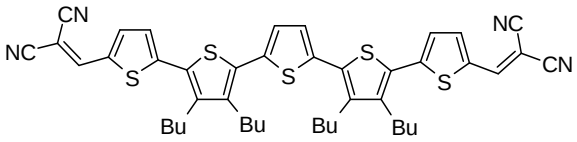

DCV5T

Figure 1: Oligothiophene end-capped with dicyanovinyl (DCV) as terminal acceptor groups.

However, in order to cover the major part of the sun emission spectrum, and thus enabling even higher conversion efficiencies, it is necessary to design compounds with a strong absorption from the visible region to the near IR. One of the approaches towards such low band gap oligomers is the implementation of a strong donor-acceptor push-pull system.[16] Various low band gap oligomers and polymers involving median acceptor units such as thienothiadiazole (TTDA),[17-18] benzothiadiazole (BTDA),[19-21] and thienopyrazine (TP)[22-23] have been reported and the presence of these planar, proquinoid building blocks in the π-conjugated systems dramatically reduced the HOMO-LUMO gap of the materials.

The objective of this thesis was to develop tailored oligothiophenes based on compound DCV5T for the application as red/NIR absorbers in "small molecule" solar cells. We intended to

adjust molecular properties such as absorption, HOMO-LUMO energy levels, long term stability, volatility, and charge carrier mobility, by introducing various acceptor moieties into the core of the oligomer and/or by replacing the terminal DCV groups with novel, promising acceptor units. Furthermore, different alkyl-substitution patterns were envisaged to retain solubility of the compounds and improve morphology in the solid state (Figure 2).

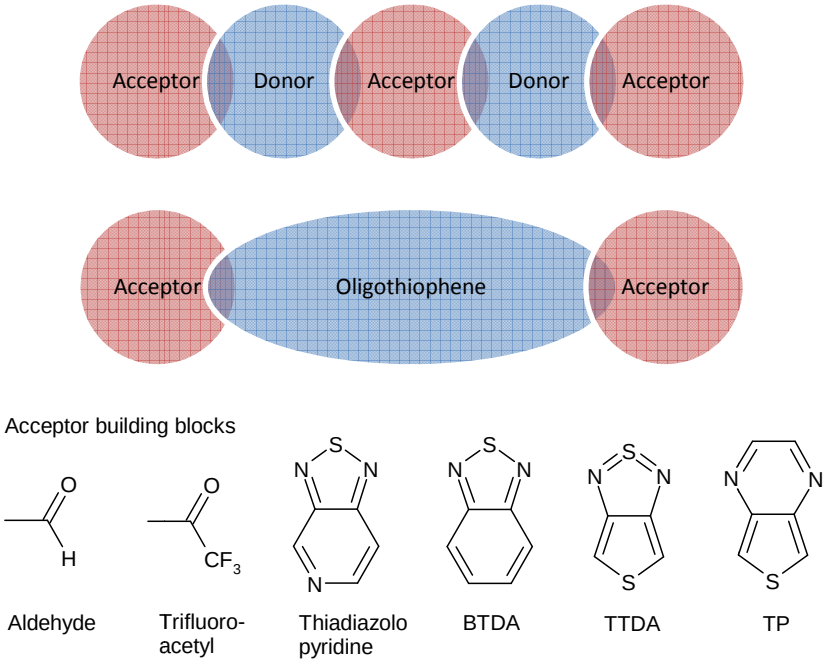

Figure 2: DCV5T-analogue donor/acceptor functionalized oligomers as red/NIR absorbers for "small molecule" solar cells.

In the course we intended to gain structure-property relations to obtain further insight into the multi-parameter problem of optimizing materials for efficient organic photovoltaic devices.

References

[1] C. J. Brabec, N. S. Sariciftci, J. C. Hummelen, *Adv. Funct. Mater.* **2001**, *11*, 15.
[2] D. Meissner, D. Wöhrle, *Adv. Mater.* **1991**, *3*, 129.
[3] N. S. Sariciftci, S. Günes, H. Neugebauer, *Chem. Rev.* **2007**, *107*, 1324.
[4] N. S. Sariciftci, H. Hoppea, *J. Mater. Res.* **2004**, *19*, 1924.
[5] G. A. Chamberlain, *Sol. Cells* **1983**, *8*, 47.
[6] Heliatek GmbH, press release, 11th Oct 2010. http://www.heliatek.com.
[7] H. Y. Chen, J. H. Hou, S. Q. Zhang, Y. Y. Liang, G. W. Yang, Y. Yang, L. P. Yu, Y. Wu, G. Li, *Nat. Photonics* **2009**, *3*, 649.
[8] W. Ma, C. Yang, X. Gong, K. Lee, A. J. Heeger, *Adv. Funct. Mater.* **2005**, *15*, 1617.

[9] Y. Kim, S. Cook, S. M. Tuladhar, S. A. Choulis, J. Nelson, J. R. Durrant, D. D. C. Bradley, M. Giles, I. McCulloch, C.-S. Ha, M. Ree, *Nat. Mater.* **2006**, *5*, 197.
[10] J. Y. Kim, K. Lee, N. E. Coates, D. Moses, T.-Q. Nguyen, M. Dante, A. J. Heeger, *Science* **2007**, *317*, 222.
[11] A. Mishra, C.-Q. Ma, P. Bäuerle, *Chem. Rev.* **2009**, *109*, 1141.
[12] K. Schulze, B. Maennig, K. Leo, Y. Tomita, C. May, J. Hüpkes, E. Brier, E. Reinold, P. Bäuerle, *App. Phys. Lett.* **2007**, *91*, 073521.
[13] K. Schulze, C. Uhrich, R. Schüppel, K. Leo, M. Pfeiffer, E. Brier, E. Reinold, P. Bäuerle, *Adv. Mater.* **2006**, *18*, 2872.
[14] C. Uhrich, R. Schüppel, A. Petrich, M. Pfeiffer, K. Leo, E. Brier, P. Kilickiran, P. Bäuerle, *Adv. Funct. Mater.* **2007**, *17*, 2991.
[15] K. Schulze, M. Riede, E. Brier, E. Reinold, P. Bäuerle, K. Leo, *J. Appl. Phys.* **2008**, *104*, 074511.
[16] M. M. Oliva, J. Casado, M. Manuela, M. Raposo, A. Maurcio, C. Fonseca, H. Hartmann, V. Hernandez, J. T. L. Navarrete, *J. Org. Chem.* **2006**, *71*, 7509.
[17] Y. Yamashita, S. Tanaka, *Synth. Metals* **1995**, *69*, 599.
[18] M. C. Ruiz Delgado, V. Hernández, J. T. López Navarrete, S. Tanaka, Y. Yamashita, *J. Phys. Chem. B* **2004**, *108*, 2516.
[19] A. J. Moulé, A. Tsami, T. W. Bünnagel, M. Forster, N. M. Kronenberg, M. Scharber, M. Koppe, M. Morana, C. J. Brabec, K. Meerholz, U. Scherf, *Chem. Mater.* **2008**, *20*, 4045.
[20] S. Song, Y. Jin, S. H. Kim, J. Moon, K. Kim, J. Y. Kim, S. H. Park, K. Lee, H. Suh, *Macromolecules* **2008**, *41*, 7296.
[21] L. H. Slooff, S. C. Veenstra, J. M. Kroon, D. J. D. Moet, J. Sweelssen, M. M. Koetse, *Appl. Phys. Lett.* **2007**, *90*, 143506.
[22] J. Casado, R. P. Ortiz, M. C. Ruiz Delgado, V. Hernández, J. T. López Navarrete, J. M. Raimundo, P. Blanchard, M. Allain, J. Roncali, *J. Phys. Chem. B* **2005**, *109*, 16616.
[23] A. P. Kulkarni, Y. Zhu, S. A. Jenekhe, *Macromolecules* **2007**, *41*, 339.

Chapter 2

Organic Solar Cells

Abstract

Solar energy today is economically not yet competitive with conventional power sources, but as the need for renewable energy sources grows, the technology to convert sunlight into electricity becomes more and more attractive. In this field, organic solar cells (OSC) have the potential to become a flexible and low-cost alternative to their inorganic counterparts. Besides organic polymers, functionalized oligothiophenes are among the most frequently used photoactive materials in such devices, since uncountable synthetic methods allow the π-conjugated systems to be modified and molecular properties to be adjusted with respect to the envisages applications. With a remarkable development from syntheses to device architecture, “small molecule” solar cells (SMSC) are today on the brink of industrial large scale production.[1-3]

2.1 Introduction

In the past hundred years, human population quadrupled to almost seven billion inhabitants and with it, the global energy consumption increased sixteen fold. The limited supply of today's main energy sources – oil, coal and uranium – will soon force us to replace most of the currently used power plants by renewable energy sources like wind-, hydroelectric- and solar power systems. With a power of 10000 TW on the surface of the Earth, the amount of energy provided by the sun is enormous and the comparison to the second largest renewable energy source, wind power (14 TW), clearly points out the importance of solar energy (Figure 1). With an average power conversion efficiency of 10%, solar panels covering only 0.08% of the surface of the Earth would provide the world's current consumption rate of energy (10 TW).

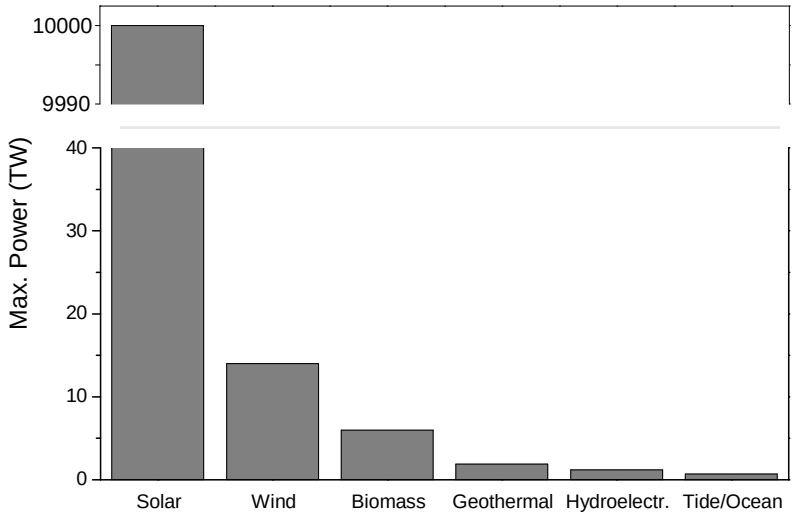

Figure 1: Maximum available power from renewable energy sources.

At present, solar cells comprising an inorganic semiconductor such as mono- or multi-crystalline silicon, have record power conversion efficiencies close to 39%[4], while commercially available solar panels show a significantly lower conversion of around 15–20%. Yet, the production of these devices requires several energy intensive processes at high temperatures up to 1400 °C, leading to high manufacturing costs.[5] In this respect, organic solar cells are very attractive, since only thin films of relatively cheap materials are needed, thus enabling low-cost roll-to-roll fabrication. Additionally, organic photovoltaics can be prepared on flexible substrates like plastic films, enabling completely new fields of application.

The first *organic semiconductors* with reasonable conductivity were reported in the 1950s and initial attempts in the field of organic solar cells date back to 1959.[6] Kallman and Pope discovered that anthracene can be used to make a photovoltaic device, but their single layer architecture provided a photovoltage of only 0.2 V with an extremely low efficiency.[7] In quick succession advances were made and a first breakthrough was presented in 1986 by Tang *et al*.: Perylene-3,4,9,10-tetracarboxyl-bis-benzimidazole (PTCBI) and copper phthalocyanine (CuPc) were evaporated in a two layer arrangement onto a transparent electrode, resulting in the first bilayer heterojunction solar cell (vide infra) with a power conversion efficiency of ca. 1% (Figure 2).[8]

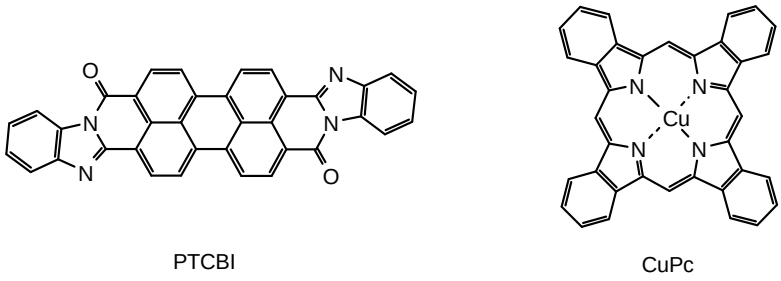

Figure 2: Photoactive compounds used by Tang *et al*. for the first bilayer heterojunction solar cell.

At present, one of the most studied photoactive materials is poly(3-hexylthiophene) (P3HT). Used as donor in solution processed bulk heterojunction solar cells (BHJSC, vide infra) with [6,6]-phenyl-C_{61}-butyric acid methyl ester (PCBM) as acceptor, a certified power conversion efficiency of over 5% with an external quantum yield of up to 88% was achieved (Figure 3).[9-14] In particular, its crystalline morphology in the solid state with almost ideal HOMO and LUMO energy levels makes P3HT a pristine material for polymer solar cells.

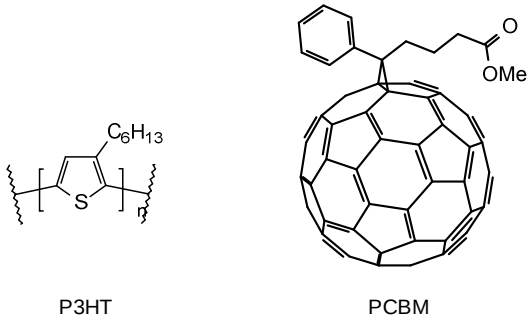

Figure 3: PCBM and P3HT, pristine compounds for highly efficient polymer BHJSC.

Another promising concept of organic photovoltaics are dye-sensitized solar cells (DSSC), which are due to a different working principle not further discussed in the thesis, but shall be

mentioned here for their extraordinary high power conversion efficiencies of more than 11%.[15-17]

Various approaches have been employed to achieve higher power conversion efficiencies and currently, both “small molecule” and polymer organic solar cells have already achieved power conversions of more than 8%.[1-3, 18-21]

2.2 Working Principle of Organic Solar Cells

2.2.1 Device Architecture

A bilayer heterojunction solar cell represents the most basic device architecture and therefore, the general working process of organic photovoltaics is explained upon such. The common assembly of a bilayer heterojunction solar cell is depicted in Figure 4.

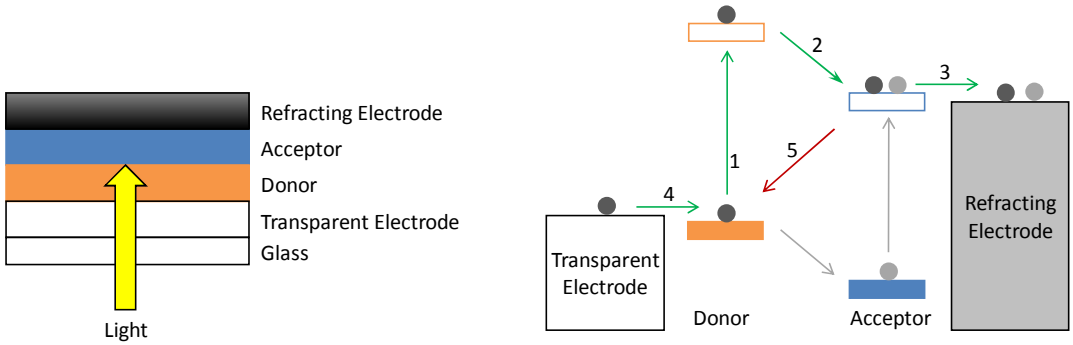

Figure 4: Device architecture (left) and schematic energy-band diagram with ideal HOMO and LUMO energy levels (right) of a bilayer heterojunction solar cell. 1: Exciton generation; 2: Charge separation; 3, 4: Charge transfer to electrodes via hopping mechanism; 5: Undesired charge recombination, lowering the device efficiency.

Two photoactive materials, donor and acceptor, are aligned in flat arrangement in separate layers, sandwiched between a transparent electrode, usually consisting of the inorganic semiconductor indium tin oxide (ITO) on a glass substrate, and a thin refracting metal contact, e.g. aluminum, silver or gold. In the case of “small molecules” the layers are preferably prepared by vacuum deposition, thus resulting in homogeneous nanostructure morphology enabling a higher charge carrier mobility (vide infra). Solution-processed polymers can be used as well, however orthogonal solubility is required, meaning one material is soluble in a solvent in which the other is not.[22] Without orthogonal solubility already processed layers are destroyed when depositing new layers. In the case of vacuum-processed devices, the different

thin films have thicknesses in the range between 5 and 20 nm and for solution-processed materials, thicknesses up to 60 nm are applied.

2.2.2 Solar Cell Operation and Processes

Upon absorption of light, electrons in the organic donor material are excited from the ground state into unoccupied molecular orbitals of higher energy and form strongly bound electron-hole pairs, the so called excitons (Figure 4; 1). For a successful charge separation (Figure 4; 2), the driving force of the electron transfer to the energetically lower lying acceptor LUMO must exceed the electron-hole binding energy. It has been shown, for this process the LUMO of the donor must be at least 0.3 eV higher in energy than the LUMO of the acceptor.[23-25] In particular fullerenes are among the best acceptor materials, since the LUMO of C_{60} is triply degenerated and a six fold reversible reduction is possible.[26-27] Furthermore, with a band gap of 2.30 eV, fullerene C_{60} is able to absorb photons of higher energy, and thus also contributes to the generation of excitons (Figure 4; gray pathway). The energetic difference between the two HOMOs of donor and acceptor is usually significantly higher as for the charge separation required (0.3 eV). Thus, caused by the strong electrostatic forces at the donor-acceptor interface (heterojunction), the excitons can dissociate into free charges, which are able to diffuse via a hopping mechanism to the anode and cathode of the device (Figure 4; 3 + 4).

This is an idealized pathway from photo excitation to the generation of free charges. However, in most organic devices, only a small part of the incident photons is converted into electricity.

2.2.3 Loss Mechanisms

In the work flow of an organic solar cell, different loss mechanisms occur, reducing the overall efficiency of the photovoltaic device. Figure 5 schematically depicts the solar cell processes with corresponding leakage pathways.

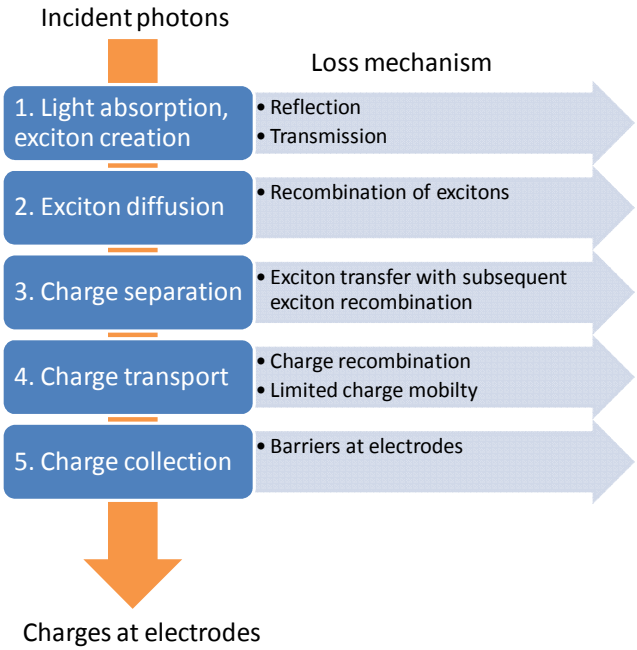

Figure 5: Work flow of an organic solar cell with loss mechanisms during the process.

1. Sunlight provides a very broad spectrum and a band gap of 1.1 eV is theoretically necessary to absorb about 77% of all incident photons, whereas the majority of organic donor materials have band gaps greater than 1.5 eV, thus limiting the absorption range of the devices' active layers. Furthermore, a significant number of photons is simply reflected by either the device casing, the electrodes or even the active layers themselves. In addition, the organic layers are too thin for absorbing all of the provided photons.

2. However, both the short exciton diffusion length (L_D, vide infra) and the low charge carrier mobility in organic materials, render thicker films inefficient: An exciton created in the organic layer has an average lifespan of only a few nanoseconds and thus, a relatively short diffusion length of ca. 10 nm after which recombination (relaxation) of the hole and the electron occurs.[28-29]

3. As a consequence, only excitons generated within this distance from the donor-acceptor interface can be separated into free charges, hence the thickness of the photoactive film is confined by this factor.

4. The charge transport in organic semiconductors can be described as a hopping mechanism, which is several orders of magnitudes slower, when compared to their inorganic counterparts. Thus, free charges are eliminated by recombination of electrons and holes on the way to the electrodes.

5. Furthermore, in order to enter the electrode materials, the charges in general have to overcome a potential barrier, which again enables recombination processes. The HOMO and LUMO energy level offsets of the electrodes must therefore be chosen very carefully, in order to reduce this potential barrier to a minimum.

2.3 Optimized Device Architecture

In order to reduce the impact of the described loss mechanisms, different strategies have been developed.

2.3.1 Bulk Heterojunction Solar Cells

The problem of incomplete exploitation of excitons caused by the short diffusion length (L_D) has been approached by developing a new type of donor-acceptor layer – the so called bulk heterojunction (BHJ) – for increasing the interfacial area between donor and acceptor (Figure 6).

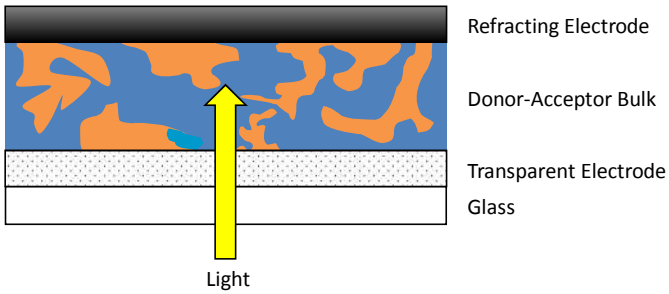

Figure 6: Bulk heterojunction architecture with blended donor and acceptor material for increasing the area of the heterojunction, thus resulting in a more efficient charge separation.

The microphase-separated bulk layer extends the photogeneration region of the device, therewith allowing more excitons to dissociate into free charges. For an optimized BHJ, the phase separation should be in the order of $2L_D$ for minimizing the rate of exciton recombination, while at the same time maximizing the thickness of the light absorbing layer.[30] Except for the morphology of the intrinsic (photoactive) layer, the device assembly and its operation is identical to the described bilayer heterojunction cell. The bulk architecture can be applied, both for vacuum deposited “small molecules” and solution-processed

polymers. In the case of vacuum deposition, the blend layer is created by co-evaporation of the two corresponding compounds.

2.3.2 M-i-p Layer Sequence

To reduce charge recombination caused by the low mobility in organic semiconductors, different layer sequences have been developed comprising additional materials for blocking electrons or holes in specific directions. One of which is the so called “m-i-p-type” solar cell architecture used for all vacuum-processed devices assembled within the scope of this study.[31-33] “*m*” stands for *m*etal and refers to the transparent front electrode (mostly ITO), “*i*” means the *i*ntrinsic, photoactive donor and acceptor materials and “*p*” is the abbreviation for a *p*-doped layer, also called hole transport or electron blocking layer. Figure 7 depicts an m-i-p-layer sequence and the corresponding, schematic energy-band diagram with ideal HOMO and LUMO energy levels.

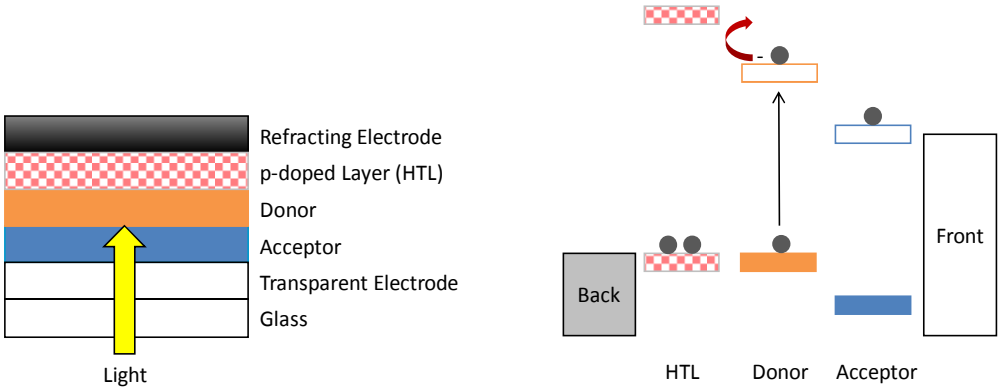

Figure 7: M-i-p-Layer sequence with ideal HOMO and LUMO energy levels.

The operation processes of this device are basically the same as for a bilayer device, except for the additional p-doped hole transport layer (HTL). The LUMO of the HTL constitutes an energetic barrier for excited electrons of the donor: While holes from the donor can freely pass through the HOMO of the HTL, electrons are forced towards the front electrode, thus charge recombination at the back electrode interface is prevented.

2.4 Characterization of Photovoltaic Devices

2.4.1 Background

For a reliable comparison of solar cell characteristics and in particular for comparing efficiencies, international standard test methods were introduced.[34-35] Furthermore, an accurate measurement is especially important for gaining structure-property relations and with it, preventing development into wrong directions.

The standard test conditions – "Air Mass 1.5 Global" (AM1.5G, IEC 904-3) – reflect the solar spectrum on the surface of the Earth with an intensity of 1000 W/m^2 under an angle of 48.2° against the average zenith angle of the sun. The simulated spectrum accounts for a model atmosphere, containing specific concentrations of e.g. water vapor and carbon dioxide, and test conditions also include a standard temperature of 25 °C.

2.4.2 *I-V*-Characteristics

The most important characteristics of a photovoltaic device are obtained from the so called *I-V*-curve (current vs. voltage curve), which is determined under AM1.5G conditions by applying a potential to the device and measuring the resulting current. A schematic diagram is depicted in Figure 8.

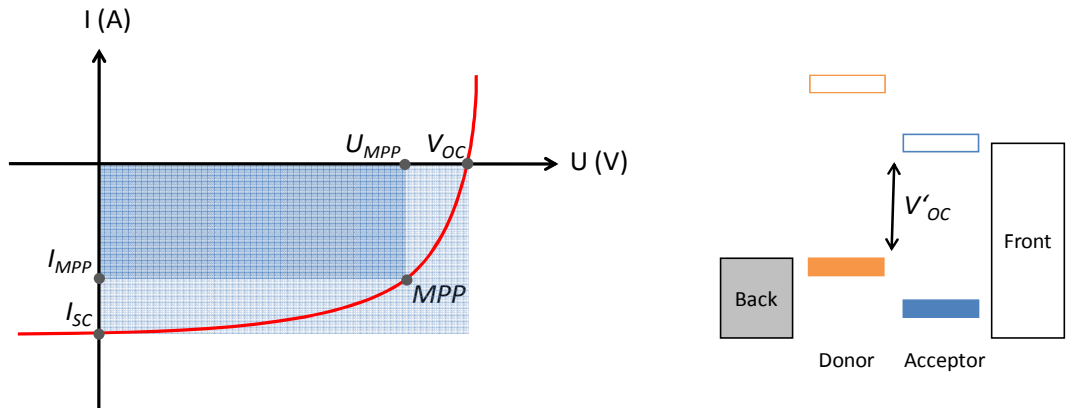

Figure 8: Schematic *I-V*-curve for determining photovoltaic characteristics and performance (left) and theoretical open-circuit voltage V'_{OC} (right).

Open-circuit voltage (V_{OC}), short-circuit current (I_{SC}), fill factor (*FF*) and efficiency (η) of a solar cell, both organic and inorganic, can be determined directly from the *I-V* curve.

2.4.3 Open Circuit Voltage (V_{OC})

The maximum potential a photovoltaic device can provide under ideal conditions is described by the open-circuit voltage (V_{OC}). The value of V_{OC} corresponds to the intersection of the *I-V* curve with the voltage-axis (Figure 8, left) under illumination conditions (AM1.5G) and is correlated to the frontier molecular orbitals of the donor and acceptor in the solar cell (Figure 8, right). The theoretical open-circuit voltage is determined by the difference of the HOMO energy level of the donor and the LUMO level of the acceptor, which in the ideal case correspond to the work-functions of the electrodes. However, the empirically found V_{OC} is in general lower, due to resistances in the device, e.g. recombination losses caused by a low charge carrier mobility of the intrinsic layers.[36]

2.4.4 Short-Circuit Current (I_{SC})

The short-circuit current (I_{SC}) is the maximum supplied current of a solar cell under AM1.5G conditions and corresponds to the intersection of the *I-V* curve with the current-axis (Figure 8, left). I_{SC} shows a linear dependency on the incident light intensity until saturation effects occur within the absorbing layers. With this respect, the value of I_{SC} is proportional to the number of absorbed photons and therefore can be improved by a broad absorption of the intrinsic layers, in particular by using a low band gap donor material in the photovoltaic device. In addition, I_{SC} also depends on the charge carrier mobility and increases with higher temperatures, due to a thermally active hopping transport.

Since the short-circuit current is directly correlated with the number of incident photons, it is also proportional to the illuminated area of the cell. For an area-independent reference, the short-circuit current density was introduced as short-circuit current divided by the active area (equation 1).

$$J_{\mathrm{SC}} = \frac{I_{\mathrm{SC}}}{\mathrm{A}} \qquad (1)$$

The short-circuit current *density* (J_{SC}) is used in publications for comparing different solar cells, however occasionally misnamed as short-circuit current (I_{SC}).

2.4.5 Fill Factor (*FF*)

The fill factor value (*FF*) describes the quality of a solar cell and is determined by the ratio of total number of generated excitons and number of free charges that reach the electrodes. In an ideal device, the fill factor is 1, but due to loss mechanisms not all the generated charges reach the electrodes, hence the empirical value is smaller.

The fill factor is defined as the quotient of maximum power point (*MPP*), which gives information on the power output a device can provide, and the product of V_{OC} and I_{SC} (equation 2). The maximum power point (*MPP*) is located on the *I-V* curve where the product of U and I is largest. U_{mpp} and I_{mpp} are the corresponding potential and current, respectively.

$$\mathrm{FF} = \frac{U_{\mathrm{mpp}} \cdot I_{\mathrm{mpp}}}{V_{\mathrm{OC}} \cdot I_{\mathrm{SC}}} \qquad (2)$$

For an ideal solar cell, V_{OC} and I_{SC} equals U_{mpp} and I_{mpp}, respectively, and the *I-V* curve becomes rectangular (Figure 10, light blue area). In a real solar cell however, loss mechanisms like charge recombination and resistances decimate the number of free charges, thus the observed *I-V* curve is bended and the product of U_{mpp} and I_{mpp} becomes smaller (Figure 10, dark blue area).

2.4.6 Power Conversion Efficiency (*η*)

The overall power conversion efficiency (*η*) of a photovoltaic device corresponds to the quotient of the maximum power (P_{out}), which can be withdrawn from the solar cell and the incident illumination intensity (P_{in}). The described factors, open-circuit voltage (V_{OC}), short-circuit current (I_{SC}) and fill factor (*FF*) contribute equally to the efficiency of a cell, which can be calculated according to equation 3.

$$\eta = \frac{\mathrm{P_{out}}}{\mathrm{P_{in}}} = \frac{U_{\mathrm{mpp}} \cdot I_{\mathrm{mpp}}}{P_{\mathrm{in}}} = \frac{V_{\mathrm{OC}} \cdot I_{\mathrm{SC}} \cdot \mathrm{FF}}{\mathrm{P_{in}}} \qquad (3)$$

For normalized test results, the illumination intensity (P_{in}) must correspond to AM1.5G conditions and the temperature must be kept at 25 °C. P_{out} is the power provided by the device at the *MPP* and is therefore calculated as the product of U_{mpp} and I_{mpp}.

2.4.7 External Quantum Efficiency (EQE)

The external quantum efficiency (EQE) or incident photon to current efficiency (IPCE) describes the power conversion of a solar cell at a specific incident wavelength.

$$\mathrm{EQE}\ (\lambda) = \frac{\text{total available charges}}{\text{total incident photons}} \qquad (4)$$

If each incident photon causes the injection of an electron into the circuit, the EQE becomes 1, meaning a power conversion efficiency of 100% for the observed wavelength. Hence, the overall efficiency (η) of the solar cell corresponds to the average value of the EQE over the full absorption spectrum. Conclusively, the EQE curve (EQE vs. wavelength) often reflects the actual absorption properties of the molecules, but deviations due to loss effects are possible.

2.5 Multi-Parameter Optimization

To sum up, there are many different parameters for tuning the efficiency of organic photovoltaic devices and some of the molecular properties, e.g. absorption and orbital energy levels, are directly correlated and therefore cannot be adjusted freely.

- The LUMO energy level of the donor needs to be at least 0.3 eV higher than the LUMO of the acceptor for an efficient charge separation at the heterojunction interface.
- A donor band gap of ca. 1.1 eV and with it, strong extinction down to 1100 nm (panchromatic absorption) is desired for exploiting the major part of the sun emission spectrum. Yet, the energy gap is directly correlated to the open circuit voltage (V_{OC}) of the device.[37-38] With a decrease of the HOMO-LUMO gap, V_{OC} is lowered as well, and since a high V_{OC} is desirable, the ideal band gap is considered to be at approximately 1.5 eV.[39-40]
- Charge carrier mobility should be as high as possible and therefore a homogeneous and well ordered nanostructure of the molecules in the thin film is advantageous. Particularly, the deposition technique of the layers determines in large extend the

morphology of the film and in general sublimation of oligomers gives the best results. The drawback here is, that in comparison to polymers, “small molecules” have a less extended conjugated system, hence it is more difficult to achieve absorption down to the red/NIR-region. Also for vacuum deposition, very high thermal stability of the compounds is imperative to obtain reasonable sublimation yields while preparing thin films.

- Concerning synthesis, alkyl chains are commonly introduced for increasing the solubility of compounds. However, the side chains also increase both, the molecular weight and the intermolecular forces. Hence, in the case of “small molecules”, higher temperatures are required for the vacuum deposition process.
- Furthermore, the morphology of thin films is strongly affected by even minor modifications to the compounds’ structures, causing hard to predict changes in the device properties.

These are some of the most prominent variables, which impose a multi-parameter problem for improving and adjusting the physical and optical properties of new materials for stable and efficient organic solar cells. Developing such compounds is therefore a trial-and-error process, since the complexity of the problem does not allow exact or reliable predictions on molecular properties.[3]

2.6 Band Gap Engineering of π-conjugated Systems

Different strategies have evolved for tuning the molecular orbital energy levels and therewith the band gap of π-conjugated systems. In the case of a hypothetical, *ideal* organic conductor, the fully π-conjugated structure should be flat with all C-C bonds having equal lengths. Graphite fulfills these requirements and therefore evinces its metallic characteristics with an extremely high charge carrier mobility. However, due to asymmetrical delocalization of the π-electrons, one-dimensional conjugated structures evince a more or less pronounced bond length alternation (BLA), resulting in a band gap aperture. However, by reducing the BLA via structural modifications of the compound’s backbone, a lowering of the band gap can be achieved.[41]

One effective strategy for decreasing the BLA – and with it the band gap itself – is to enforce quinoid character on the π-system. Unlike polyenes, the mesomeric structures of aromatic systems have degenerated ground states: Aromatic form **1** in Figure 9 is energetically more stable, while the quinoid form **2** is higher in energy, but evinces a smaller band gap.[42]



1 (aromatic) **2** (quinoid)

Figure 9: Aromatic (left) and quinoid form (right) of a terthiophene: The aromatic form is lower in energy, while the quinoid form has a smaller band gap.

In the aromatic form, the π-electrons are distinctly localized on the thiophene moieties. In the quinoid form however, the thiophene rings loose their aromatic character, while the backbone of the oligomer becomes fully conjugated, thus the π-electrons are more delocalized over the complete structure. In the case of an oligothiophene, the quinoid character can be increased e.g. by introducing a fused aromatic unit of higher resonance energy into the conjugated system. The π-electrons are localized mainly on the most stable aromatic unit, thus by fusing a phenyl ring with thiophene, the latter tends to dearomatize in favor of the quinoid form. For example, while simple polythiophene shows a band gap of 2.00 eV, phenyl fused polymer **4** in Figure 10 evinces a reduced band gap of only 1.10 eV.[43]

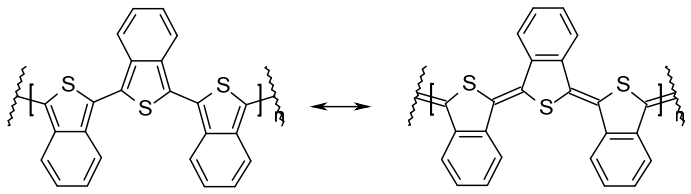

3 (aromatic) **4** (quinoid)

Figure 10: Enforcing the quinoid form in an oligothiophene. In a fused structure, the aromatic unit of higher resonance energy localizes the π-electrons, thus in the case of polythiophene fused with phenyl rings, quinoid character is enforced on the thienyl part.

Another important band gap controlling factor is planarity of the conjugated system: Sterical hindrance leading to torsion angles between consecutive aromatic units reduces the overlap of the molecular orbitals and results in a lowered resonance energy and an increase of the energy gap. Substituents at the conjugated backbone must therefore be carefully chosen in order to avoid twisted aromatic structures.[44] Full planarity of a system can be enforced by implementing a rigid, covalently interconnected backbone as depicted in Figure 11.[45-46] While

polymer **5** shows dihedral angles of around 20° between the aromatic units, the β-bridge in **6** prevents the thiophene rings from twisting out of plane, resulting in fully planar building blocks.



5 (twisted) **6** (planar)

Figure 11: Covalent interconnections between the thiophene moieties lead to a rigidification of the backbone, hence to full planarity of the aromatic units.

Another effective and commonly applied methods for achieving a reduced band gap is the introduction of electron-rich and electron-deficient moieties in an alternate fashion into the backbone of a conjugated system. Electron-releasing building blocks locally increase the electron density, thus the oxidation potential of the compound is lowered, while electron withdrawing groups decrease the electron density, hence the reduction potential is shifted to less energetic values. In other words, by implementing a push-pull system of electron donors and acceptors, the highest molecular orbital (HOMO) energy level is raised, while the lowest unoccupied molecular orbital (LUMO) energy level is decreased, resulting in a reduction of the band gap. Representative donor-acceptor substituted push-pull trimers are depicted in Figure 12.[47-48]

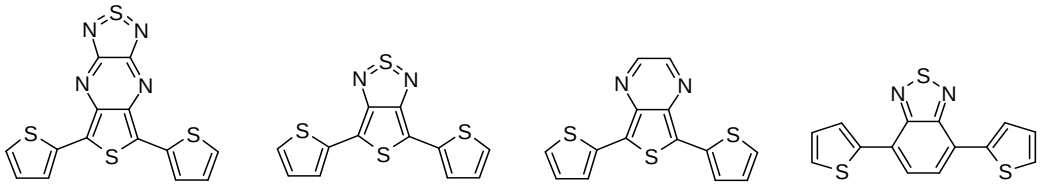

7 (ΔE = 1.25 eV) **8** (ΔE = 2.01 eV) **9** (ΔE = 2.34 eV) **10** (ΔE = 2.77 eV)

Figure 12: Donor-acceptor substituted push-pul: The magnitude of the band gap reduction is directly correlated to the electron withdrawing force of the core acceptor. The electron-rich thiophene rings constitute the donor moieties in these systems.[47-48]

The thiophene rings in these compounds (**7**-**10**) are electron-rich moieties, while the core components are strong electron acceptors. Thienopyrazine-based polymers **11** and **12** in Figure 13 show the importance of the donor-acceptor regularity: In the case of a 1:1 relation (**11**), a band gap of 0.80 eV is observed, whereas a donor-acceptor variation of 2:1 (**12**) results in an increased band gap of 1.10 eV.[49]

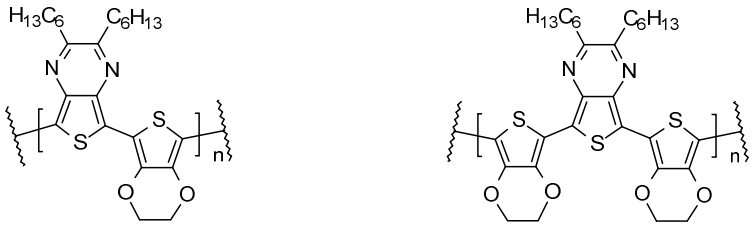

11 (DE = 0.80 eV) **12** (DE = 1.10 eV)

Figure 13: Donor-acceptor regularity in push-pull systems drastically influences the size of the band gap.

Intermolecular interactions may also influence the band gap, in particular in the solid state: Dipole-induced self-assembly or π-π-stacking of molecules can lead to H- or J-aggregates, resulting in an hypsochromic or bathochromic shift in absorption, respectively. The impact of this factor on the band gap is difficult to predict and in many cases strong π-π-stacking in combination with blue-shifting H-aggregates is taken into account in favor of better morphology in thin films.

To sum up, different structural parameters allow the adjustment and optimization of the band gap of conjugated systems: Rigidification of the backbone, enforcing quinoid character and imposing strong push-pull systems are among the most prominent methods for enabling a small bond length alternation (BLA), thus optimizing the band gap for organic solar cells.

2.7 Applied Materials in "Small Molecule" Solar Cells

2.7.1 Solution-processed Photovoltaic Devices

Figure 14 displays recent successes in oligomers for solution-processed organic solar cells and Table 1 summarizes corresponding device characterizations.

Chen *et al*. presented in 2010 a DCV-capped regioregular octylseptithiophene (**13**), which shows absorption down to 800 nm in thin films.[50-51] Applied as donor in BHJSCs with phenyl-C_{61}-butyric acid methyl ester ($PC_{61}BM$) as the acceptor, spin-coated from chloroform solution in a ratio of 1:1.4, a cell with an efficiency of 3.7% was achieved. A low fill factor value (*FF*) of 0.34 was compensated by a very high shortcut current density (J_{SC}) of 12.4 mA cm^{-2} and a reasonable V_{OC} of 0.88 V (Table 1).

Table 1: Device characteristics of solution-processed "small molecule" solar cells under AM1.5G conditions.

Device architecture	J_{SC} (mA cm^{-2})	V_{OC} (V)	*FF*	η (%)	Ref.
ITO/PEDOT:PSS (40 nm)/**13**:$PC_{61}BM$ (1:1.4, 110 nm)/ LiF (1 nm)/Al	12.4	0.88	0.34	3.7	[51]
ITO/PEDOT:PSS (50 nm)/**14**:$PC_{71}BM$ (~100 nm)/Al	10.0	0.92	0.48	4.4	[52]
ITO/PEDOT:PSS/P3HT:$PC_{71}BM$:**15** (1:1:0.2)/Al	8.6	0.63	0.59	3.2	[53]
ITO/PEDOT:PSS/P3HT:$PC_{71}BM$:**16** (2:2:0.5)/Ca/Al	10.6	0.69	0.61	4.5	[54]
ITO/**17**:$PC_{61}BM$ (1:1)/Al (annealed)	5.3	0.87	0.54	2.5	[55]
ITO/**18**:$PC_{61}BM$ (1:1)/Al (annealed)	5.2	0.85	0.53	2.3	[55]
ITO/ PEDOT:PSS (30 nm)/**19**:$PC_{71}BM$ (1:2, 80 nm)/Ca (10 nm)/Al	7.76	0.88	0.44	3.0	[56]

In 2009, Nguyen *et al*. prepared DPP compound **14,** which incorporates benzofurane as terminal acceptor groups. Blended with $PC_{71}BM$ in a 6:4 ratio and thermally annealed at 110 °C, the photovoltaic device showed a high current density (J_{SC}) of 10 mA cm^{-2}, a voltage (V_{OC}) of 0.92 V, and hence a record power conversion efficiency of 4.4%.[52] Impact of the blend ratios and annealing temperatures on the film morphology and the device performances were investigated in detail.[52, 57-58] The same group published another highly efficient DPP derivative (**15**), in which the terminal acceptor moieties were replaced with electron rich oligothiophenes. A device incorporating **15** in a D-A mixture of 1:1 showed an efficiency of 3.0% and a current density (J_{SC}) of 9.2 mA cm^{-2}.[57] For improving the photon exploitation on the near-IR-region, compound **15** was also applied as an additive in a P3HT:$PC_{71}BM$ BHJ device.[53] The cell performance of the bulk-system P3HT:$PC_{71}BM$:**15** (10:10:2 mg/mL) showed an increase in efficiency from 2.9% to 3.2%, when compared to the P3HT/$PC_{71}BM$-only architecture, which can be assigned to the additional near-IR absorption properties of DPP-compound **15**.

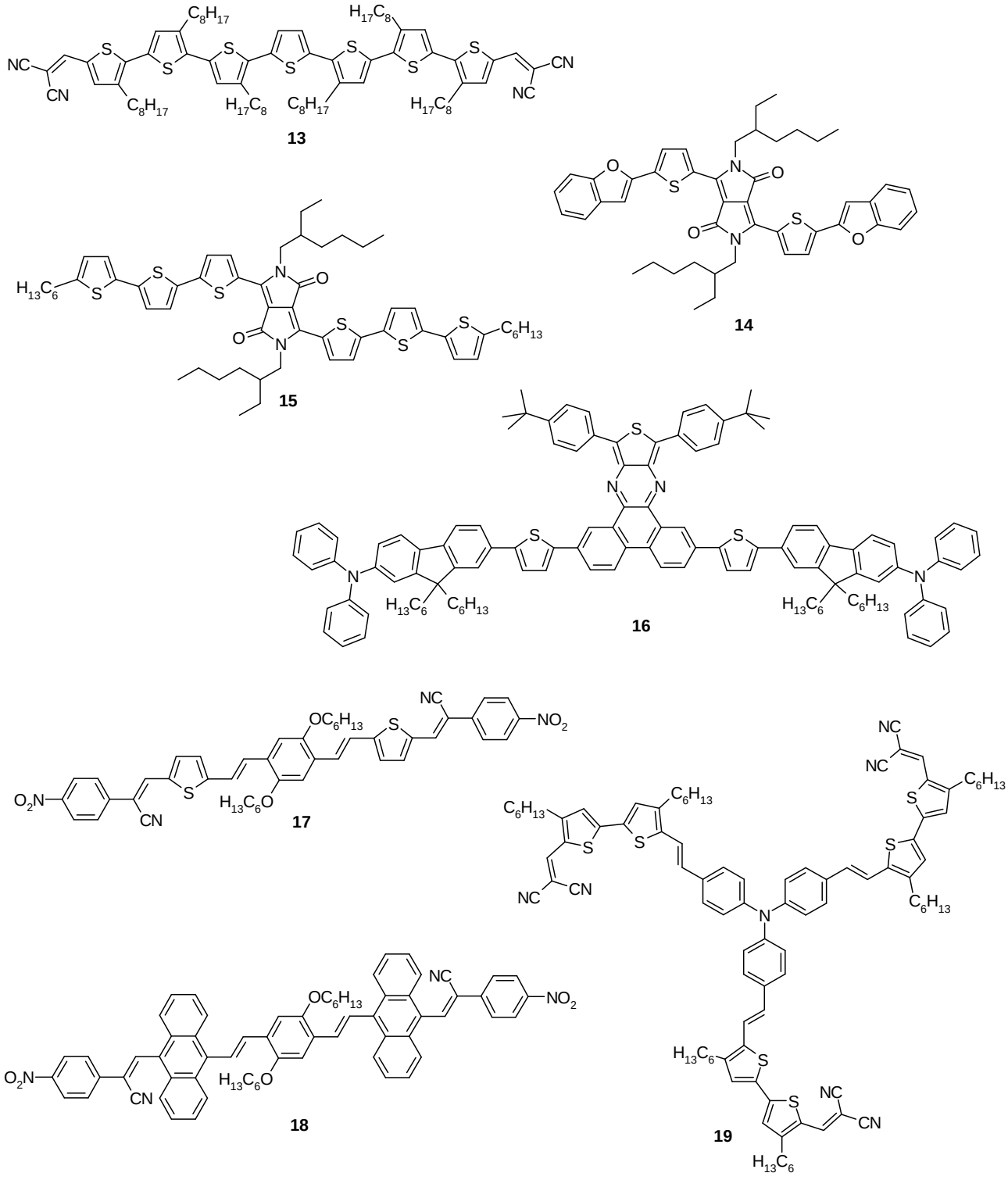

Figure 14: Oligomers for solution-processed organic solar cells.

Diphenylaminofluorene end-capped compound **16** incorporates a dibenzo[f,h]thieno[3,4-b]quinoxaline as electron accepting core, constituting a pronounced donor-acceptor push-pull system with a charge-transfer band at around 580 nm and a narrow band gap of 1.82 eV. BHJSCs, assembled by spin-coating from chloroform solutions of **16** and $PC_{61}BM$ in a ration of

33:67 (wt%), showed an efficiency of 1.7%.[59] Compound **16** was also used as an additional donor in a P3HT-based device, to improve the light harvesting properties of the cell.[54] Relative to P3HT, compound **16** acts as an electron acceptor, while at the same time it serves as an electron donor to $PC_{71}BM$. Photovoltaic devices based on a mixture of P3HT:$PC_{71}BM$:**16** in a ratio of 2:2:0.5, showed an improved PCE of 4.5%, which is by 0.6% higher than the original device without **16** as additive.

A-D-A compounds **17** and **18** showed a longest wavelength absorption maximum at 630 and 640 nm, respectively. Applied as donor with $PC_{61}BM$ as the acceptor in BHJSCs, **17** and **18** gave efficiencies of 1.4 and 1.7%, respectively, with open-circuit voltages (V_{OC}) as high as 0.94 and 0.92 V.[55] The efficiencies were optimized to 2.3 and 2.5%, respectively, by thermal annealing of the active layers. Both J_{SC} and *FF* increased with this process, indicating an improved charge carrier mobility due to better packing in the film, when compared to non-annealed devices.

Most recently, Li and co-workers reported a novel star-shaped triphenylamin-based compound (**19**) with terminal DCV-groups connected via vinylene-bridged bithiophene units. The absorption in solid state covers a broad wavelength range from 380 to 750 nm, which is benefited from its pronounced D-A structure. Applied in BHJSCs with $PC_{71}BM$ as the acceptor, a PCE of 3.0% with an open-circuit voltage (V_{OC}) of 0.88 V and a current density of 7.76 mA/cm^{-2} was achieved.

2.7.2 Vacuum-processed Photovoltaic Devices

Table 2 lists recent advances in the field of vacuum-processed organic solar cells and Figure 15 depicts the corresponding structures. In particular, linear donor-acceptor push-pull systems and phthalocyanine-based dyes are among the most efficient structures. Since vacuum deposition does not allow arbitrary bulky building blocks for keeping the sublimation temperature as low as possible, these compounds are more restricted in their structural demands than the above presented solution-processed compounds.

In 2005, Xue *et al*. developed a bulk heterojunction architecture, in which copper phthalocyanine **20** (CuPc) gave with fullerene C_{60} as the electron acceptor an open circuit voltage (V_{OC}) of 1.00 V, a shortcut current density (J_{SC}) of 9.66 mA cm^{-2}, a fill factor value of 0.59, and thus a conversion efficiency of 5.0%. Bundled in a sophisticated tandem cell, con-

sisting of two hybrid planar-mixed heterojunction cells, an improved efficiency of 5.9% was achieved.[1, 60]

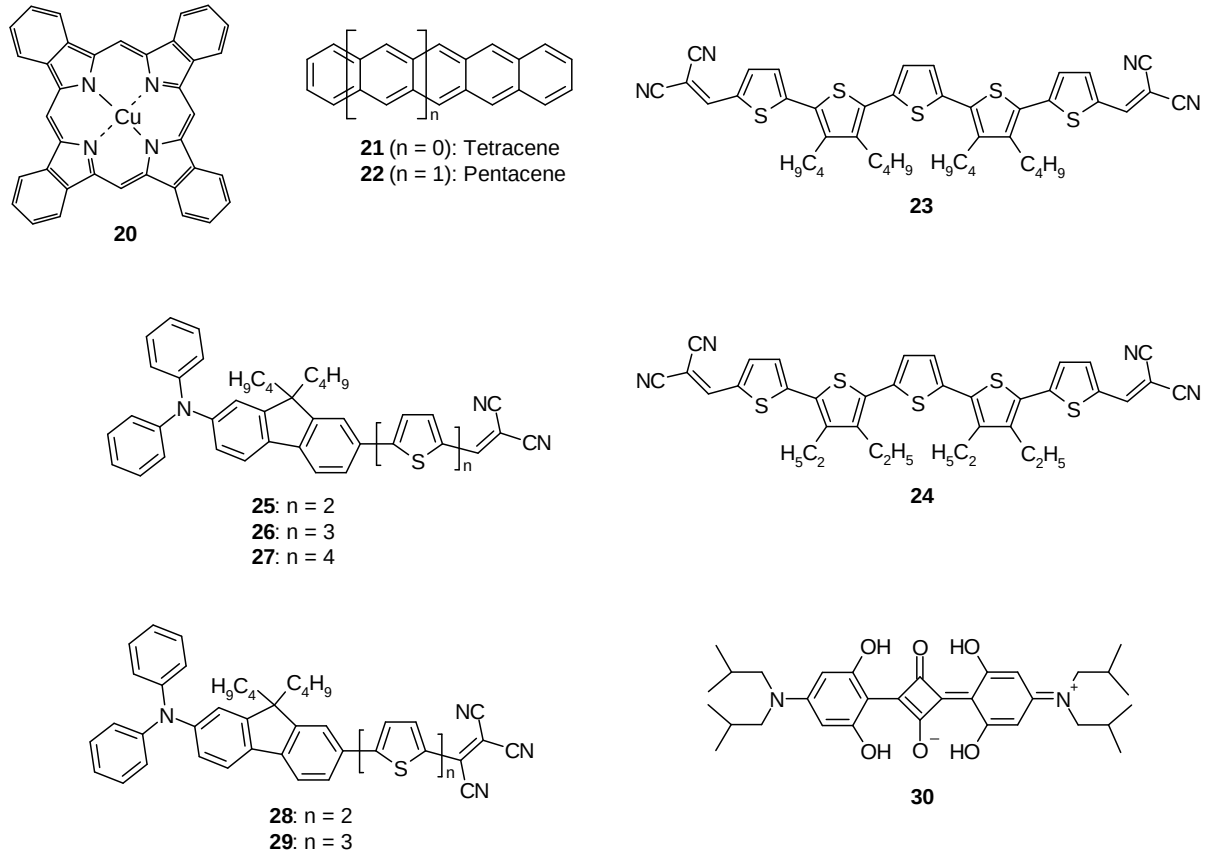

Figure 15: Oligomers for vacuum-processed organic solar cells.

Due to their high charge carrier mobility, tetracene **21** and pentacene **22** are among the best investigated conjugated oligomers for p-type materials, in particular for OFETs. Photovoltaic devices using tetracene **21** and fullerene C_{60} in bulk heterojunction layers gave conversion efficiencies as high as 2.3% under AM1.5G conditions.[61] The completely flat structure results in a well-defined morphology in the active film, leading to a high charge carrier mobility and an excellent efficiency. Kippelen *et al*. assembled solar cells applying a BHJ layer of pentacene **22** and fullerene C_{60} with BCP as exciton blocking layer, which showed a record shortcut current density (J_{SC}) of around 15 mA cm^{-2} and thus an improved overall efficiency of 2.7%.[29]

Table 2: Device characteristics of vacuum-processed "small molecule" solar cells under AM1.5G conditions.

Device architecture	J_{SC} (mA cm^{-2})	V_{OC} (V)	*FF*	η (%)	Ref.
ITO/**20** (7.5 nm)/**20**:C_{60} [1:1](12.5 nm)/C_{60} (8 nm)/PTCBI (50 nm)/Ag (0.5nm)/p-*m*-MTDATA (50 Å)/**20** (6 nm)/**20**:C_{60} [1:1](13 nm)/C_{60} (16 nm)/BCP (10 nm)/Ag	9.7	1.03	0.59	5.7	[1]
ITO/**21** (80 nm)/C_{60}(30 nm)/BCP (8 nm)/Al	7.0	0.58	0.56	2.3	[61]
ITO/**22** (45 nm)/C_{60} (50 nm)/BCP (10 nm)/Al	15.0	0.36	0.50	2.7	[29]
ITO/Au (1 nm)/p-doped α-NPD (10 nm)/α-NPD (5 nm)/**23** (9.8 nm)/C_{60} (52 nm)/Bphen (6 nm)/Al	8,9	1.00	0.50	3.4 [a]	[62]
ITO/Au (1 nm)/p-doped α-NPD (10 nm)/α-NPD (5 nm)/**24** (10 nm)/C_{60} (52 nm)/Bphen (6 nm)/Al	8.4	1.00	0.40	2.5 [a]	[62]
ITO/PEDOT:PSS/**25** (20 nm)/C_{60} (30 nm)/BCP (8 nm)/Ag	4.9	0.89	0.36	1.6	[63]
ITO/PEDOT:PSS/**26** (20 nm)/C_{60} (30 nm)/BCP (8 nm)/Ag	6.3	0.89	0.38	2.1	[63]
ITO/PEDOT:PSS/**27** (20 nm)/C_{60} (30 nm)/BCP (8 nm)/Ag	6.1	0.91	0.48	2.7	[63]
ITO/PEDOT:PSS/**28** (20 nm)/C_{60} (30 nm)/BCP (8 nm)/Ag	4.0	0.82	0.40	1.3	[64]
ITO/PEDOT:PSS/**29** (20 nm)/C_{60} (30 nm)/BCP (8 nm)/Ag	3.5	0.79	0.39	1.1	[64]
ITO/**30** (6.5 nm)/C_{60} (40 nm)/BCP (10 nm)/Al	7.1	0.75	0.60	3.2	[65]

[a] A spectral mismatch between sun simulator and the AM1.5 sun spectrum is taken into account.

Our group reported in 2006 linear oligothiophenes, terminally functionalized on both ends with dicyanovinyl groups as low band gap p-type materials for photovoltaic applications.[3, 31-32, 62, 66-68] Due to the electron-accepting nature of the DCV-groups, the optical band gap of DCV5T (**23**) was reduced from about 2.5 eV to 1.77 eV as compared to the unsubstituted quinquethiophene. A p/n-planar heterojunction solar cell comprising **23** as donor with fullerene C_{60} as acceptor, showed an open circuit voltage (V_{OC}) of 0.98 V, an excellent shortcut current density (J_{SC}) of 10.6 mA cm^{-2}, a fill factor (*FF*) value of 0.49 and a power conversion efficiency of 3.4%.[31, 69] The EQE covers the full spectral range from 350 to 650 nm, reaching a maximum of nearly 50% at 570 nm. Different chain lengths and alkylation patterns were investigated and e.g. derivative **24**, in which the butyl chains were replaced with ethyl groups, showed in a similar photovoltaic device an efficiency of 2.5%.[62] The decrease in efficiency is attributed to a lower fill factor value (*FF*), which can mainly be assigned to better packing of the butyl derivative in the thin film. An analogous sexithiophene gave in a bilayer architecture an efficiency of 3.1%[70] and in tandem cells up to 7.7% on an area of 1.1 cm^2, which is currently the among the highest values reported.[3] Wong and co-workers reported in 2007

linear oligothiophenes asymmetrically functionalized on one α-position with diphenylaminofluorenyl and on the other with dicyanovinyl groups (**25**-**27**).[63] Assembled BHJSCs showed efficiencies in the range of only 0.45-0.9%. However, by thermal annealing, the efficiencies increased significantly to 1.6% for **25**, to 2.1% for **26** and to 2.7% for **27**, respectively, which indicates an improved morphology in the thin films and with it a strong increase in J_{SC} and *FF*.

The same group also reported analogous structures **28** and **29**, in which the terminal dicyanovinyl group is replaced with the stronger acceptor moiety tricyanovinyl.[64] A similar device architecture as for **25**-**27** gave an open circuit voltage (V_{OC}) of 0.82 V, a shortcut current density (J_{SC}) of 4.03 mA cm^{-2}, a fill factor value of 0.44 and an efficiency of only 1.33%. The decrease in efficiency demonstrates, that a stronger push-pull system, and hence a smaller band gap, does not necessarily lead to an improvement in solar cell performance. In this case, the small difference of the LUMO energy level offset of the donor (-3.9 eV) and the LUMO energy level offset of the acceptor C_{60} (-4.0 eV) resulted in an inefficient exciton separation at the heterojunction interface.

Recently, Forrest *et al*. prepared squaraine **30**, which shows a longest wavelength absorption maximum at 652 nm in solution and a bathomchromic shift to 700 nm in the solid state. [65] A photovoltaic device using the squaraine as donor with fullerene C_{60} as the acceptor resulted in a PCE of 3.2% with a V_{OC} of 0.75 V.

To sum up, various approaches have been made for improving materials in order to achieve higher efficiencies in organic photovoltaic devices. Currently all presented strategies imply advantages as well as disadvantages, making it difficult to decide, which is the most promising direction.

2.8 References

[1] J. Xue, S. Uchida, B. P. Rand, S. R. Forrest, *Appl. Phys. Lett.* **2004**, *85*, 5757.
[2] H. Y. Chen, J. H. Hou, S. Q. Zhang, Y. Y. Liang, G. W. Yang, Y. Yang, L. P. Yu, Y. Wu, G. Li, *Nat. Photonics* **2009**, *3*, 649.
[3] Heliatek GmbH, press release, 11th Oct 2010. http://www.heliatek.com.
[4] M. A. Green, K. Emery, D. L. King, Y. Hishikawa, W. Warta, *Prog. Photovoltaics* **2006**, *14*, 455.

[5] H. J. Lewerenz, H. Jungblut, in *Photovoltaic - Grundlagen und Anwendungen*, Springer, Berlin, Heidelberg, New York, **1995**.
[6] H. Akamatu, H. Inokuchi, Y. Matsunaga, *Nature* **1954**, *173*, 168.
[7] H. Kallmann, M. Pope, *J. Chem. Phys.* **1959**, *30*, 585.
[8] C. W. Tang, *Appl. Phys. Lett.* **1986**, *48*, 183.
[9] K. Kim, J. Liu, M. A. G. Namboothiry, D. L. Carroll, *Appl. Phys. Lett.* **2007**, *90*, 163511.
[10] W. Ma, C. Yang, X. Gong, K. Lee, A. J. Heeger, *Adv. Funct. Mater.* **2005**, *15*, 1617.
[11] Y. Kim, S. Cook, S. M. Tuladhar, S. A. Choulis, J. Nelson, J. R. Durrant, D. D. C. Bradley, M. Giles, I. McCulloch, M. R. C.-S. Ha, *Nat. Mater.* **2006**, *5*, 197.
[12] V. S. G. Li, J. Huang, Y. Yao, T. Moriarty, K. Emery, Y. Yang, *Nat. Mater.* **2005**, *4*, 864.
[13] F. Padinger, R. S. Rittberger, N. S. Sariciftci, *Adv. Funct. Mater.* **2003**, *13*, 85.
[14] J. Y. Kim, S. H. Kim, H. H. Lee, K. Lee, W. L. Ma, X. Gong, A. J. Heeger, *Adv. Mater.* **2006**, *18*, 572.
[15] B. O'Regan, M. Grätzel, *Nature* **1991**, *353*, 737.
[16] M. K. Nazeeruddin, P. Pechy, T. Renouard, S. M. Zakeeruddin, R. Humphry-Baker, P. Comte, P. Liska, L. Cevey, E. Costa, V. Shklover, L. Spiccia, G. B. Deacon, C. A. Bignozzi, M. Grätzel, *J. Am. Chem. Soc.* **2001**, *123*, 1613.
[17] F. Gao, Y. Wang, J. Zhang, D. Shi, M. Wang, R. Humphry-Baker, P. Wang, S. M. Zakeeruddin, M. Grätzel, *Chem. Comm.* **2008**, 2635.
[18] W. Ma, C. Yang, X. Gong, K. Lee, A. J. Heeger, *Adv. Funct. Mater.* **2005**, *15*, 1617.
[19] Y. Kim, S. Cook, S. M. Tuladhar, S. A. Choulis, J. Nelson, J. R. Durrant, D. D. C. Bradley, M. Giles, I. McCulloch, C.-S. Ha, M. Ree, *Nat. Mater.* **2006**, *5*, 197.
[20] J. Y. Kim, K. Lee, N. E. Coates, D. Moses, T.-Q. Nguyen, M. Dante, A. J. Heeger, *Science* **2007**, *317*, 222.
[21] A. Mishra, C.-Q. Ma, P. Bäuerle, *Chem. Rev.* **2009**, *109*, 1141.
[22] S. A. Jenekhe, S. Yi, *Appl. Phys. Lett.* **2000**, *77*, 2635.
[23] C. J. Brabec, C. Winder, N. S. Sariciftci, J. C. Hummelen, A. Dhanabalan, P. A. v. Hal, R. A. J. Janssen, *Adv. Funct. Mater.* **2002**, *12*, 709.
[24] C. Winder, G. Matt, J. C. Hummelen, R. A. J. Janssen, N. S. Sariciftci, C. J. Brabec, *Thin Solid Films* **2002**, *403-404*, 373.
[25] V. I. Arkhipov, H. Bässler, *Phys. Status Solidi A* **2004**, *201*, 1152.
[26] N. S. Sariciftci, L. Smilowitz, A. J. Heeger, F. Wudl, *Science* **1992**, *258*, 1474.
[27] S. Günes, H. Neugebauer, N. S. Sariciftci, *Chem. Rev.* **2007**, *107*, 1324.
[28] P. Peumans, A. Yakimov, S. R. Forrest, *J. Appl. Phys.* **2003**, *93*, 3693.
[29] S. Yoo, B. Domercq, B. Kippelen, *Appl. Phys. Lett.* **2004**, *65*, 5427.
[30] B. C. Thompson, J. M. J. Fréchet, *Angew. Chem. Int. Ed.* **2008**, *47*, 58.
[31] K. Schulze, C. Uhrich, R. Schüppel, K. Leo, M. Pfeiffer, E. Brier, E. Reinold, P. Bäuerle, *Adv. Mater.* **2006**, *18*, 2872.
[32] C. Uhrich, R. Schüppel, A. Petrich, M. Pfeiffer, K. Leo, E. Brier, P. Kilickiran, P. Bäuerle, *Adv. Funct. Mater.* **2007**, *17*, 2991.
[33] K. Schulze, *Dissertation* **2008**, *Technical University of Dresden*, 31.
[34] K. A. Emery, C. R. Osterwald, *Solar Cells* **1986**, *17*, 253.
[35] V. Shrotriya, Y. Y. G. Li, T. Moriarty, K. Emery, Y. Yang, *Adv. Funct. Mater.* **2006**, *16*, 2016.
[36] H. Kies, H. Rehwald, *Sol. Energy Mater. Sol. Cells* **1995**, *38*, 45.
[37] C. J. Brabec, A. Cravino, D. Meissner, N. S. Sariciftci, M. T. Rispens, L. Sanches, J. C. Hummelen, T. Fromherz, *Thin Solid Films* **2002**, *403-404*, 368.
[38] H. Kim, S.-H. Kim, H. Suh, K. Lee, in *Organic Photovoltaics IV* (Eds.: Z. H. Kafafi, P. A. Lane), Bellinghem, **2004**, pp. 111.

[39] M. C. Scharber, D. Mühlbacher, M. Koppe, P. Denk, C. Waldauf, A. J. Heeger, C. J. Brabec, *Adv. Mater.* **2006**, *18*, 789.
[40] G. Dennler, M. C. Scharber, T. Ameri, P. Denk, K. Forberich, C. Waldauf, C. J. Brabec, *Adv. Mater.* **2008**, *20*, 579.
[41] I. Jestin, P. Frère, N. Mercier, E. Levillain, D. Stiévenard, J. Roncali, *J. Am. Chem. Soc.* **1998**, *120*, 8150.
[42] J.-L. Brédas, *J. Chem. Phys.* **1985**, *82*, 3808.
[43] F. Wudl, M. Kobayashi, A. J. Heeger, *J. Org. Chem.* **1984**, *49*, 3382.
[44] M. H. Petersen, O. Hagemann, K. T. Nielsen, M. Jørgensen, F. C. Krebs, *Sol. Energy Mater. and Sol. Cells* **2007**, *91*, 996.
[45] H. Briset, A. Thobi-Gautier, M. Gorgues, J. Jubault, J. Roncali, *Chem. Comm.* **1994**, *1305*.
[46] P. Blanchard, H. Brisset, A. Riou, R. Hierle, J. Roncali, *J. Org. Chem.* **1998**, *63*, 8310.
[47] H. A. M. Van Mullekom, J. A. J. M. Vekemans, E. W. Meijer, *Chem. Eur. J.* **1998**, *4*, 1235.
[48] Y. Yamashita, S. Tanaka, *Synth. Metals* **1995**, *69*, 599.
[49] J. Casado, R. P. Ortiz, M. C. Ruiz Delgado, V. Hernández, J. T. López Navarrete, J. M. Raimundo, P. Blanchard, M. Allain, J. Roncali, *J. Phys. Chem. B* **2005**, *109*, 16616.
[50] Y. Liu, J. Zhou, X. Wan, Y. Chen, *Tetrahedron* **2009**, *65*, 5209.
[51] B. Yin, L. Yang, Y. Liu, Y. Chen, Q. Qi, F. Zhang, S. Yin, *Appl. Phys. Lett.* **2010**, *97*, 023303.
[52] B. Walker, A. B. Tamayo, X.-D. Dang, P. Zalar, J. H. Seo, A. Garcia, M. Tantiwiwat, T.-Q. Nguyen, *Adv. Funct. Mater.* **2009**, *19*, 3063.
[53] J. Peet, A. B. Tamayo, X. D. Dang, J. H. Seo, T. Q. Nguyen, *Appl. Phys. Lett.* **2008**, *93*, 163306.
[54] J.-H. Huang, M. Velusamy, K.-C. H. J.-T. Lin, C.-W. Chu, *J. Mater. Chem.* **2010**, *20*, 2820.
[55] J. A. Mikroyannidis, M. M. Stylianakis, P. Balraju, P. Suresh, G. D. Sharma, *ACS Appl. Mater. Interfaces* **2009**, *1*, 1711.
[56] J. Zhang, D. Deng, C. He, Y. He, M. Zhang, Z.-G. Zhang, Z. Zhang, Y. Li, *Chem. Mater.* **2010**, *DOI:10.1021/cm102077j*.
[57] A. B. Tamayo, X.-D. Dang, B. Walker, J. Seo, T. Kent, T.-Q. Nguyen, *Appl. Phys. Lett.* **2009**, *94*, 103301.
[58] A. B. Tamayo, B. Walker, T.-Q. Nguyen, *J. Phys. Chem. C* **2008**, *112*, 11545.
[59] M. Velusamy, J.-H. Huang, Y.-C. Hsu, H.-H. Chou, K.-C. Ho, P.-L. Wu, W.-H. Chang, J. T. Lin, C.-W. Chu, *Org. Lett.* **2009**, *11*, 4898.
[60] J. Xue, B. P. Rand, S. Uchida, S. R. Forrest, *J. Appl. Phys.* **2005**, *98*, 124903.
[61] C.-W. Chu, Y. Shao, V. Shrotriya, Y. Yang, *Appl. Phys. Lett.* **2005**, *86*, 243506.
[62] K. Schulze, M. Riede, E. Brier, E. Reinold, P. Bäuerle, K. Leo, *J. Appl. Phys.* **2008**, *104*, 074511.
[63] P. F. Xia, X. J. Feng, J. Lu, S.-W. Tsang, R. Movileanu, Y. Tao, M. S. Wong, *Adv. Mater.* **2008**, *20*, 4810.
[64] P. F. Xia, X. J. Feng, J. Lu, R. Movileanu, Y. Tao, J.-M. Baribeau, M. S. Wong, *J. Phys. Chem. C* **2008**, *112*, 16714.
[65] S. Wang, E. I. Mayo, M. D. Perez, L. Griffe, G. Wei, P. I. Djurovich, S. R. Forrest, M. E. Thompson, *Appl. Phys. Lett.* **2009**, *94*, 233304.
[66] K. Schulze, B. Maennig, K. Leo, Y. Tomita, C. May, J. Hüpkes, E. Brier, E. Reinold, P. Bäuerle, *App. Phys. Lett.* **2007**, *91*, 073521.
[67] R. Schüppel, C. Uhrich, M. Pfeiffer, K. Leo, E. Brier, E. Reinold, P. Baeuerle, *ChemPhysChem* **2007**, *8*, 1497.
[68] R. Schüppel, K. Schmidt, C. Uhrich, K. Schulze, D. Wynands, J. L. Brédas, E. Brier, E. Reinold, H.-B. Bu, *Phys. Rev. B* **2008**, *77*, 085311.

[69] K. Schulze, C. Uhrich, R. Schüppel, K. Leo, M. Pfeiffer, E. Brier, E. Reinold, P. Bäuerle, *Proc. SPIE Int. Soc. Opt. Eng.* **2006**, *6192*, 61920.

[70] D. Wynands, B. Männig, M. Riede, K. Leo, E. Brier, E. Reinold, P. Bäuerle, *J. Appl. Phys.* **2009**, *106*, 054509.

Chapter 3

Thienothiadiazole and Thienopyrazine as Core Acceptor in A-D-A-D-A-type Oligothiophenes

Abstract

Novel A-D-A-D-A-type oligothiophenes comprising heterocyclic thieno[3,4-*c*][1,2,5]thiadiazole (TTDA) or thieno[3,4-*b*]pyrazine (TP) as core and dicyanovinyl (DCV) or trifluoroacetly (TFA) as terminal acceptors have been developed as red/near-IR absorbers for vacuum-processed "small molecule" solar cells. The insertion of such a core acceptor unit into the conjugated backbone of quinquethiophene DCV5T, reported earlier by our group,[1-2] resulted in a large bathochromic shift. The compounds show absorption extending over 950 nm in thin films ($\Delta E_g \leq 1.2$ eV) with HOMO and LUMO energy levels well located to be used as donor with fullerene C_{60} as acceptor in m-i-p-type planar heterojunction solar cells. Devices based on TTDA or TP showed an overall power conversion efficiency of around 1.1% under AM1.5G illumination.

3.1 Introduction

One of the approaches towards low band gap materials is the application of strong donor and acceptor push-pull systems or the incorporation of *o*-quinoid heterocycles into conjugated oligomers.[3] Various low band gap oligomers and polymers comprising the proquinoid acceptor units thienothiadiazole (TTDA)[4-6] and thienopyrazine (TP)[5, 7-9] have been reported.[10-11]

Thieno[3,4-*b*]pyrazine (TP) was theoretically calculated in 1976 and first synthesized in 1983 by Skancke and Paulmier.[12-13] The structure has been demonstrated as an excellent building block in the development of low band gap materials for organic electronic applications such as OLEDs, OFETs and OSCs.[5, 14-28] Chan and co-workers published in 2008 stable polymers containing phenyl-substituted thienopyrazine moieties with narrow band gaps of 1.47 eV and efficiencies of preliminary solar cells of up to 0.63%.[18] In 2009, Bao *et al*. presented another stable thienopyrazine polymer with a narrow band gap of 1.6 eV (λ_{Onset} = 800 nm) and corresponding photovoltaic devices with a fill factor (FF) value of 0.50, an open circuit voltage (V_{OC}) of 0.52 V, a shortcut current density (J_{SC}) of 5.35 mA cm^2, and hence an efficiency of 1.4%.[29] The same year, Janssen *et al*. reported a thienopyrazine-comprising polymer with an ultra small band gap of ΔE = 0.94 eV and absorption down to 1400 nm, but very poor solar cell performance with efficiencies < 0.1%.[30] A pentamer with up to three consecutive thienopyrazine units was presented in 2008 by Janssen and co-workers with an onset of absorption at 871 nm, yet no solar cells were assembled. In 2009, the same group published a series of polymers with alternating bithiophene- and thienopyrazine units with small band gaps of 1.2 eV to 1.5 eV and solar cells reaching power conversion efficiencies of up to 1.5%.[31-32]

In contrast to thienopyrazine, the chemistry of nonclassical bicyclic thieno[3,4-*c*][1,2,5]thiadiazole (TTDA) has scarcely been explored in detail, in particular with respect to the application in photovoltaic devices.[4-6, 33] In 1969, Bower and Schlessinger have first reported the synthesis of a phenyl-capped TTDA unit by reaction of 3,4-dibenzoyl-1,2,5-thiadiazole with phosphorus pentasulfide in dioxane at 110 ^{o}C. The compound showed its longest wavelength absorption band at 558 nm in dichloromethane.[33] Later in 1993, Tanaka and Yamashita synthesized a simple non-substituted terthiophene containing TTDA as core unit, using a Stille-type coupling reaction. The trimeric compound absorbs at 618 nm in solution, with a narrow band gap of 2.01 eV.[4-6] A very low band gap of 0.9 eV (λ_{max} = 934 nm) was reported for the corresponding polymer. Later, they successfully prepared nonsubstituted TTDA (λ_{max} = 415 nm)

and *tert*-butyl capped TTDA (λ_{max} = 478 nm) moieties, while the former was found to be unstable at room temperature in solid state and in concentrated solution.[34] Recently, alkylated and non-alkylated quinquethiophenes comprising a core TTDA unit were synthesized, showing a longest wavelength absorption band at around 700 nm.[35] There is only one report of a solar cell in which TTDA was used in a conjugated polymer containing oligothiophene as donor units, and the photovoltaic devices blended with $PC_{61}BM$ (1:1) generated low power conversion efficiencies of only 0.11%.[36] However, there is no report on photovoltaic cells based on low band gap oligomers containing TTDA moieties.

The objective in this study is to shift the longest wavelength absorption of oligothiophene DCV5T[1-2]-analoguous structures to the near-IR regime by the insertion of TTDA or TP as an additional core electron-acceptor. Dicyanovinylene (DCV) and trifluoroacetyl (TFA) are applied as terminal acceptor groups to optimize the physical and optical properties of these materials and alkyl chains are attached for solubility reasons and to influence the morphology in the solid state (Figure 1).

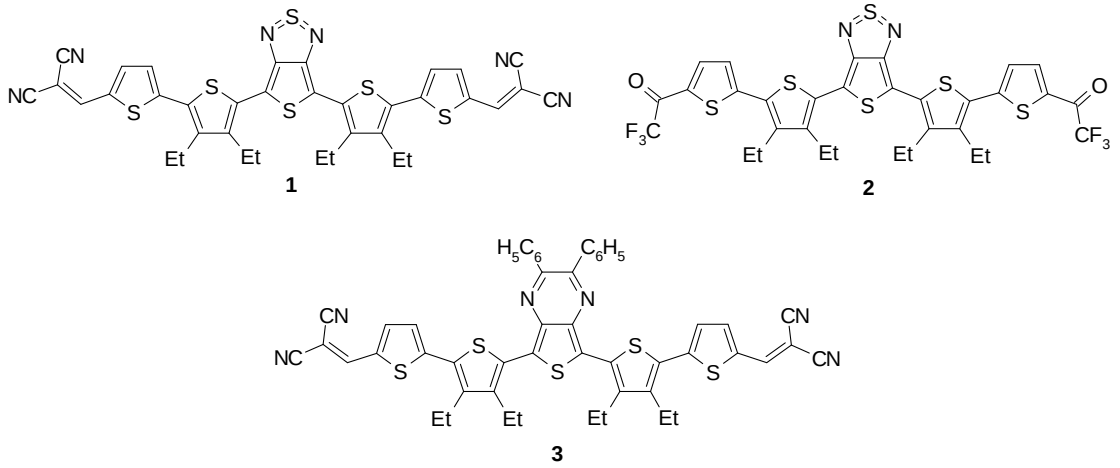

Figure 1. DCV5T-analogous target structures **1**-**3** with TTDA or TP as core and TFA or DCV as terminal acceptor units.

We investigated the influence of the TTDA- and TP-group on the conjugated oligothiophene and applied these novel materials as donor with fullerene C_{60} as acceptor in vacuum-processed m-i-p-type flat heterojunction solar cells.

3.2 Synthesis

A Stille-type cross-coupling reaction of stannylated diethylthiophene **4**[37] and 2,5-dibromo-3,4-dinitrothiophene using $Pd(PPh_3)_4$ as catalyst in dry THF gave terthiophene **5** in 81% yield

(Scheme 1). Reduction of the nitro group of **5** by tin(II)-chloride/EtOH or Pd/hydrogen was found to be difficult, resulting in low conversion yields. The transformation from **5** to amine **6** was therefore performed by Pd/C and hydrazine hydrate in ethanol (88% yield), which was used without further purification. Reaction of amine **6** with thionyl aniline and trimethylsilyl chloride in pyridine afforded the trimeric thienothiadiazole **7** in a yield of 69%.

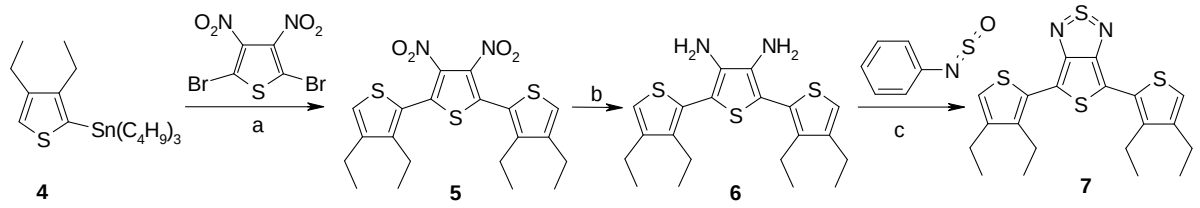

Scheme 1: a) $Pd(PPh_3)_4$, THF, reflux, 3 d, 81%; b) hydrazine hydrate, Pd/C (10%), ethanol, rt, 1 h, 88%; c) TMS-chloride, pyridine, rt, 1 h, 69%.

Bromination of terthiophene **7** using NBS followed by a Stille-type cross-coupling reaction with stannylated thiophene afforded quinquethiophene **9** in 72% yield (Scheme 2). Vilsmeier-Haack formylation of quinquethiophene **9** afforded bis-aldehyde **10** in a yield of 33%, and the corresponding mono-aldehyde was formed in 12% (Scheme 3). The use of excess formylating reagent or prolonged reaction time did not improve the yield. A Knoevenagel condensation of aldehyde **10** with malononitrile and piperidine in 1,2-dichloroethane gave target compound **1** (DCV5T-TTDA) in a yield of 87%.

We further introduced the electron-withdrawing TFA moiety in order to study the influence of fluorine substituents on the thermal stability and the device performance. TFA-substituted compound **2** was prepared in 65% yield by reaction of quinquethiophene **9** with trifluoroacetic anhydride under microwave irradiation (Scheme 2).

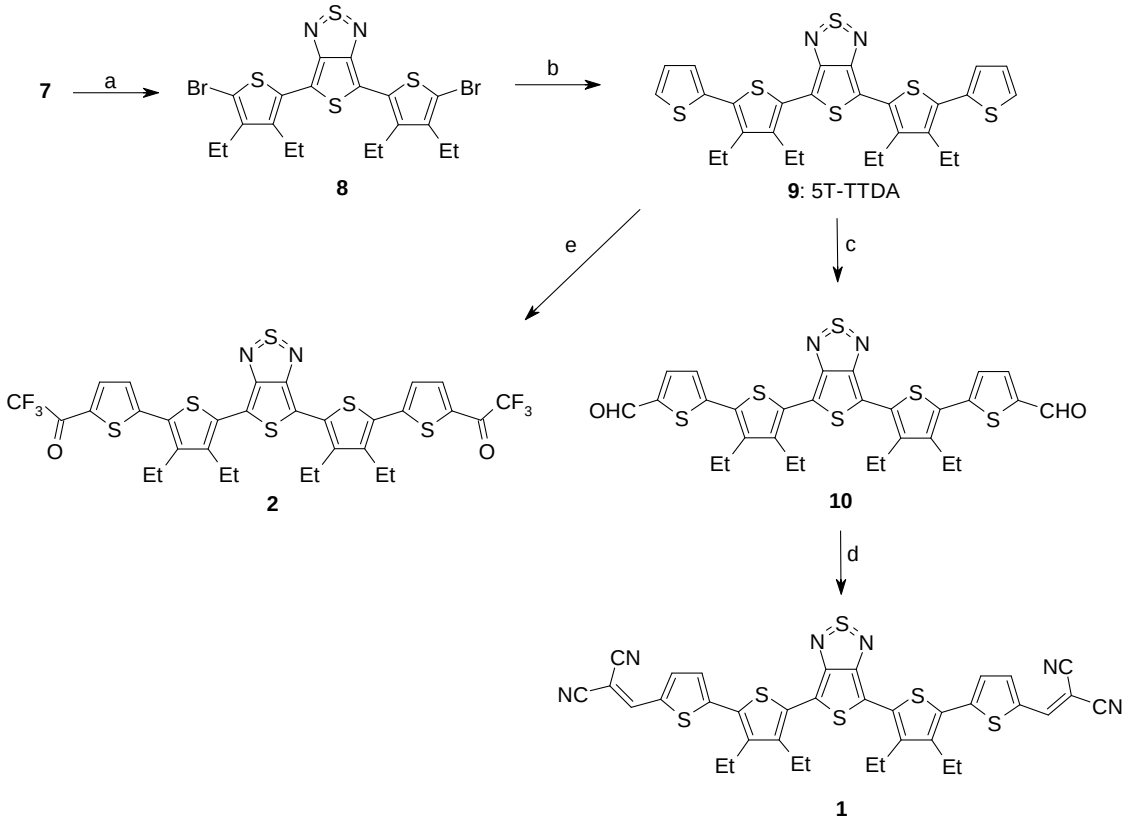

Scheme 2: a) NBS, DCM, 0 °C to rt, 1 d, 92%; b) 2-(tributylstannyl)-thiophene, Pd_2dba_3, Tri-2-furylphosphine, THF, reflux, 3 d, 72%; c) DMF, $POCl_3$, DCM, rt, 1 d, 32%; d) malonitrile, piperidine, 1,2-dichloroethane, reflux, 1.5 h, 87%; e) Trifluoroacetic anhydride, 1,2-dichloroethane, microwave, 120 °C, 4 h, 65%.

We also optimized the mono-formylation of **9**, to investigate the asymmetric product and its DCV-derivative in more detail (Scheme 3). By tuning the reaction temperature and time, mono-aldehyde **11** was obtained via Vilsmeier-Haack reaction in 33% yield. Compound **11** was then transformed in analogy to compound **1** via Knoevenagel condensation with malononitrile and piperidine in 1,2-dichloroethane to DCV-derivative **12** in a yield of 91%.

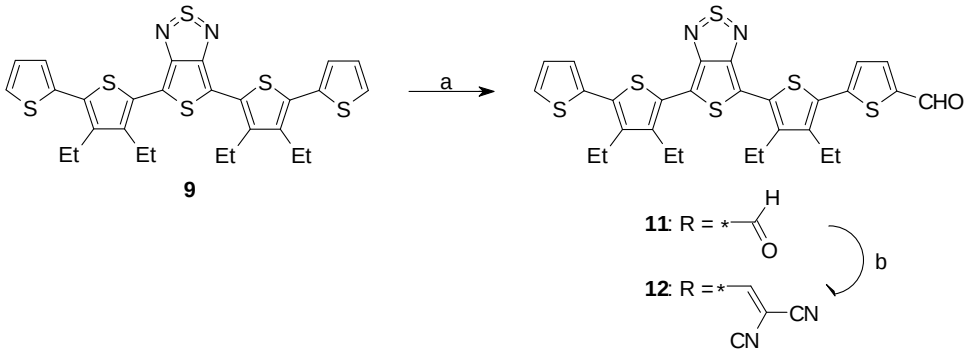

Scheme 3: a) DMF, $POCl_3$, DCM, rt, 1 d, 33%; b) malonitrile, piperidine, 1,2-dichloroethane, reflux, 1.5 h, 91%.

The synthesis of thienopyrazine **3** (DCV5T-TP) is outlined in Scheme 4. Thieno[3,4-*b*]pyrazine **13** was obtained in 68% yield by condensation of diamine **6** with benzile in methanol.

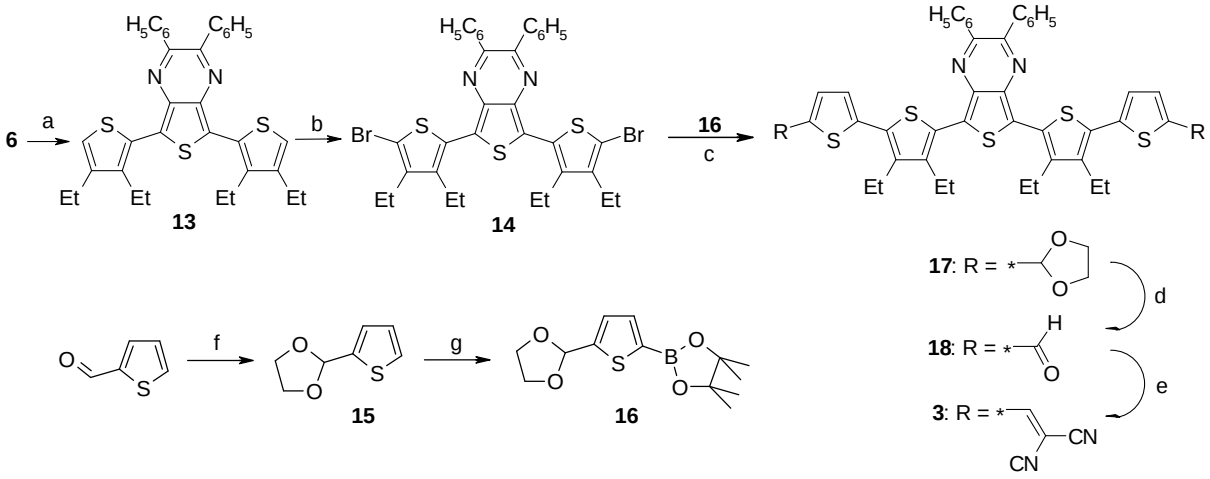

Scheme 4: a) Benzile, methanol, 60 °C, 4 h, 68%; b) NBS, acetic acid, chloroforme, 2 h, rt, 85%; c) Pd_2dba_3, $HP(^tBu)_3BF_4$, THF/Water (4:1), sodium phosphate, 100 °C, 1 h, microwave, 89%; d) p-toluenesulfonic acid, THF/water, rt, 24 h, 54%; e) Malonitrile, piperidine, 1,2-dichloroethane, rt, 4-6 h, 66%; f) p-Toluenesulfonic acid, toluene, glycol, Dean-Stark-apparatus, reflux, 3 h, 63%; g) 1. *n*BuLi, THF, -78 °C, 1 h. 2. ITDB, THF, -78 °C – rt, 1 h, 87%.

Bromination of **13** using NBS in chloroforme and acetic acid afforded trimer **14** in 85% yield. Boronic ester **16**, which is used in the next step, was prepared by protecting the carbonyl function of commercially available thiophene-2-carbaldehyde as dioxolane (**15**, 68% yield), followed by lithiation and subsequent quenching with 2-Isopropoxy-4,4,5,5-tetramethyl-1,3,2-dioxaborolane (ITDB) at -78 °C (87% yield). A Suzuki-type cross coupling reaction of **14** and boronic ester **16** gave quinquethiophene **17** in 89% yield. The aldehyde groups were de-protected, using a catalytic amount of *p*-toluenesulfonic acid in an acidic solution of THF and water, which afforded bis-aldehyde **18** in 54%. Finally, Knoevenagel condensation of pentamer **18** with malonitrile in presence of piperidine furnished title compound **3** in 66% yield.

3.3 Physical Properties

One of our aims was to investigate optical and redox properties of the obtained A-D-A-D-A-type systems, which are important parameters for the application in organic

electronics, and to deduced novel structure-property relations for the new series of compounds.

3.3.1 Steady-State Spectroscopy

Figure 2 depicts representative absorption spectra of title compounds **1**-**3** measured in a) dichloromethane and b) in solid state and Table 1 summarizes corresponding absorption properties and optical energy gaps.

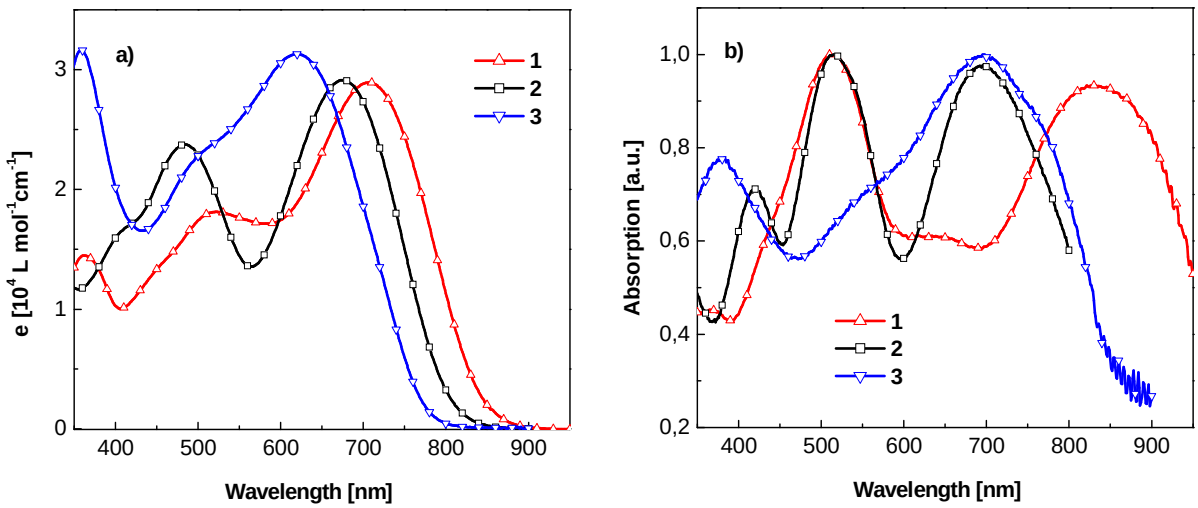

Figure 2: Representative absorption spectra of compounds **1**-**3** in a) solution and b) solid state, 30 nm thin film prepared by vacuum evaporation.

When compared to the absorption of parent compound DCV5T in solution (λ_{max} = 507 nm, ε = 51000 L mol^{-1} cm^{-1}), the insertion of a TTDA unit in **1** and **2** resulted in a strong red shift of the longest wavelength absorption band by Δλ = 201 and Δλ = 169 nm, respectively (**1**: λ_{max} = 708 nm, **2**: λ_{max} = 676 nm), while the molar extinction coefficient is lowered by a factor of nearly two (**1**: ε = 29000 L mol^{-1} cm^{-1}, **2**: ε = 30000 L mol^{-1} cm^{-1}) (Figure 2a). Thienopyrazine **3** showed a broad absorption band with its maximum at 620 nm (ε = 31000 L mol^{-1} cm^{-1}), which is 113 nm shifted to the red, when compared to DCV5T. From the onset of the absorption spectrum optical band gaps (E_g) of 1.47, 1.54 and 1.59 eV were estimated for **1**, **2** and **3**, respectively. We further observed broad multiple absorption bands between 400 to 500 nm, which are red shifted with increasing terminal acceptor strength in the order H < CHO < $COCF_3$ < DCV (Table 1). These high-energy absorption transitions can be assigned to multiple excitations arisen from a combination of the TTDA/TP chromophore and the main π-conjugated chain.

Table 1: UV-vis data of title compounds **1**-**3** and intermediates **9**-**12** in dichloromethane solution ([c] = 10^{-5} M) and solid state, 30 nm thin film prepared by vacuum evaporation.

Compound	λ_{abs} (nm)	ε [a] ($L\ mol^{-1}\ cm^{-1}$)	λ_{Onset} (nm)	E_g^{opt} (eV)	λ_{abs}^{solid} (nm)
DCV5T-TTDA (**1**)	319, 362, 458 (sh), 516, 707	29000	842	1.47	512, 830
TFA5T-TTDA (**2**)	317, 408 (sh), 483, 675	30000	805	1.54	515, 695
DCV5T-TP (**3**)	620, 512 (sh), 358	31000	780	1.59	700
5T-TTDA (**9**)	313, 391, 665	14600	815	1.52	-
Bis-aldehyde(**10**)	313, 404(sh), 446, 669	20700	815	1.52	-
Mono-aldehyde(**11**)	313, 398, 434, 667	17200	815	1.52	-
Mono-DCV (**12**)	316, 379, 515, 686	25000	835	1.49	-

[a] The molar extinction coefficient values are given for the longest wavelength absorption band.

The solid-state spectrum of **1** extends over 950 nm to the near-IR region and the second broad absorption band, at around 500 nm in the solution spectrum, appeared more strongly at 512 nm in the solid-state (Figure 2b). Thienopyrazine **3** shows in the film an absorption maximum at 700 nm with an onset extending over 850 nm. The strong bathochromic shifts in the solid state compared to the solution spectra of 123 and 80 nm on the low energy bands for **1** and **3**, respectively, could be due to strong intermolecular π-π-stacking in the film. TFA compound **2**, however, showed in solid state a longest wavelength absorption maximum at 695 nm, which is red-shifted by only 20 nm when compared to the solution spectra. This indicates a weaker stacking ability, possibly due to the non-planar terminal TFA-units. A second absorption band for **2** in the solid state is observed at 515 nm, which appears at 483 nm in the solution spectrum.

The photophysical analysis of compounds **1** and **2** in solvents of different polarity (DMF, DCM, toluene and mixtures ethanol:DCM (9:1) and n-hexane:DCM (9:1)) reveals no solvatochromic effect (Table 2). This finding demonstrates that the electronic transition at the longest wavelength absorption bands in these dyes has no charge-transfer character.

Table 2: Longest wavelength absorption maxima of TTDA-derivatives **1** and **2** in solvents of different polarity.

Compounds	EtOH:DCM (9:1)	DMF	DCM	Toluene	n-Hexane:DCM (9:1)
DCV5T-TTDA (**1**)	701	703	707	704	-
TFA5T-TTDA (**2**)	667	667	676	681	665

3.3.2 Light-induced decomposition of thienopyrazines

It has been demonstrated, that thienopyrazine-substituted compounds rapidly degrade upon exposure to UV light and air at the same time.[15] In this study, we introduced a thienopyrazine unit as an additional core acceptor group in oligothiophene **3**. Phenyl substituents were attached at the 2- and 3-position of the thienopyrazine moiety as sterical units in order to improve light and air stability. Figure 3 depicts the UV-vis absorption spectra of compound **3** in DCM solution and as thin film over time, when exposed to air and light.

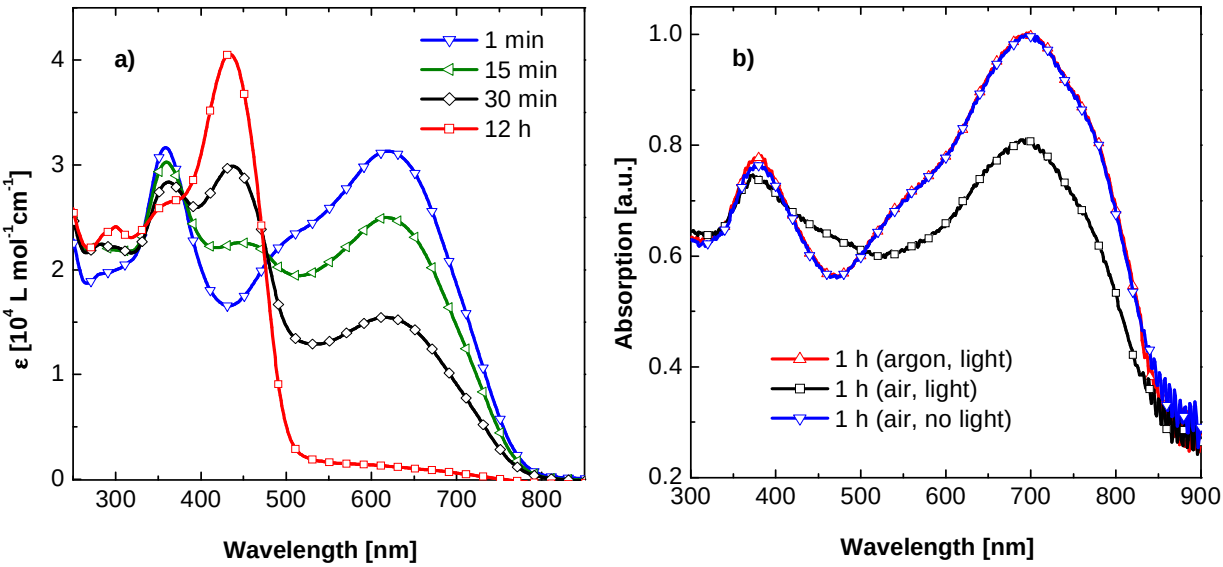

Figure 3: Absorption spectra of compounds **1**-**3** in a) solution (DCM) and b) solid state, 10 nm thin film prepared by vacuum deposition.

When exposed to sun light under ambient atmosphere, the longest wavelength absorption of **3** in dichloromethane solution rapidly decreased, while a new absorption maximum appeared at 420 nm. After 12 hours of irradiation the original band at 620 nm completely disappeared in favour of the new main absorption band at 420 nm. In the solid state and in the absence of oxygen, no change in absorption was found after one hour of sun light irradiation. After exposure to ambient atmosphere, degradation was observed, yet in a significantly lower rate than in solution. In addition, the change in absorption in the solid state is only observed by a slight decrease of the longest wavelength absorption without appearance of any new band. In comparison to a previously reported analogous compound,[38] in which the phenyl rings are replaced with methyl groups, a dramatic increase of stability is found, confirming the expected sterical influence of the bulky phenyl rings.

The photodegradation mechanism was derived on the basis of MALDI-TOF mass spectral analysis (Figure 4). We assume that in the first step, singlet oxygen plays an important role in

the photodegradation process of the compound, probably via a [2+4] cycloaddition to the TP moiety (Scheme 5).

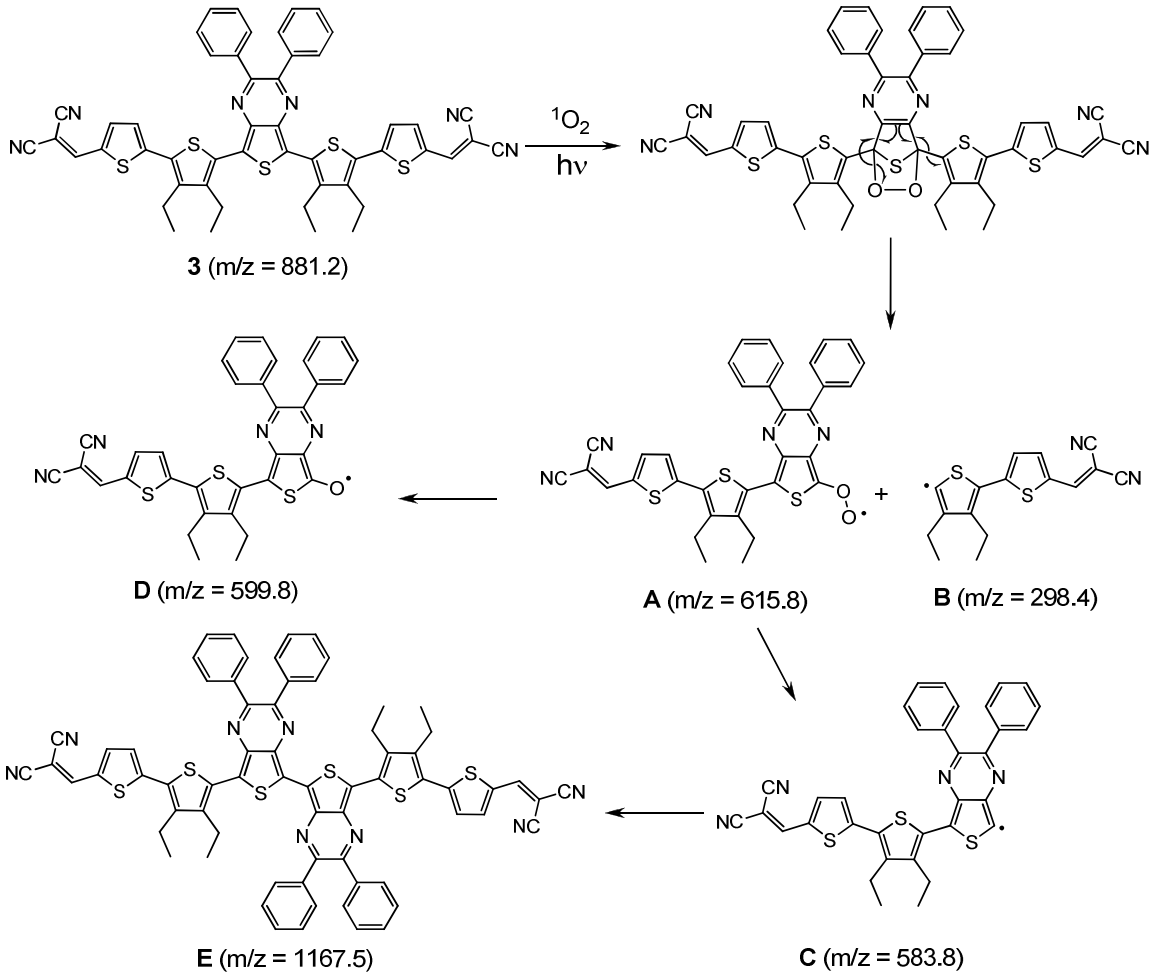

Scheme 5: Proposed photodegradation mechanism for TP **3** based on MALDI-TOF measurements.

The bound oxygen should react further in a radical pathway, leading to a C-C bond cleavage between the TP moiety and the adjacent thiophene ring (Fragment **A** and **B**). The mass peak of **A** was not observed, probably due to its further fragmentation to either species **D** (m/z = 599.8) or **C** (m/z = 583.8). Radical dimerization of intermediate **C** gave a mass peak at m/z 1167.7, which is the diagnostic peak for the dimerized product **E**. A similar photodegradation mechanism was earlier proposed for bengal rose-induced photodegradation of lignin in the presence of singlet oxygen.[39]

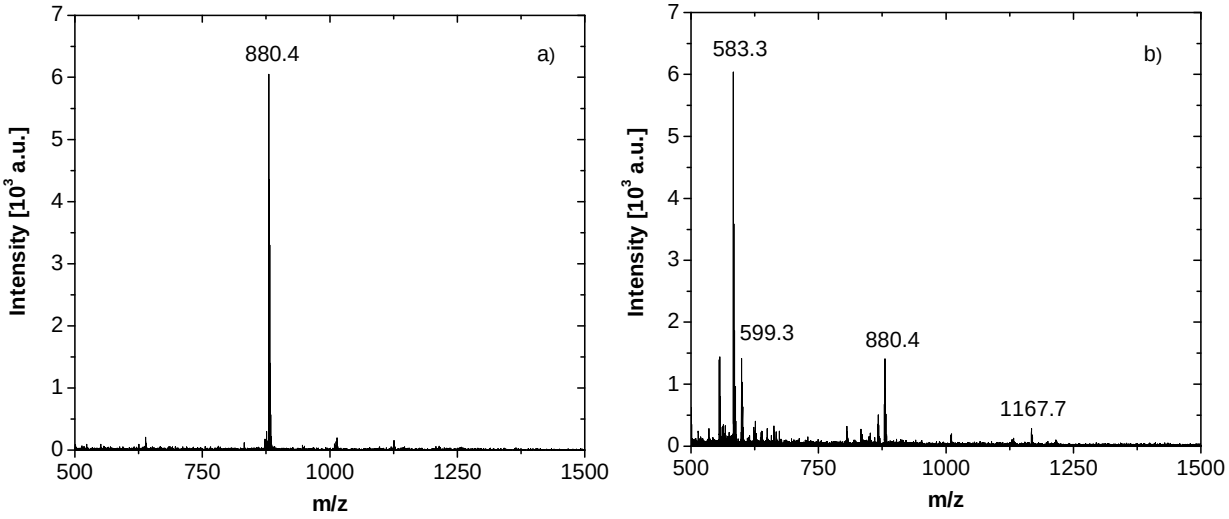

Figure 4: MALDI-TOF spectra of TP **3** a) before and b) after decomposition by light and oxygen.

3.3.3 Theoretical calculations

We investigated the influence of the TTDA/TP-unit on the π-system and the nature of the electronic transitions by theoretical calculations of the compounds at a semiempirical level (Austin Model 1). The most stable conformation for all compounds shows an all-trans arrangement of the aromatic units with small torsion angles (< 170°). The small BLA along the main chain further confirms the less aromatic character (quinoid-type character) of these oligomers compared to the linear quinquithiophene. The analysis of the calculated electronic spectra shows no charge-transfer character on the low energy transition and is in good agreement with the experimentally verified absence of solvatochromism for TTDA.

Figure 5 depicts the distribution of the frontier molecular orbitals (HOMO and LUMO) of DCV5T and title compounds **1**-**3**. For DCV5T, both HOMO and LUMO are distributed over the entire molecule. In TTDA compounds **1** and **2**, the HOMO expands over almost the entire molecule, whereas the LUMO is localized mostly on the three central rings around the TTDA acceptor unit. Analyzing these frontier orbitals in more detail, a very low (in the HOMO) and even no-overlap (in the LUMO) of the isosurfaces at the TTDA units can be recognized (Figure 5, red circles). In TP-based compound **3**, we found a homogenous distribution of both, HOMO and LUMO, over the entire conjugated backbone with a slight concentration of electron density of the LUMO on the core acceptor moiety. The phenyl rings attached to the pyrazine are strongly twisted out of plane, hence, do not contribute to the molecular orbital distribution, which is in agreement with reported systems.[40] In conclusion, although the

delocalization of the exciton can be favored by the decrease in the BLA in **1**-**3**, the central TTDA/TP unit localizes the highest electron density in the excited state, presumably acting as a trap for the exciton. This could be an indication for the moderate device performances.

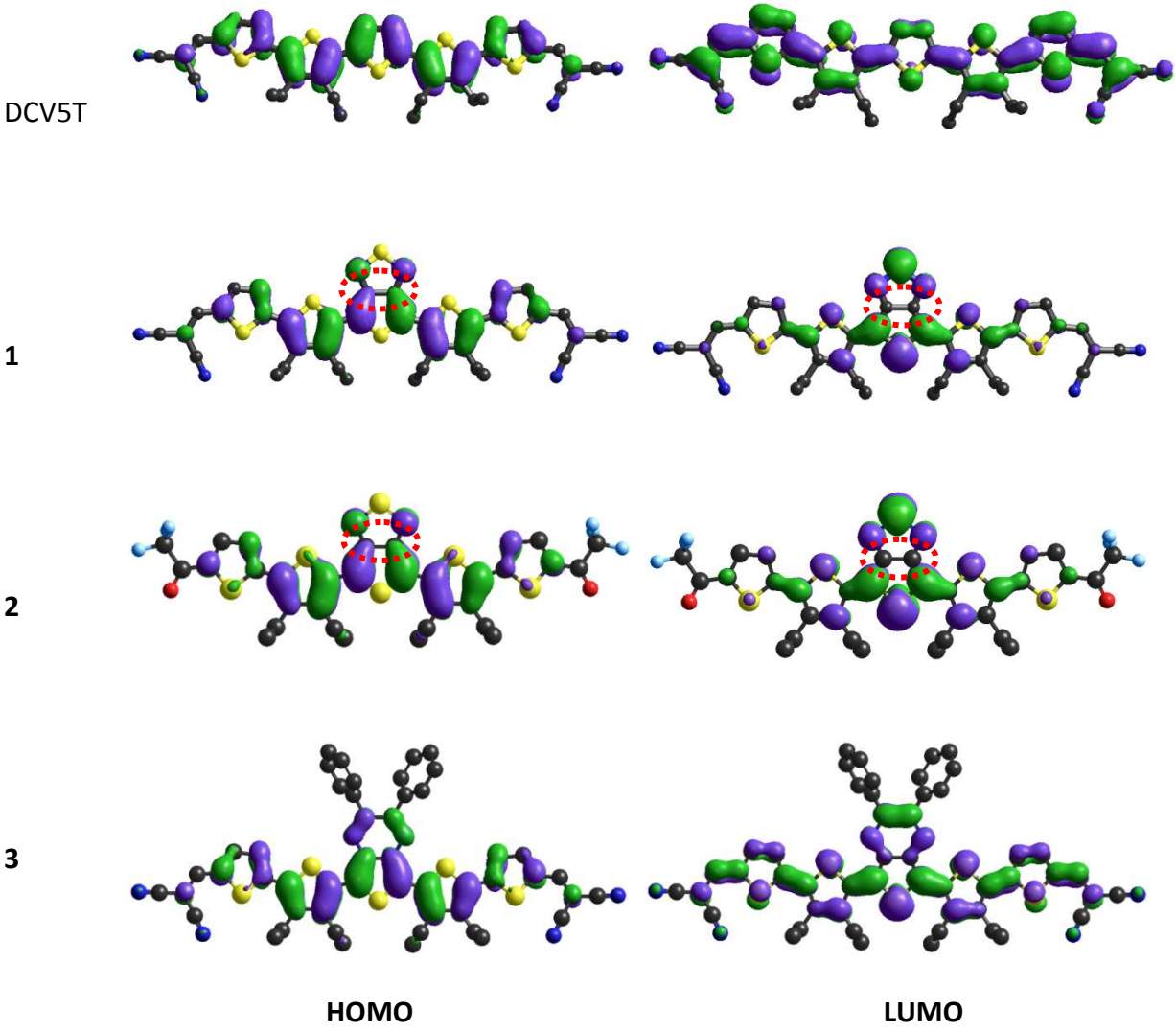

Figure 5: Electron density distribution of the frontier orbitals in derivatives **1**-**3** and DCV5T obtained from semi-empirical AM1 calculations (carbon atoms in black, fluorine in light blue, nitrogen in blue, oxygen in red, sulfur in yellow and hydrogen atoms are omitted for clarity reasons).

3.3.4 Electrochemical studies

Figure 6 depicts cyclic voltammograms of compounds **1**-**3**, measured in dichloromethane solution, and Table 3 summarizes the corresponding electrochemical data. The investigated compounds showed each two fully reversible $1e^-$ oxidation waves, which can be assigned to the oligothiophene backbone. At the anodic potential, we observed one $2e^-$ reversible wave corresponding to the TTDA and TP unit and one $1e^-$ quasi-reversible reduction wave for the

DCV and TFA groups, respectively. These results indicate the formation of stable radical anions and cations.

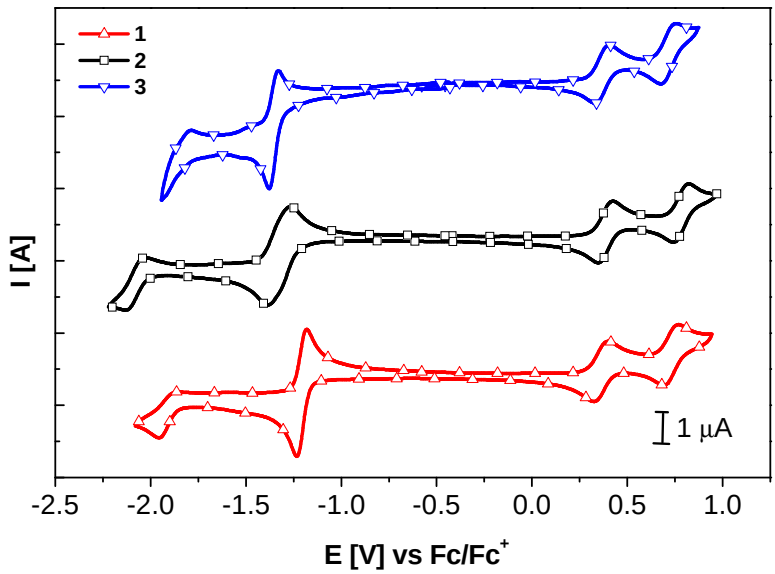

Figure 6: Representative cyclic voltammograms of TTDA-based compounds **1** and **2** and thienopyrazine **3** (1×10^{-3} mol·L^{-1}) in dichloromethane-$TBAPF_6$ (0.1M), scan speed 100 mV/s, potentials *vs.* Fc/Fc^+.

The HOMO and LUMO energy levels of the investigated compounds were calculated from the onset of the first oxidation and reduction wave using the standard approximation that the Fc/Fc^+ HOMO level is -5.1 eV vs. vacuum (Table 3).

Table 3: Summarized cyclovoltammetry data of title compounds **1**-**3** (DCM, HOMO/LUMO vs. Fc/Fc^+_{vac} = 5.1 eV).

Compound	$E°_{ox1}$ (V)	$E°_{ox2}$ (V)	$E°_{red1}$ (V)	$E°_{red2}$ (V)	HOMO (eV)	LUMO (eV)	ΔE^{CV} (eV)
DCV5T-TTDA (**1**)	0.35	0.73	-1.21	-1.91	-5.39	-3.94	1.45
TFA5T-TTDA (**2**)	0.39	0.78	-1.33	-2.08	-5.41	-3.88	1.53
DCV5T-TP (**3**)	0.36	0.71	-1.36	-1.86	-5.36	-3.83	1.53
5T-TTDA (**9**)	0.23	0.56	-1.35	-	-5.24	-3.84	1.40
Bis-aldehyde(**10**)	0.32	0.69	-1.37	-1.66	-5.34	-3.83	1.51
Mono-aldehyde(**11**)	0.24	0.58	-1.43	-1.82	-5.26	-3.80	1.46
Mono-DCV (**12**)	0.26	0.61	-1.33	-1.47	-5.28	-3.84	1.44

The low band gap materials **1**-**3** studied here showed strong positive shifts of the reduction potentials and consequently lower LUMO energy levels compared to those of DCV5T demonstrating that the TTDA/TP units behave as strong electron acceptors. It has been reported that upon attachment of electron-withdrawing moieties at the terminal α-positions of linear π-conjugated chains, the relative HOMO and LUMO energies shift toward lower energy values with respect to the unsubstituted system. The LUMOs are more affected than the HOMOs and

thus the band gaps are lowered.[41-42] However, the determined orbital energies for **1**-**3** revealed a different trend. The insertion of *o*-quinoidal TTDA/TP units in the core of an oligomer stabilizes the LUMO, but destabilizes the HOMO energy at the same time, thus reducing the band gap to a large extent relative to DCV5T (Figure 7).

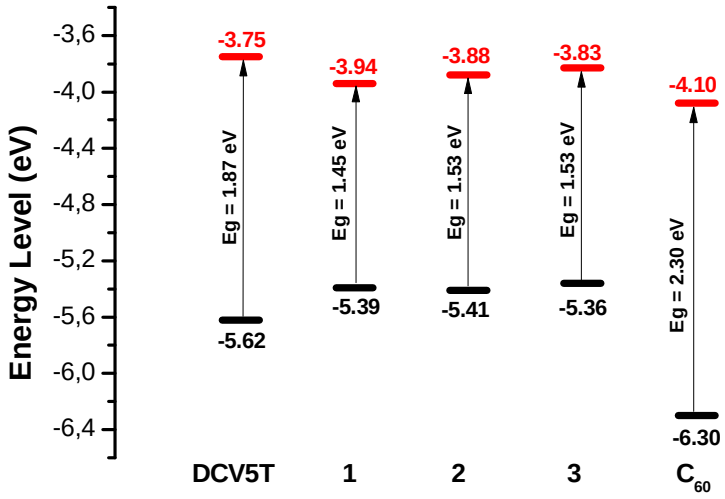

Figure 7: HOMO-LUMO energy levels of the investigated oligomers **1**-**3** deduced from electrochemical data and compared to C_{60}.

For the TTDA-series we found, both, LUMO energy level (calculated from cyclic voltammetry measurements) and molar extinction coefficient, depend on the terminal substituents (H, OHC, DCV, TFA) of the compounds (Figure 8).

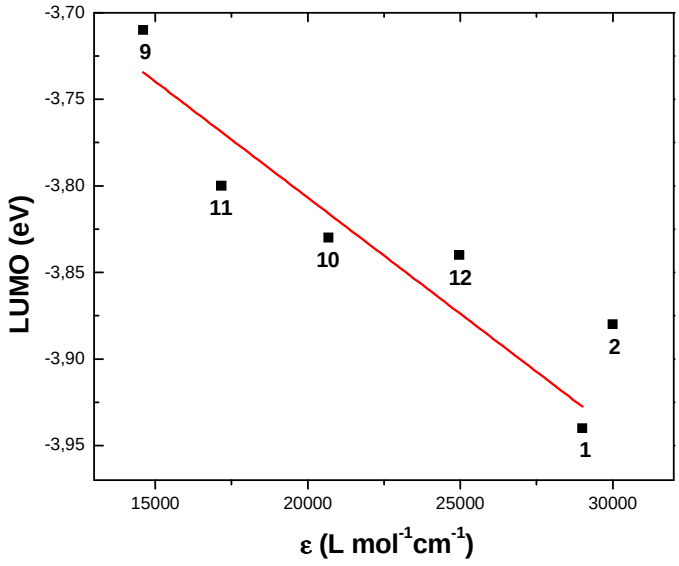

Figure 8: Correlation between LUMO level and extinction coefficient at the longest wavelength absorption band of TTDA-based compounds. The red line indicates the linear fit excluding compound **2** (R^2 = 0.89).

The stronger the electron-withdrawing force of the acceptor in the α-position of the pentamer, the larger the bathochromic shift of the longest wavelength absorption band and the higher the extinction coefficient of the compound, except for TFA-derivative **2**, which has a weaker terminal acceptor than bis-DCV **1**.

3.3.5 Thermal properties

The thermal stability of organic materials is one of the important parameter for device fabrication. Therefore, thermal properties of **1**-**3** were determined by differential scanning calorimetry (DSC) and thermogravimetric analysis (TGA) under an inert atmosphere at heating rate of 10 ^{o}C min^{-1} as depicted in Figure 9. The TGA analysis reveals that the onset temperatures with 5% weight-loss (T_d) of **1**, **2** and **3** are 312, 324 and 365 °C, respectively. This result indicates that the thermal stability of the oligomers could be critical for the vacuum-processing during device fabrication. DCV-substituted TTDA-derivative **1** showed a low sublimation yield (~20%), since during the sublimation process most of the material was decomposed. To overcome this thermal instability, the DCV groups were replaced with TFA units in TTDA-pentamer **2** to lower the sublimation temperature and hence reduce the thermal decomposition.[43]

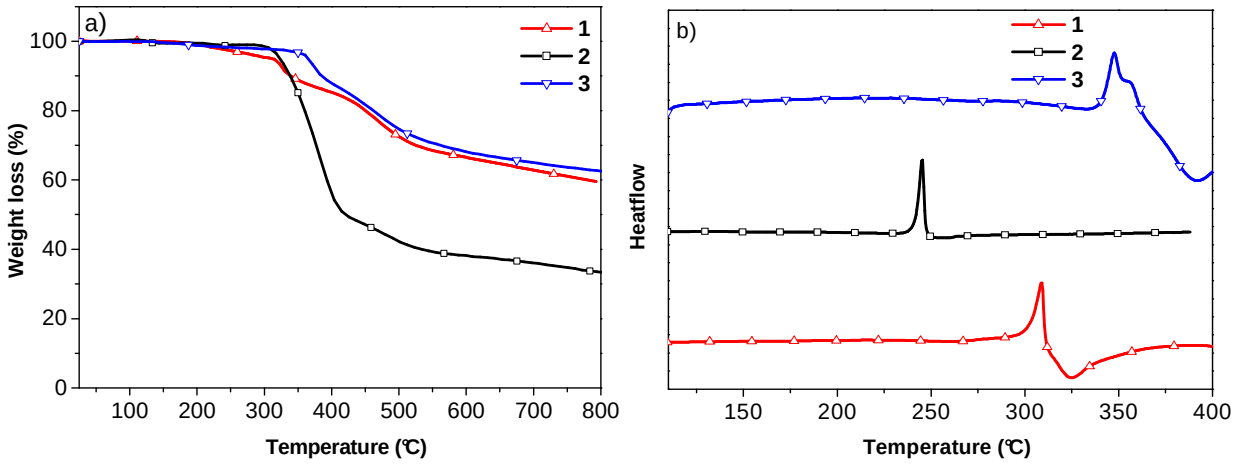

Figure 9: a) TGA thermograms of oligomers **1**-**3** measured under N_2. Conditions: N_2 flow, 50 mL/min; heating rate, 10 ^{o}C/min. b) DSC trace of all derivatives measured under Ar flow at heating rate of 10 ^{o}C/min.

The melting temperaures (T_m) of **1**-**3** determined by DSC were 306, 237 and 341 °C, respectively. In DSC, DCV-oligomers **1** and **3** showed a strong exothermic peak immediately after melting, while no such behavior was observed for TFA derivative **2**. NMR analysis of **1**

after melting showed that the compound reacted in the melt and we suspect, that the TTDA group undergoes an intermolecular Diels-Alder reaction with the DCV groups as reported in literature.[33, 44-46] This behavior was not observed for TFA derivative **2**.

3.4 Photovoltaic Performance

Figure 10 shows the current density-voltage (*J*-*V*) characteristics of planar heterojunction (PHJ) solar cells comprising the cell structure: ITO/C_{60} (15 nm)/**1**-**3**/Di-NPB (5 nm)/ Di-NPB:NDP (40 nm 5wt%)/p-ZnPc (10 nm 2.7wt%)/Au (50 nm). The corresponding solar cell data are summarized in Table 4.

Table 4: Characteristic solar cell data of m-i-p-type heterojunction solar cells of title compounds **1**-**3**.

Compound	V_{OC} (mV)	J_{SC} (mA cm^{-2})	*FF*	η (%)
1 (6 nm)	0.70	2.76	0.43	0.83
2 (6 nm)	0.77	2.89	0.48	1.08
2 (10 nm)	0.78	2.65	0.44	0.91
3 (6 nm)	0.66	2.86	0.58	1.09

With DCV-compound **1** as donor, we observed an open circuit voltage (V_{OC}) of 0.7 V, a shortcut current density (J_{SC}) of 2.76 mA cm^{-2}, a fill factor value of 0.43, and hence an efficiency of 0.83%. Devices based on TFA **2** as donor showed a fill factor value (*FF*) of 0.48, an open circuit voltage (V_{OC}) of 0.77 V and a shortcut current density (J_{SC}) of 2.89 mA cm^{-2}, resulting in a power conversion efficiency (η) of 1.08%. Increasing the photoactive layer thickness to 10 nm mainly resulted in a lowered shortcut current density (J_{SC}) of 2.65 mA cm^{-2}, leading to a lowered overall efficiency of 0.91%. A photovoltaic cell with TP **3** as donor gave an open circuit voltage (V_{OC}) of 0.66 V, a shortcut current density (J_{SC}) of 2.86 mA cm^{-2} and a fill factor (*FF*) of 0.58, resulting in an overall efficiency of 1.09%.

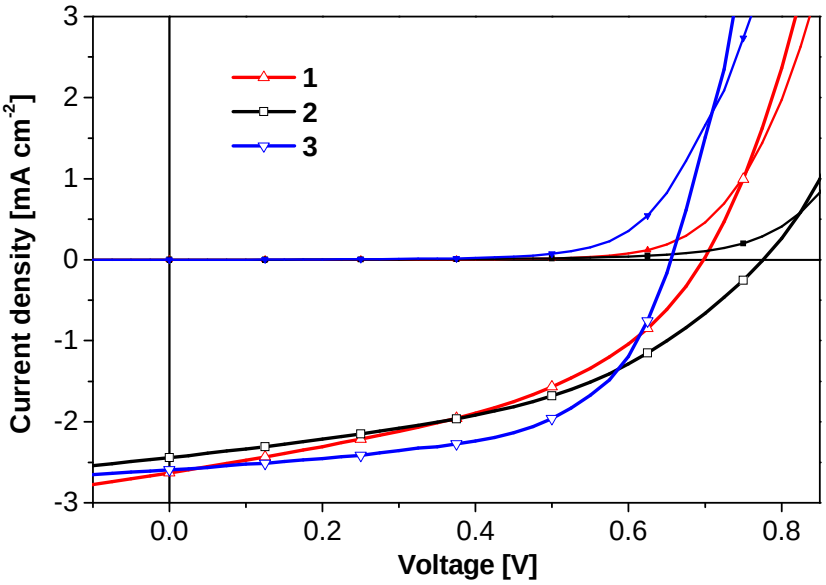

Figure 10: *J-V* characteristics of PHJ solar cells using oligothiophenes **1**-**3** as donors under AM 1.5G white light illumination at 100 mW cm^{-2}.

Thus, all compounds showed moderate short-circuit current density (J_{SC}) values between 2.6-2.9 mA cm^{-2}. This could be ascribed to the lack of transport of the photo-generated electrons and holes at the D-A interface, resulting in significant recombination and low values of J_{SC} and *FF* (0.43-0.58). All the studied materials displayed as well moderate V_{oc} values in the range of 0.66 to 0.77 V, which is due to the fact that V_{OC} is limited by the difference between the HOMO energy level of the donor and the LUMO energy level of the acceptor[47-48] restricting the overall device efficiency (η), which were determined to 0.8, 1.1 and 1.1% for oligomers **1**-**3**, respectively. To ensure an efficient charge separation, it has been suggested a minimum LUMO(D)–LUMO(A) offset of about 0.3–0.4 eV is necessary.[48] The difference between the LUMO of these oligomers and the LUMO of C_{60} is only about 0.27-0.16 eV, which indeed appears to be insufficient for efficient electron transfer at the donor/acceptor interface from the excited state of these low band gap oligomers. Therefore, only a small fraction of the absorbed photons could be dissociated into charge carriers that can reach the electrodes under influence of the internal electric field.

Conclusions: Novel conjugated A-D-A-D-A-type oligothiophenes were synthesized up to the pentamer with thienothiadiazole or thienopyrazine as core and dicyanovenylene or trifluoroacetyl as end-capping acceptor moieties. The obtained materials showed strong absorption down to the near IR-region with narrow band gaps down to 1.2 eV in thin films.

The red-shifted absorption bands of these compounds is ascribed to the influence of the various acceptor units on the π-conjugation and is not a charge-transfer band. Substitution of dicyanovinyl units with electron withdrawing trifluoroacetyl groups resulted in highly stable compounds, hence thermal decomposition while processing the materials by vacuum technique was reduced. Photovoltaic devices based on the new materials as donor with fullerene C_{60} as acceptor in m-i-p-type solar cells showed efficiencies as high as 1.1%. A low fill factor value of the assembled photovoltaic cells indicates, that thienothiadiazole and thienopyrazine may act as a hole trap, resulting possibly in a reduced charge carrier mobility.

3.5 Experimental Section

General remarks:

NMR spectra were recorded on a *Bruker AMX 500* (^{1}H NMR: 500 MHz, ^{13}C NMR: 125 MHz) or an *Avance 400* spectrometer (^{1}H NMR: 400 MHz, ^{13}C NMR: 100 MHz), unless mentioned otherwise at 25 °C. Chemical shift values (δ) are expressed in parts per million using residual solvent protons (^{1}H NMR, δ_H = 7.26 for $CDCl_3$, δ_H = 5.32 for $[D_2]$DCM, δ_H = 5.91 for $[D_2]$TCE and δ_H = 3.57 for $[D_8]$THF; ^{13}C NMR, δ_C = 77.0 for $CDCl_3$, δ_C = 53.8 for $[D_2]$DCM, δ_C = 74.2 for $[D_2]$TCE and δ_C = 67.2 for $[D_8]$THF) as internal standard. The splitting patterns are designated as follows: s (singulet), d (doublet), t (triplet) and m (multiplet). The assignments are Ar-H (H-atoms of aromatic systems) and Th-H (H-atoms of thiophene rings). Melting points were determined using a *Büchi B-545* apparatus and were not corrected. Elemental analyses were performed on an *Elementar Vario EL* (University of Ulm) and a *Carlo Erba 1104* (University of Stuttgart). Thin layer chromatography was carried out on aluminum plates, pre-coated with silica gel, *Merck Si60* F_{254}. Preparative column chromatography was performed on glass columns packed with silica gel, *Merck Silica 60*, particle size 40 − 43 µm. CI and EI mass spectra were recorded on a *Finnigan MAT SSQ-7000* or a *Varian Saturn 2000* GC-MS, MALDI-TOF on a *Bruker Daltonics Reflex III*. UV/Vis absorption spectra were recorded in 1 cm cuvettes with *Merck* Uvasol grade solvents on a *Perkin Elmer Lambda 19* spectrometer. Cyclic voltammetry experiments were performed with a computer-controlled *EG&G PAR 273* potentiostat in a three-electrode single-compartment cell with a platinum working electrode, a platinum wire counter electrode, and an Ag/AgCl reference electrode. All potentials were internally referenced to the ferrocene / ferrocenium couple. Tetrahydrofurane (*Merck*) was dried under

reflux over sodium/benzophenone (*Merck*) and dichloromethane (*Merck*) over calcium hydride (*Merck*). All synthetic steps were carried out under argon atmosphere. *N*-Bromo succinimide (NBS), NaOH and K_2CO_3 were purchased from *Merck*, $Pd(PPh_3)_2Cl_2$, trifurylphosphine (TFP) and *n*BuLi (1.6 mol/L in hexane) from *Acro*s, tri-*n*-butyltin chloride and tri-*n*-methyltin chloride from *Aldrich*.

Vacuum-processed solar cells: N,N′-di(naphthalen-1-yl)-N,N′-diphenyl-benzidine (Di-NPB) and zinc phthalocyanine (ZnPc), doped with proprietary compounds NDP2 or NDP9 of *Novaled GmbH* (Dresden) were used as p-doped hole transport layers. Doping concentrations of Di-NPB and ZnPc were 2-5 wt%. C_{60} and ZnPc have been provided by *Alfa Aesar* and Di-NPB by *Sensient Imaging Technologies*. Except the oligothiophenes, all materials were cleaned at least twice by thermal gradient sublimation before evaporation. The organic layers and metal contacts were thermally deposited in an ultra high vacuum system ("UFO", *Bestec GmbH*) at 10^{-8} to 10^{-7} mbar through shadow masks onto semitransparent indium tin oxide (ITO) coated glass substrates (*Thin Film Devices Inc.*, sheet resistance < 30 Ω / sq) without breaking the vacuum. Ceramic or graphite crucibles were used as sublimation sources (*Creaphys GmbH*, Reinhardtsgrimma), temperatures were set by a *Eurotherm* controller and film thicknesses were determined by quartz crystal monitors (*Leybold Inficon Inc.*). Substrates were cleaned using detergent, acetone, and ethanol. The active area of the cells had an average size of 4-7 mm^2. *J-V* characteristics were measured using a Source Measurement Unit 236 SMU (*Keithley*) in an N_2-filled glovebox without exposing the samples to air. Illumination was provided by a sun simulator SOL 1200 (*Hoehnle*) with an intensity of 127 mW cm^{-2}, which was calibrated using an outdoor reference cell provided by the *Fraunhofer Institute for Solar Energy Systems* (Freiburg). External quantum efficiency (EQE) spectra were recorded using a homemade setup based on a xenon lamp (*ILC-Technologies*) and a grating monochromator. Calibration was done using a *Newport Corporation* powermeter or a *Hamamatsu Photonics* photo diode. Organic films for spectral analysis were vapor deposited onto quartz substrates under ultra high vacuum with deposition rates of about 0.1 Å s^{-1}. A commercial *Shimadzu* UV-2101/3101 spectrophotometer was used for absorption measurements. Luminescence spectra were recorded using a *Spex* FluoroMAX with separated monochromators for excitation and luminescence light.

Synthesis:

3,4:3'',4''-Tetraethyl-3'4'-dinitro-2,2':5'2''-terthiophene (**5**). To a solution of 2,5-dibromo-3,4-dinitrothiophene (10.0 g, 30.2 mmol) in absolute THF (200 mL) under argon atmosphere were added tributyl-(3,4-diethyl-thien-2-yl)-stannane (**4**) (31.0 g, 72.2 mmol) and $Pd(Ph_3)_4$ (346 mg, 0.30 mmol). After refluxing for 3 h, a second portion of catalyst (346 mg) was added and the reaction mixture was refluxed for another 19 h. The solvent was evaporated to a large extend and the raw product was precipitated by addition of n-hexane. Subsequent recrystallization from ethanol, followed by column chromatography (SiO_2, petroleum ether/dichloromethane = 3 : 2 v/v, R_f = 0.25) afforded **5** (11.08 g, 24.6 mmol) in 81.4 % yield as yellow crystals. **M.p.:** 100–101°C. **^{1}H NMR** ($CDCl_3$, TMS, 400 MHz): δ [ppm] = 7.17 (s, 2H, Th-H), 2.61 (q, ^3J = 7.5 Hz, 4H, CH_2), 2.60 (q, ^3J = 7.5 Hz, 4H, CH_2), 1.31 (t, ^3J = 7.5 Hz, 6H, CH_3), 1.11 (t, ^3J = 7.5 Hz, 6H, CH_3). **^{13}C NMR** ($CDCl_3$, δ ppm) 146.0, 144.5, 138.5, 135.2, 123.7, 120.5, 22.1, 21.1, 14.6, 13.6. **MS** (CI): m/z = 450 (M^+, 40 %); 451 (M^+ + H, 60 %). **Elemental analysis:** $C_{20}H_{22}N_2O_4S_3$: calc. C, 53.31; H, 4.92; N, 6.22%; found C, 53.25; H, 4.89; N, 6.23%.

3,4,3'',4''-Tetraethyl-3'4'-diamino-2,2':5'2''-terthiophene (**6**). To a suspension of grinded 3,4:3'',4''-tetraethyl-3'4'-dinitro-2,2':5'2''-terthiophene **5** (0.90 g, 2.0 mmol) in ethanol (16 ml) under argon atmosphere were added Pd/C (0.45 g, 10% Pd by weight) and hydrazine monohydrate (10.0 g, 200 mmol). After stirring for 2 h, the Pd/C catalyst was removed by filtration through a celite pad and washed with dichloromethane (*caution: dry catalyst is pyrophorous*). The organic phase was washed with aqueous ammonium chloride, saturated aqueous sodium bicarbonate solution and water. The organic phase was then dried ($MgSO_4$), filtered, concentrated by rotary evaporator. The crude product was column chromatograph (SiO_2, n-hexane / THF = 2 : 1 v/v; R_f = 0.37) to yield **6** (691 mg, 1.77 mmol, 88.4%) as a slightly brownish viscous liquid which was pure enough to use without further purification. **^{1}H NMR** ($CDCl_3$, δ ppm) 6.98 (s, 2H, Th-H), 3.47 (broad s, 4H, NH_2), 2.61 (q, ^3J = 7.5 Hz, 4H, CH_2), 2.60 (q, ^3J = 7.5 Hz, 4H, CH_2), 1.30 (t, ^3J = 7.5 Hz, 6H, CH_3), 1.10 (t, ^3J = 7.5 Hz, 6H, CH_3). **^{13}C NMR** ($CDCl_3$, δ ppm) 144.3, 144.5, 142.8, 134.5, 128.0, 120.0, 109.4, 22.3, 20.8, 15.0, 13.7. **MS**(CI): m/z = 390 (M^+, 55 %); 391 (M^+ + H, 100 %). **Elemental analysis:** $C_{20}H_{26}N_2S_3$: calc. C, 61.50; H, 6.71; N, 7.17%; found C, 61.60; H, 6.74; N, 7.06%.

4,6-Di-(3,4-diethyl-thien-2-yl)-thieno[3,4-c][1,2,5]thiadiazole (**7**). To a stirred solution of 3,4:3'',4''-tetraethyl-3'4'-diamino-2,2':5'2''-terthiophene **6** (1.53 g, 3.92 mmol) in dry pyridine (22 ml) under argon atmosphere was added freshly distillated N-thionylaniline (1.09 g, 7.84 mmol, b.p. 77 °C/15 mbar) via syringe. Then, trimethylsilyl chloride (2.98 g, 27.4 mmol) was added, resulting in a dark blue color. After 2 h stirring at ambient temperature, dichloromethane (250 ml) was added and the solution was washed with 1N hydrochloric acid (2 × 150 ml) and with water. The organic phase was dried over $MgSO_4$ and then the solvent was removed under vacuum yielding the crude product. The excess of N-thionylaniline was removed by extraction with *n*-hexane (100 ml). The solid product was filtered and recrystallized from n-hexane (300 ml) to give **6** (1.14 g, 2.73 mmol,) in a yield of 69.5 % as dark blue colored crystal. **M.p.:** 115°C. **TLC:** R_f = 0.53 (n-hexane/THF = 2 : 1 v/v), R_f = 0.74 (dichloromethane/petroleum ether = 2 : 1). **^{1}H NMR** ($CDCl_3$, δ ppm) 7.07 (s, 2H, Th-H), 2.92 (q, ^3J = 7.5 Hz, 4H, CH_2), 2.64 (q, ^3J = 7.5 Hz, 4H, CH_2), 1.32 (t, ^3J = 7.5 Hz, 6H, CH_3), 1.26 (t, ^3J = 7.5 Hz, 6H, CH_3). **^{13}C NMR** ($CDCl_3$, δ ppm) 156.7, 144.8, 140.4, 128.9, 121.0, 112.9, 22.1, 21.3, 14.0, 13.8. **MS** (CI): m/z = 418 (M^+, 51%); 419 (M^+ + H, 100%). **Elemental analysis:** $C_{20}H_{22}N_2S_4$: calc. C, 57.38; H, 5.30; N, 6.69%; found C, 57.43; H, 5.34; N, 6.72%.

4,6-Bis(5-bromo-3,4-diethylthien-2-yl)-thieno[3,4-c][1,2,5]thiadiazole (**8**). To a solution of terthiophene **5** (654 mg, 1.56 mmol) in DMF (49 ml) was added dropwise a solution of NBS (612 mg, 3.44 mmol) in DMF (33 ml) at 0 °C. The cooling bath was removed and the solution was kept stirring at room temperature until completion of the reaction. The reaction was controlled by TLC using dichloromethane:*n*-hexane (1:1) as eluent. After 5 h stirring, the mixture was dissolved in dichloromethane (150 ml) and washed with water (3 × 200 ml). The organic phase was dried over sodium sulfate and the solvent was removed by vacuum. The product was purified by column chromatography (SiO_2, dichloromethane 1:1 n-hexane) to obtained **8** (818 mg, 1.42 mmol) as deep blue crystals in a yield of 92%. **M.p.:** 130.5-132 °C. **^{1}H NMR** ($CDCl_3$, δ ppm) 2.93 (q, ^3J = 7.6 Hz, 4H, CH_2), 2.65 (q, ^3J = 7.6 Hz, 4H, CH_2), 1.27 (t, ^3J = 7.5 Hz, 6H, CH_3), 1.20 (t, ^3J = 7.5 Hz, 6H, CH_3). **^{13}C NMR** ($CDCl_3$, δ ppm) 156.6, 143.6, 143.2, 140.8, 139.9, 129.2, 22.3, 21.8, 14.3, 14.2. **MS** (CI): *m/z* 573.7 $[M]^+$ (calc. for $C_{20}H_{20}Br_2N_2S_4$: 573.9). **Elemental analysis:** $C_{20}H_{20}Br_2N_2S_4$: calc. C, 41.67; H, 3.50; N, 4.86%; found: C, 41.86; H, 3.62; N, 4.84%.

4,6-Bis(3,4-diethyl-2,2'-bithien-5-yl)-thieno[3,4-c][1,2,5]thiadiazole (**9**). Dibromo-terthiophene **8** (817 mg, 1.42 mmol), tri-2-furylphosphine (131.6 mg, 0.57 mmol) and $Pd_2(dba)_3 \bullet CHCl_3$ (73.35 mg, 0.07 mmol) were dissolved in freshly dried THF (140 ml). After stirring at room temperature for 20 min, 2-(tributylstannyl)-thiophene (1.85 g, 4.96 mmol) was added and the mixture heated up to 60 °C. Stirring was continued at this temperature for two days. After cooling, aqueous ammonium chloride solution was added and the mixture was extracted with dichloromethane (300 ml). The organic phase was dried over sodium sulfate and the solvent was removed under reduced pressure. The product was purified by column chromatography (SiO_2, DCM:*n*-hexane (1:1)) to obtain **9** (654 mg, 1.12 mmol) in 79% as deep green powder. **M.p.:** 196 °C. **^{1}H NMR** ($CDCl_3$, δ ppm) 7.36-7.34 (dd, *J* = 5.1 Hz, *J* = 1.2 Hz, 2H, Th-H^{β}), 7.25-7.24 (dd, *J* = 3.6 Hz, *J* = 1.1 Hz, 2H, Th-H^{β}), 7.11-7.08 (dd, *J* = 5.1 Hz, *J* = 3.6 Hz, 2H, Th-H^{α}), 3.00 (q, ^3J = 7.5 Hz, 4H, CH_2), 2.83 (q, ^3J = 7.5 Hz, 4H, CH_2), 1.33 (t, ^3J = 7.5 Hz, 6H, CH_3) , 1.27 (t, ^3J = 7.5 Hz, 6H, CH_3). **^{13}C NMR** ($CDCl_3$, δ ppm) 141.5, 141.2, 135.9, 132.5, 130.2, 128.3, 127.5, 126.6, 126.1, 125.6, 99.9, 21.9, 15.3, 14.2. **MS** (MALDI): *m/z* 581.9 $[M]^+$ (calc. for $C_{28}H_{26}N_2S_6$: 582.0). **Elemental analysis:** $C_{28}H_{26}N_2S_6$: calc. C, 57.69; H, 4.50; N, 4.81%; found: C, 57.86; H, 4.69; N, 4.63%.

5',5''-(Thieno[3,4-c][1,2,5]thiadiazole-4,6-diyl)bis(3',4'-diethyl-2,2'-bithiophene-5-carbaldehyde) (**10**). Phosphoryl chloride (0.78 ml, 8.50 mmol) and dimethylformamide (0.66 ml, 8.50 mmol) were dissolved in 1,2-dichloroethane (8.5 ml) and stirred at room temperature for two hours. Quinquethiophene **9** (110 mg, 0.19 mmol) was dissolved in 1,2-dichloroethane (6 ml) and the formed Vilsmeier-reagent was added. The mixture was stirred under reflux (110-120 °C) for 4 h. After cooling, dichloromethane (80 ml) and aqueous solution of sodium hydrogen carbonate (240 ml) were added. Stirring was continued overnight at room temperature. The organic phase was washed several times with water, dried over sodium sulfate, filtered, and evaporated. Column chromatography with dichloromethane and ethyl acetate (9:1) as mobile phase afforded compound **10** (40 mg, 0.06 mmol) in a yield of 33%. The corresponding monoaldehyde was also isolated in a yield of 12%. **M.p.:** 251 °C. **^{1}H NMR** ($CDCl_3$, δ ppm) 9.91 (s, 2H, OHC), 7.74 (d, ^3J = 4.0 Hz, 2H, ThH), 7.37 (d, ^3J = 4.0 Hz, 2H, ThH), 3.03 (q, ^3J = 7.5 Hz, 4H, CH_2), 2.91 (q, ^3J = 7.5 Hz, 4H, CH_2), 1.35 (t, ^3J = 7.5 Hz, 6H, CH_3), 1.31 (t, ^3J = 7.5 Hz, 6H, CH_3). **^{13}C NMR** ($CDCl_3$, δ ppm) 206.5, 159.9, 157.1, 145.8, 143.6, 142.5, 142.1, 136.7, 131.5, 130.6, 126.4, 21.9,

21.2, 14.9, 14.0. **MS** (MALDI): *m/z* 637.7 $[M]^+$ (calc. for $C_{30}H_{26}N_2O_2S_6$: 638.0). **Elemental analysis:** $C_{30}H_{26}N_2O_2S_6$: calc. C, 56.40; H, 4.10; N, 4.38%; found: C, 56.66; H, 4.32; N, 4.11%.

2,2'-(5',5''-(Thieno[3,4-c][1,2,5]thiadiazole-4,6-diyl)bis(3',4'-diethyl-2,2'-bithien-5,5'-diyl))bis(methan-1-yl-1-ylidene)dimalononitrile (**1**, DCV5T-TTDA). Bis-aldehyde **10** (30 mg, 0.05 mmol), malonitrile (40 mg, 0.61 mmol) and piperidine (8,0 mg, 0.09 mmol) were dissolved in 1,2-dichloroethane (10 ml) and stirred at room temperature for 1h. The mixture was then heated up to 70 °C and stirred again for one hour. The reaction was controlled by TLC using dichloromethane and ethyl acetate (9:1) as mobile phase. After cooling down to room temperature, the solid product was filtered, washed with *n*-hexane and dried under vacuum. Column chromatography on silica using dichloromethane as solvent afforded title compound **1** (30 mg, 0.04 mmol, 87%) as deep lilac color powder. **M.p.** (DSC): 305 °C. **^{1}H NMR** (1,1,2,2-Tetrachloroethane-d_2, 500 MHz, 100 °C) δ ppm: 7.71 (d, ^3J = 4.2 Hz, 2H, ThH), 7.70 (s, 2H, Vinyl-H), 7.36 (d, ^3J = 4.2 Hz, 2H, ThH), 3.01 (q, ^3J = 7.5 Hz, 4H, CH_2), 2.90 (q, ^3J = 7.5 Hz, 4H, CH_2) , 1.33 (t, ^3J = 7.5 Hz, 6H, CH_3) , 1.29 (t, ^3J = 7.5 Hz, 6H, CH_3). **^{13}C NMR** (1,1,2,2-Tetrachloroethane-d_2, 125 MHz, 100 °C) δ ppm: 157.50, 149.50, 148.16, 145.09, 143.01, 138.56, 134.53, 132.05, 131.14, 126.98, 120.49, 114.33, 113.57, 113.38, 21.94, 21.51, 14.65, 14.02. **MS** (MALDI): *m/z* 733.7 $[M]^+$ (calc. for $C_{36}H_{26}N_6S_6$: 734.1). **Elemental analysis:** $C_{36}H_{26}N_6S_6$: calc. C, 58.83; H, 3.57; N, 11.43%; found: C, 58.57; H, 3.58; N, 11.50%.

1,1'-(5',5''-(Thieno[3,4-c][1,2,5]thiadiazole-4,6-diyl)bis(3',4'-diethyl-2,2'-bithien-5,5'-diyl))bis(2,2,2-trifluoroethanone) (**2**, TFA5T-TTDA). To a solution of quinquethiophene **9** (300 mg, 0.51 mmol) in 1,2-dichloroethane (32 ml) was added trifluoroacetic anhydride (21 ml). The mixture was irradiated by microwave for four hours at 120 °C. After completion of the reaction, the solvent was removed under reduced pressure and the product was purified by column chromatography (SiO_2) eluting with pure dichloromethane. Recrystallization, using a Soxhlet apparatus with 1,2-dichloroethane as solvent, afforded **2** (259 mg, 0.33 mmol, 65%) as dark brown powder. **M.p.** (DSC): 221 °C. **^{1}H NMR** (1,1,2,2-Tetrachloroethane-d_2, 500 MHz, 100 °C) δ ppm: 7.90-7.85 (m, 2H, ThH), 7.32 (d, ^3J = 4.2 Hz, 2H, ThH), 2.99 (q, ^3J = 7.5 Hz, 4H, CH_2), 2.88 (q, ^3J = 7.5 Hz, 4H, CH_2), 1.31 (t, ^3J = 7.5 Hz, 6H, CH_3), 1.28 (t, ^3J = 7.5 Hz, 6H, CH_3). **^{13}C NMR** (1,1,2,2-Tetrachloroethane-d_2, 125 MHz, 100 °C) δ ppm: 157.5, 144.8, 142.9, 136.8, 134.9, 131.6, 131.1, 127.1, 120.5, 113.3, 21.9, 21.4, 14.8, 14.1. **MS** (MALDI): *m/z* 775.0 $[M]^+$ (calc. for

$C_{32}H_{24}F_6N_2O_2S_6$: 774.0). **Elemental analysis:** $C_{32}H_{24}F_6N_2O_2S_6$: calc. C, 49.60; H, 3.12; N, 3.61%; found: C, 49.66; H, 3.08; N, 3.43%.

5'-(6-(3,4-Diethyl-2,2'-bithien-5-yl)-thieno[3,4-c][1,2,5]thiadiazol-4-yl)-3',4'-diethyl-2,2'-bithiophene-5-carbaldehyde (**11**). Phosphoryl chloride (0.05 mL, 0.55 mmol) was added at 5 °C to dry dimethylformamide and the mixture was stirred at room temperature for 45 minutes. Quinquethiophene **9** (60 mg, 0.10 mmol) was added and the resulting mixture was stirred for 3 h at 100 °C. The desired product formed as main product and no further turn over was observed by TLC (silica, DCM : *n*-hexane = 1 : 1) after stirring over night at room temperature. Dichloromethane (80 mL) and aqueous solution of sodium hydrogen carbonate (200 mL) was added and stirring was continued for two hours. The organic phase was separated, dried over sodium sulfate, filtered, and the solvent was removed under reduced pressure. The product (21 mg, 0.03 mmol) was isolated by column chromatography (silica, DCM : *n*-hexane = 1 : 1) as deep green solid in 33% yield. **M.p.:** 205-206 °C. **^{1}H NMR** ($CDCl_3$, 400 MHz) δ ppm: 9.90 (s, 1H, OHC), 7.73 (d, 2H, Th-H), 7.36 (d, 2H, Th-H), 7.10 (q, 1H, Th-H), 7.01 (d, 1H, Th-H), 6.91 (d, 1H, Th-H), 3.58-2.74 (m, 8H, CH_2), 1.39-1.24 (m, 12H, CH_3). **^{13}C NMR** ($CDCl_3$, 100 MHz) δ ppm: 182.6, 157.0, 156.7, 146.0, 143.5, 142.1, 141.8, 141.4, 141.2, 136.8, 135.7, 133.0, 130.8, 130.8, 128.2, 127.5, 126.1, 126.1, 125.8, 113.7, 111.1, 21.9, 21.8, 21.2, 20.9, 15.3, 14.9, 14.1, 14.0. **MS** (MALDI-TOF): *m/z* 609.7 $[M]^+$ (calc. for $C_{29}H_{26}N_2OS_6$: 610.0). **Elemental analysis**: $C_{29}H_{26}N_2OS_6$: calc. C, 57.02; H, 4.29; N, 4.59%; found: C, 57.15; H, 4.36; N, 4.58%.

2-((5'-(6-(3,4-Diethyl-2,2'-bithien-5-yl)-thieno[3,4-c][1,2,5]thiadiazol-4-yl)-3',4'-diethyl-2,2'-bithien-5-yl)methylene)malononitrile (**12**). Mono-aldehyde **11** (25 mg, 0.04 mmol), malonitrile (32 mg, 0.48 mmol) and piperidine (7.0 mg, 0.08 mmol) were dissolved in 1,2-dichloroethane (10 mL) and the resulting solution was stirred under reflux for 1.5 hours. The solvent was removed under reduced pressure and the obtained solid was subjected to column chromatography (silica, dichloromethane) yielding the product (24 mg, 0.04 mmol) as dark-blue polycrystalline solid in 91% yield. **M.p.:** 256-257 °C. **^{1}H NMR** ($[d_2]$TCE, 500 MHz, 100 °C) δ ppm: 7.70 (d, 1H, ThH), 7.69 (s, 1H, Vinyl-H), 7.35 (d, 1H, ThH), 7.33 (dd, 1H, ThH), 7.22 (dd, 1H, ThH), 7.07 (dd, 1H ThH), 2.99 (quintet, 4H, CH_2) , 2.89 (q, 2H, CH_2) , 2.80 (q, 2H, CH_2), 1.34 - 1.26 (m, 9H, CH_3), 1.23 (t, 3H, CH_3). **^{13}C NMR** ($[d_2]$TCE, 125 MHz, 100 °C) δ [ppm]: 157.2, 156.8, 149.2, 148.2, 144.8, 142.4, 142.1, 141.6, 138.3, 135.7, 134.0, 133.4, 132.2, 130.1, 128.0, 127.3,

126.5, 126.3, 125.8, 117.9, 114.8, 114.2, 113.4, 111.0, 21.7, 21.6, 21.2, 20.8, 14.9, 14.3, 13.9, 13.8. **MS** (MALDI-TOF): *m/z* 657.7 $[M]^+$ (calc. for $C_{32}H_{26}N_4S_6$: 658.0). **Elemental analysis:** $C_{32}H_{26}N_4S_6$: calc. C, 58.33; H, 3.98; N, 8.50%; found: C, 58.12; H, 3.95; N, 8.78%.

5,7-Bis(3,4-diethylthien-2-yl)-2,3-diphenylthieno[3,4-b]pyrazine (**13**). 3,4,3'',4''-Tetraethyl-[2,2';5',2'']terthiophen-3',4'-diamin **6** (4.08 g, 10.4 mmol, 1.0 eq.) and benzil (2.43 g, 11.6 mmol, 1.1 eq.) were dissolved in methanol (250 ml). The mixture was heated up to 70 °C and stirred for 12 h under argon atmosphere. After cooling down, the formed precipitate was filtered off, washed with a small amount of methanol and dried under vacuum. Column chromatography (silica, DCM : *n*-hexane = 7 : 3) furnished product **13** (4.02 g, 7.1 mmol) as deep red powder in a yield of 68%. **M.p.:** 168-169 °C. **^{1}H NMR** ($CDCl_3$, 400 MHz) δ ppm: 7.58-7.54 (m, 4H, Ar-H), 7.37-7.27 (m, 6H, Ar-H), 7.12 (ws, 2H, Th-H) , 2.96 (q, ^3J = 7.6 Hz, 4H, $-CH_2$), 2.65 (dq, *J* = 7.5 Hz, *J* = 1.0 Hz, 4H, $-CH_2$), 1.33 (t, ^3J = 7.4 Hz, 6H, CH_3), 1.27 (t, ^3J = 7.5 Hz, 6H, CH_3). **^{13}C NMR** ($CDCl_3$, 100 MHz) δ ppm: 152.3, 144.1, 141.2, 139.0, 137.8, 129.9, 128.7, 128.0, 127.8, 125.4, 121.8, 22.0, 21.3, 14.4, 13.8. **MS** (MALDI-TOF): *m/z* 564.2 $[M]^+$ (calc. for $C_{34}H_{32}N_2S_3$: 564.2). **Elemental analysis:** $C_{34}H_{32}N_2S_3$: calc. C, 72.30; H, 5.71; N, 4.96%; found: C, 72.10; H, 5.77; N, 4.83%.

5,7-Bis(5-bromo-3,4-diethylthien-2-yl)-2,3-diphenylthieno[3,4-b]pyrazine (**14**). Thieno-pyrazine **13** (888 mg, 1.57 mmol) was dissolved under heat in chloroform (83 ml) and after cooling down to 0 °C conc. acetic acid (83 ml) was added. To this solution, NBS (588 mg, 3.3 mmol, 2.1 eq.) was added in one portion and the mixture was stirred in darkness at ambient temperature for one hour. Then the mixture was extracted carefully with saturated solution of sodium hydrogen carbonate and several times with water. The organic phase was dried over sodium sulfate and removed of the solvent under reduced pressure. Column chromatography (silica, DCM : *n*-hexane = 2 : 1) yielded the desired product (965 mg, 1.34 mmol, 85%) as deep blue powder. **M.p.:** 198-200 °C. **^{1}H NMR** ($CDCl_3$, 400 MHz) δ ppm: 7.58 – 7.53 (m, 4H, Phenyl), 7.40 – 7.30 (m, 6H, Phenyl), 2.98 (q, ^3J = 7.6 Hz, 4H, CH_2) , 2.66 (q, ^3J = 7.6 Hz, 4H, CH_2), 1.30 (t, ^3J = 7.5 Hz, 6H, CH_3), 1.19 (t, ^3J = 7.5 Hz, 6H, CH_3). **^{13}C NMR** ($CDCl_3$, 100 MHz) δ ppm: 152.79, 142.88, 140.76, 138.89, 137.97, 130.07, 129.03, 128.54, 128.13, 124.39, 112.74, 22.37, 21.77, 14.73, 14.19. **MS** (MALDI-TOF): 720.0 $[M]^+$ (calc. for $C_{34}H_{30}Br_2N_2S_3$: 720.0). **Elemental analysis:** $C_{34}H_{30}Br_2N_2S_3$: calc. C, 56.51; H, 4.18; N, 3.88%; found C, 56.49; H, 4.21; N, 3.73%.

Thien-2-yl-[1,3]dioxolane (**15**). Thiophene-2-carbaldehyde (15.5 g, 134 mmol), ethylene glycol (12.58 g, 203 mmol) and a catalytic amount of p-toluenesulfonic acid (38 mg, 0.20 mmol) were dissolved in toluene (50 ml). The solution was refluxed and stirred for 2 hours at 160 °C oil bath temperature and water was continuously removed by a Dean-Stark apparatus. Reaction control was done by gas chromatography (GC), showing that ethylene glycol was in parts removed with the formed water. Therefore, more glycol was added drop wise, until complete turnover was observed by GC. Then the reaction mixture was washed with aqueous solution of sodium hydrogen carbonate and water. The organic phase was separated, dried over sodium sulphate and removed of the solvent under reduced pressure. Fractional distillation over Vigreux gave the product (13.1 g, 84 mmol) as colorless liquid in a yield of 63%. **B.p.:** 108-110 °C (14 mbar). **^{1}H NMR** ($CDCl_3$, 400 MHz) δ ppm: 7.33 (dd, *J* = 5.0, *J* = 1.3 Hz, 1H, Th-H), 7.18 (ddd, *J* = 3.5 Hz, 1.2 Hz, *J* = 0.7 Hz, 1H, Th-H), 7.00 (dd, *J* = 5.0 Hz, *J* = 3.5 Hz, 1H, Th-H), 6.11 (s, 1H, OCH), 4.15-4.06 (m, 2H, CH_2), 4.02-3.94 (m, 2H, CH_2). **^{13}C NMR** ($CDCl_3$, 100 MHz) δ ppm: 126.6, 126.3, 126.2, 100.3, 67.8, 66.8, 65.2. Analytical data according to literature.[49-50]

2-(5-[1,3]Dioxolan-2-yl-thien-2-yl)-4,4,5,5-tetramethyl-[1,3,2]dioxaborolane (**16**). To a solution of 2-thiophen-2-yl-[1,3]dioxolane (**15**) (6.0 g, 38.4 mmol) in freshly dried THF (60 ml) was added slowly *n*BuLi (25.2 ml of a 1.6M solution in n-hexane, 40.3 mmol, 1.05 eq.) at -78 °C and under argon atmosphere. Stirring was continued for 15 minutes at -78 °C. Then the cooling bath was removed and the reaction mixture was stirred for 45 minutes. The mixture was cooled again to -78 °C and 2-Isopropoxy-4,4,5,5-tetramethyl-[1,3,2]dioxaborolane (ITDB) (8.62 ml, 42.2 mmol, 1.1 eq.) was added slowly. The cooling bath was removed and stirring was continued for two hours. Finally the mixture was extracted with diethyl ether and aqueous solution of bicarbonate. The organic phase was separated, dried over sodium sulphate and removed of the solvent under reduced pressure. The product (9.46 g, 33.5 mmol) crystallized as wax like yellow solid in a yield of 87%. The obtained material was pure enough for further syntheses. **^{1}H NMR** ($CDCl_3$, 400 MHz) δ ppm: 7.51 (d, ^{3}J = 3.5 Hz, 1H, Th-H), 7.20 (dd, *J* = 3.5 Hz, *J* = 0.5 Hz, 1H, Th-H), 6.17 (s, 1H, OCH), 4.15-4.06 (m, 2H, CH_2), 4.06-3.97 (m, 2H, CH_2), 1.33 (s, 12H, CH_3). **^{13}C NMR** ($CDCl_3$, 100 MHz) δ ppm: 149.2, 136.8, 127.1, 100.1, 84.1, 65.1, 24.7. **MS** (EI): m/z = 282 ($[M]^+$, 100), 195 (50) , 124 (45), 73 (Dioxolane, 30).

5,7-Bis(5'-(1,3-dioxolan-2-yl)-3,4-diethyl-2,2'-bithien-5-yl)-2,3-diphenylthieno[3,4-b]pyrazine (**17**). Dibromo-terthiophene **12** (600 mg, 0.83 mmol), Dioxoborolane **14** (773 mg, 2.74 mmol,

3.3 eq.), $HP(^tBu)_3BF_4$ (77 mg, 0.27 mmol) and $Pd_2(dba)_3{\cdot}CHCl_3$ (69 mg, 0.08 mmol) were dissolved in freshly dried THF (50 ml). Aqueous solution of K_3PO_4 (2 mol L^{-1}, 4.25 g in 10 ml of water) was added and the mixture was irradiated by microwave for 40 minutes at 90 °C. TLC (silica, DCM : cyclohexane : triethylamine = 67 : 30 : 3) showed complete turn over and the mixture was then extracted with water and DCM. The organic phase was dried over Na_2SO_4 and freed from the solvent under reduced pressure. Column chromatography (silica, DCM : cyclohexane : triethylamine = 67 : 30 : 3) furnished **15** (58 mg, 0.07 mmol) as green powder (lilac in solution) in a yield of 89%. **M.p.:** 183-185 °C. **^{1}H NMR** ([D_2]DCM, 400 MHz) δ ppm: 7.54 -7.49 (m, 4H, Phenyl), 7.35-7.25 (m, 6H, Phenyl), 7.10 (dd, ^3J = 3.7 Hz, J = 0.52 Hz, 2H, Th-H), 7.07 (s, 1H, Th-H) , 7.06 (s, 1H, Th-H), 6.07 (s, 2H, C-H), 4.12-4.08 (m, 4H, O-CH_2), 3.99-3.95 (m, 4H, O-CH_2), 2.98 (q, ^3J = 7.5 Hz, 4H, C$\underline{H}_2$-CH_3), 2.80 (q, ^3J = 7.5 Hz, 4H, C$\underline{H}_2$-CH_3), 1.27 (t, ^3J = 7.5 Hz, 6H, CH_3), 1.22 (t, ^3J = 7.5 Hz, 6H, CH_3). **^{13}C NMR** ([D_2]DCM, δ ppm) 152.94, 143.39, 142.42, 141.46, 139.52, 138.62, 137.53, 133.34, 130.36, 129.25, 128.40, 127.91, 127.06, 126.00, 125.32, 100.62, 65.71, 22.17, 21.26, 15.64, 14.96. **MS** (MALDI-TOF): *m/z* 872.3 $[M]^+$ (calc. for $C_{48}H_{44}N_2O_4S_5$: 872.2). **Elemental analysis:** $C_{48}H_{44}N_2O_4S_5$: calc. C, 66.02; H, 5.08; N, 3.21%; found C, 66.02; H, 5.19; N, 3.12%.

5',5''-(2,3-Diphenylthieno[3,4-b]pyrazine-5,7-diyl)bis(3',4'-diethyl-2,2'-bithiophene-5-carbaldehyde) (**18**). Dioxolane **17** (88 mg, 0.1 mmol) was dissolved in THF (8 ml). Water (2 ml) and a catalytic amount of p-toluenesulfonic acid (10 mg) were added. The solution was stirred for 12 h at rt. After that, reaction control by TLC (100% DCM) showed complete turnover and the solvent was removed under reduced pressure. The solution was then extracted with DCM and water. The organic phase was dried over Na_2SO_4 and the solvent was removed by rotary evaporation. The product (43 mg, 0.05 mmol) was isolated by column chromatography on silica (100% DCM) as deep green powder in a yield of 54%. **M.p.:** 248-250 °C. **^{1}H NMR** ($CDCl_3$, 400 MHz) δ ppm: 9.91 (s, 2H, OHC), 7.67 (d, ^3J = 4.0 Hz, 2H, Th-H), 7.62 – 7.57 (m, 4H, Ar-H), 7.42-7.31 (m, 8H, Ar-H), 3.06 (q, ^3J = 7.5 Hz, 4H, CH_2) , 2.91 (q, ^3J = 7.5 Hz, 4H, CH_2), 1.36 (t, ^3J = 7.5 Hz, 6H, CH_3), 1.30 (t, ^3J = 7.5 Hz, 6H, CH_3). **^{13}C NMR** ($CDCl_3$, 100 MHz) δ ppm: 182.60, 152.87, 146.49, 143.04, 142.90, 142.38, 138.80, 138.43, 136.86, 132.21, 130.10, 129.69, 129.19, 128.18, 126.22, 124.84, 21.89, 21.14, 15.06, 14.63. **MS** (HR MALDI-TOF): 785.1459 $[M+H]^+$ (calc. for $C_{44}H_{36}N_2O_2S_5$: 785.1453).

2,2'-(5',5''-(2,3-Diphenylthieno[3,4-b]pyrazine-5,7-diyl)bis(3',4'-diethyl-2,2'-bithien-5',5-diyl))bis(methan-1-yl-1-ylidene)dimalononitrile (**3**, DCV5T-TP). Bis-aldehyde **18** (482 mg, 0.61 mmol) was dissolved in 1,2-dichloroethane (170 ml) and Malonitrile (812 mg, 12.3 mmol, 20 eq.) was added at room temperature. Finally Piperidine (0.12 ml, 1.23 mmol) was added and the resulting solution was stirred at room temperature for twelve hours, after which reaction control by TLC (100% DCM) showed complete conversion. After extracting the mixture with DCM, the organic phase was washed with water, dried over Na_2SO_4 and freed from the solvent under reduced pressure. To remove most of the side products, column chromatography on silica with first pure DCM and later a mixture of DCM and ethyl acetate (9:1) was applied. A second column chromatography (silica, methanol : ethyl acetate = 1 : 1) was performed to eluate impurities, while the product remained on the column head. The product was then extracted from silica with pure DCM. Removal of the solvent under reduced pressure furnished title compound **3** (31 mg, 0.04 mmol) as dark violet powder in a yield of 66%. **M.p.** (DSC): 336 °C. **^{1}H NMR** ([D_2]TCE, 500 MHz, 100 °C) δ ppm: 7.73 (d, ^3J = 4.2 Hz, 2H, Th-H), 7.70 (s, 2H, Vinyl), 7.60 – 7.56 (m, 2H, Th-H), 7.39 – 7.29 (m, 8H, Phenyl), 3.06 (q, ^3J = 7.6 Hz, 4H, CH_2), 2.92 (q, ^3J = 7.6 Hz, 4H, CH_2), 1.35 (t, ^3J = 7.4 Hz, 6H, CH_3), 1.30 (t, ^3J = 7.4 Hz, 6H, CH_3). **^{13}C NMR** ([D_2]TCE, 125 MHz, 100 °C): n/a (insufficient solubility). **MS** (MALDI-TOF): *m/z* 880.4 $[M]^+$ (calc. for $C_{50}H_{36}N_6S_5$: 880.2). **Elemental analysis:** $C_{50}H_{36}N_6S_5$: calc. C, 68.15; H, 4.12; N, 9.45%; found C, 68.24; H, 4.22; N, 9.60%.

3.6 References

[1] K. Schulze, C. Uhrich, R. Schüppel, K. Leo, M. Pfeiffer, E. Brier, E. Reinold, P. Bäuerle, *Adv. Mater.* **2006**, *18*, 2872.

[2] R. Schüppel, K. Schmidt, C. Uhrich, K. Schulze, D. Wynands, J. L. Brédas, E. Brier, E. Reinold, H.-B. Bu, *Phys. Rev. B* **2008**, *77*, 085311.

[3] M. M. Oliva, J. Casado, M. Manuela, M. Raposo, A. Maurcio, C. Fonseca, H. Hartmann, V. Hernandez, J. T. L. Navarrete, *J. Org. Chem.* **2006**, *71*, 7509.

[4] S. Tanaka, Y. Yamashita, *Synth. Met.* **1993**, *55*, 1251.

[5] Y. Yamashita, S. Tanaka, *Synth. Metals* **1995**, *69*, 599.

[6] M. C. Ruiz Delgado, V. Hernández, J. T. López Navarrete, S. Tanaka, Y. Yamashita, *J. Phys. Chem. B* **2004**, *108*, 2516.

[7] C. Kitamura, S. Tanaka, Y. Yamashita, *J. Chem. Soc., Chem. Commun.* **1994**, 1585.

[8] J. Casado, R. P. Ortiz, M. C. Ruiz Delgado, V. Hernández, J. T. López Navarrete, J. M. Raimundo, P. Blanchard, M. Allain, J. Roncali, *J. Phys. Chem. B* **2005**, *109*, 16616.

[9] A. P. Kulkarni, Y. Zhu, S. A. Jenekhe, *Macromolecules* **2007**, *41*, 339.

[10] A. K. Bakhshi, H. Ago, K. Yoshizawa, K. Tanaka, T. Yamabe, *J. Chem. Phys.* **1996**, *104*, 5528.
[11] W. Shen, M. Li, R. He, J. Zhang, W. Lei, *Polymer* **2007**, *48*, 3912.
[12] F. Outurquin, C. Paulmier, *Bull. Soc. Chim.* **1983**, *5-6*, 159.
[13] S. W. Schneller, F. W. Clough, P. N. Skancke, *J. Het. Chem.* **1976**, *13*, 581.
[14] F. Zhang, E. Perzon, X. Wang, W. Mammo, M. R. Andersson, O. Inganäs, *Adv. Funct. Mater.* **2005**, *15*, 745.
[15] A. P. Kulkarni, Y. Zhu, S. A. Jenekhe, *Macromolecules* **2008**, *41*, 339.
[16] M. M. Wienk, M. G. R. Turbiez, Martin P. Struijk, M. Fonrodona, R. A. J. Janssen, *Appl. Phys. Lett.* **2006**, *88*, 153511.
[17] H. A. Becerril, N. Miyaki, M. L. Tang, R. Mondal, Y.-S. Sun, A. C. Mayer, J. E. Parmer, M. D. McGehee, Z. Bao, *J. Mater. Chem.* **2008**, *19*, 591.
[18] X. Z. Wang, W. Y. Wong, K. Y. Cheung, M. K. Fung, A. B. Djurišić, W. K. Chan, *Dalton Trans.* **2008**, 5484.
[19] R. S. Ashraf, H. Hoppe, M. Shahid, G. Gobsch, S. Sensfuss, E. Klemm, *J. Polym. Sci. Part A* **2006**, *44*, 6952.
[20] B. P. Karsten, R. Janssen, A. J., *Org. Lett.* **2008**, *10*, 3513.
[21] Y. Zhu, R. D. Champion, S. A. Jenekhe, *Macromolecules* **2006**, *39*, 8712.
[22] C.-L. Liu, J.-H. Tsai, W.-Y. Lee, W.-C. Chen, S. A. Jenekhe, *Macromolecules* **2008**, *41*, 6952.
[23] R. Mondal, N. Miyaki, H. A. Becerril, J. E. Norton, J. Parmer, A. C. Mayer, M. L. Tang, J.-L. Bredas, M. D. McGehee, Z. Bao, *Chem. Mater.* **2009**, *21*, 3618.
[24] Q. M. Zhou, Q. Hou, L. P. Zheng, X. Y. Deng, G. Yu, Y. Cao, *Appl. Phys. Lett.* **2004**, *84*, 1653.
[25] X. J. Wang, E. Perzon, F. Oswald, F. Langa, S. Admassie, M. R. Andersson, O. Inganas, *Adv. Funct. Mater.* **2005**, *15*, 1665.
[26] S. Admassie, O. Inganas, W. Mammo, E. Perzon, M. R. Andersson, *Synth. Met.* **2006**, *156*, 614.
[27] M. X. Chen, E. Perzon, N. Robisson, S. K. M. Jonsson, M. R. Andersson, M. Fahlman, M. Berggren, *Synth. Met.* **2004**, *146*, 233.
[28] M. H. Petersen, S. A. Gevorgyan, F. C. Krebs, *Macromolecules* **2008**, *41*, 8986.
[29] H. A. Becerril, N. Miyaki, M. L. Tang, R. Mondal, Y. S. Sun, A. C. Mayer, J. E. Parmer, M. D. McGehee, Z. Bao, *J. Mater. Chem.* **2009**, *19*, 591.
[30] A. P. Zoombelt, M. Fonrodona, M. M. Wienk, A. B. Sieval, J. C. Hummelen, R. A. J. Janssen, *Org. Lett.* **2009**, *11*, 903.
[31] A. P. Zoombelt, J. Gilot, M. M. Wienk, R. A. J. Janssen, *Chem. Mater.* **2009**, *21*, 1663.
[32] A. P. Zoombelt, M. Fonrodona, M. G. R. Turbiez, M. M. Wienk, R. A. J. Janssen, *J. Mater. Chem.* **2009**, *19*, 5336.
[33] R. H. Schlessinger, J. D. Bower, *J. Am. Chem. Soc.* **1969**, *91*, 6891.
[34] S. Tanaka, M. Tomura, Y. Yamashita, *Heterocycles* **1994**, *37*, 693.
[35] I. Kmínek, V. Cimrová, D. Výprachtický, P. Pavlaková, *Macromol. Symp.* **2008**, *268*, 100.
[36] Y. Xia, L. Wang, X. Deng, D. Li, X. Zhu, Y. Cao, *Appl. Phys. Lett.* **2006**, *89*, 081106.
[37] S. Steinberger, A. Mishra, E. Reinold, C. M. Müller, C. Uhrich, M. Pfeiffer, P. Bäuerle, *Org. Lett.* **2010**, *Submitted*.
[38] S. Steinberger, E. Reinold, P. Bäuerle, *Diploma Thesis* **2005**, *University of Ulm, Institut of Organic Chemistry II and Advanced Materials*, 44.
[39] C. Crestini, M. D'Auria, *J. Photochem. Photobiol. A* **1996**, 69.
[40] M. H. Petersen, O. Hagemann, K. T. Nielsen, M. Jørgensen, F. C. Krebs, *Sol. Energy Mater. and Sol. Cells* **2007**, *91*, 996.

[41] J. Casado, T. M. Pappenfus, L. L. Miller, K. R. Mann, E. Ortí, P. M. Viruela, R. Pou-Amérigo, V. Hernández, J. T. L. Navarrete, *J. Am. Chem. Soc.* **2003**, *125*, 2524.
[42] R. Fitzner, E. Reinold, A. Mishra, E. Mena-Osteritz, H. Ziehlke, C. Körner, K. Leo, M. Riede, M. Weil, O. Tsaryova, A. Weiß, C. Uhrich, M. Pfeiffer, P. Bäuerle, *Adv. Funct. Mater.* **2011**, *21*, 897.
[43] D. Wouters, C. Bedoya, G. G. Condorelli, A. D. Mauro, G. Anastasi, I. L. Fragala, J. G. Lisoni, *Mater. Sci. Eng. B* **2005**, *B118*, 264.
[44] M. Behforouz, R. Benrashid, *Tetrahedron Lett.* **1979**, *46*, 4193.
[45] O. Tsuge, T. Takata, *J. Org. Chem.* **1980**, *45*, 2956.
[46] O. Tsuge, M. Noguchi, T. Takata, *Chem. Lett.* **1980**, 1031.
[47] A. Gadisa, M. Svensson, M. R. Andersson, O. Inganas, *Appl. Phys. Lett.* **2004**, *84*, 1609.
[48] M. C. Scharber, D. Mühlbacher, M. Koppe, P. Denk, C. Waldauf, A. J. Heeger, C. J. Brabec, *Adv. Mater.* **2006**, *18*, 789.
[49] Johnson, *J. Org. Chem.* **1976**, *41*, 1320.
[50] A. J. Carpenter, D. J. Chadwick, *Tetrahedron* **1985**, *41*, 3803.

Chapter 4

Benzothiadiazole as Core Acceptor in A-D-A-D-A-type Oligothiophenes

Abstract

Novel A-D-A-D-A-type oligothiophenes incorporating electron-withdrawing benzo[*c*][1,2,5]thiadiazole (BTDA) as core and trifluoroacetyl (TFA) or dicyanovinyl (DCV) as terminal acceptor groups have been developed. The obtained oligomers show strong absorption in solution down to 600 nm with high thermal stability. Vacuum-processed organic solar cells with fullerene C_{60} as acceptor showed very high open circuit voltages up to 1.2 V, resulting in power conversion efficiencies as high as 1.56% under AM1.5G conditions.

4.1 Introduction

Today, benzo[*c*][1,2,5]thiadiazole (BTDA) is one of the most widely used acceptor moieties in low band gap materials for organic electronic applications, such as organic solar cells (OSC).[1-7] For this purpose, the BTDA unit has been combined with carbazoles, fluorines, pyrroles, thiophenes and other electron-rich building blocks.[1, 8-15] Motivation for the incorporation of the heterocyclic BTDA unit into π-conjugated systems is its excellent thermal stability, high absorption coefficient, suitable HOMO and LUMO energy levels, and strong intermolecular π-π interactions, leading to ordered morphologies in the solid state.[9, 15-24]

In literature we find many examples of BTDA comprising polymers for bulk heterojunction solar cells with efficiencies up to 5.4% (Figure 1).[5, 25-42]

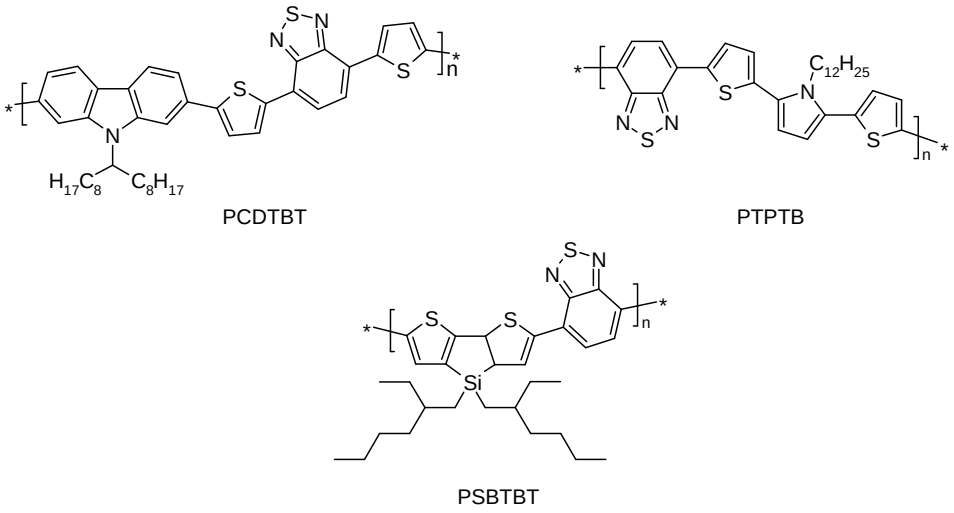

Figure 1: Highly efficient benzothiadiazole (BTDA) comprising polymers for BHJSCs: PCDTBT[5], PSBTBT[6], PTPTB[1].

In the field of "small molecule" solar cells (SMSC), however, the BTDA moiety is hardly explored. Compounds for organic field-effect transistors (OTFT) have been reported[43] and in 2010, a BTDA-comprising oligothiophene has been prepared by Kim and co-workers for the application in vacuum-deposited organic solar cells (Figure 2). The assembled cells showed a shortcut current density (J_{SC}) of 4.75 mA/cm^2, an open circuit voltage (V_{OC}) of 0.53 V, a fill factor (*FF*) of 0.38, resulting in a power conversion efficiency (PCE) of 0.97%.[44]

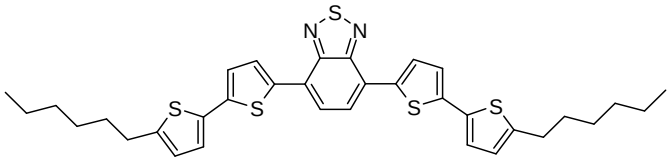

DH5TB

Figure 2: First oligothiophene comprising a BTDA as acceptor moiety for vacuum-processed SMSCs.[44]

The objective of this study was to prepare and characterize novel DCV5T-analogous[45-48] compounds comprising the electron-deficient BTDA unit as core and trifluoroacetyl (TFA) or dicyanovinyl (DCV) as terminal acceptor moieties (Figure 3).

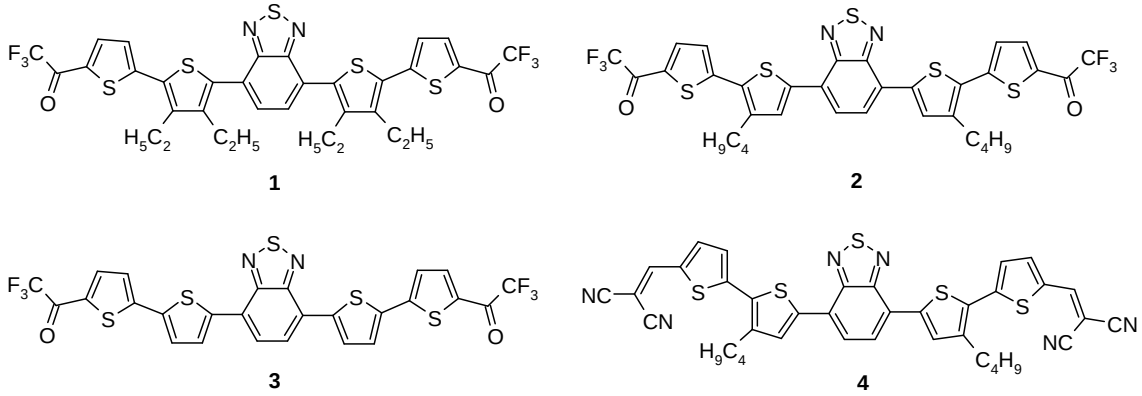

1 **2** **3** **4**

Figure 3: Target compounds **1** – **4**: Benzo[*c*][1,2,5]thiadiazole (BTDA) functionalized oligothiophenes based on reported DCV5T.[46, 48]

Various alkyl chain patterns were introduced to enhance solubility and at the same time retain planarity of the conjugated systems. The application of these materials in m-i-p-type planar heterojunction solar cells prepared by vacuum sublimation technique is described.

4.2 Synthesis

The new A-D-A-D-A-type oligomers were synthesized according to Scheme 1. 3,4-Diethylthiophene was synthesized as described in literature.[49] Lithiation of 3,4-diethyl-thiophene followed by quenching with tributyltin chloride afforded tributyl(3,4-diethylthien-2-yl)stannane **5a** in 87% yield. Terthiophene **6a** was prepared by Pd^0-catalyzed Stille-type cross-coupling reaction of 4,7-dibromobenzo[*c*][1,2,5]thiadiazole **4**[50] and **5a** in a yield of 69%. Bis-bromination of **6a** with NBS in chloroform gave terthiophene **7a** as yellow-orange crystals in 65% yield. Subsequent microwave-assisted Stille-type coupling of **7a** with tributyl(thien-2-

yl)stannane afforded pentamer **8a** in a yield of 77%. By reacting **8a** with trifluoroacetic anhydride under microwave irradiation, title compound **1** was obtained as orange powder in 60% yield. Derivative **2** was prepared following the procedure of title compound **1**. Therefore, tributyl-(4-butyl-thien-2-yl)-stannane **5b** was synthesized in analogy to literature.[51] A Stille-type coupling reaction of **4** and **5b** gave trimer **6b** in a yield of 41%. The subsequent dibromination of **6b** with NBS followed by a Stille-type coupling reaction with tributyl(thien-2-yl)stannane gave **8b** in a yield of 66%. Reaction of **8b** with trifluoroacetic anhydride under microwave irradiation afforded title compound **2** in a yield of 69%. Pentamer **9** was synthesized via microwave-assisted Stille-type cross coupling of dibromobenzo[c][1,2,5]-thiadiazole[50] and monostannylated bithiophene[52] in analogy to literature.[9] By adding cesium fluoride and applying microwave irradiation yields for the synthesis of **9** were improved from 14% to nearly 60%. Reaction of **9** with trifluoroacetic anhydride under microwave conditions gave title compound **3** as dark red powder in 67% yield.

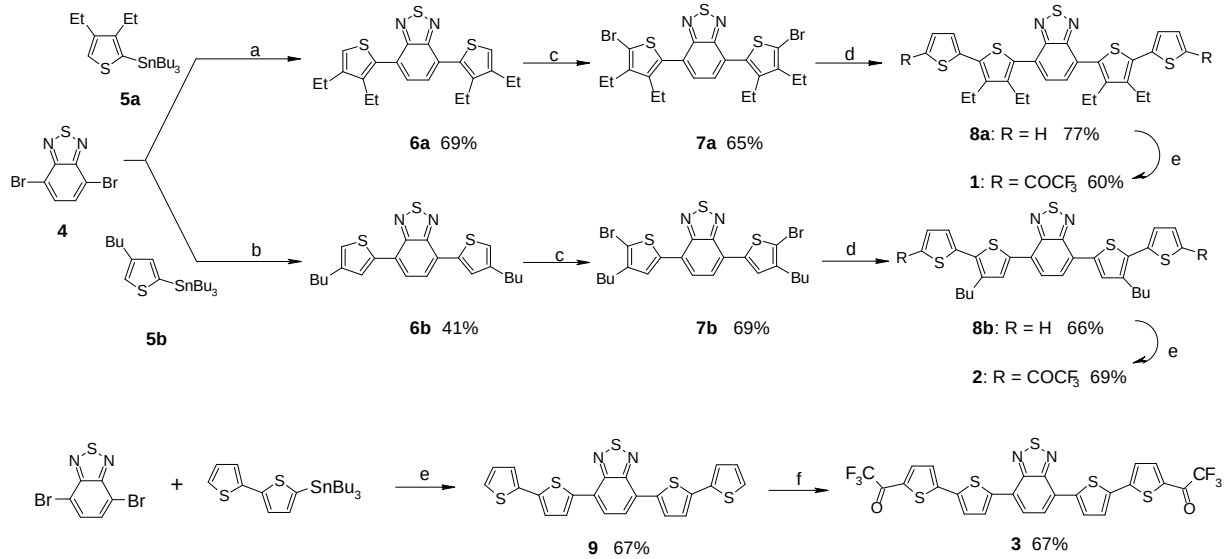

Scheme 2: a) $Pd(PPh_3)_2Cl_2$, THF, reflux, 48 h; b) $Pd(PPh_3)_2Cl_2$, CsF, 1,2-dichloroethane, microwave, 3.5 h, 110 °C; c) NBS, chloroform, 0 °C – r.t., 2 – 48 h; d) 2-Tributylstannyl thiophene, $Pd(PPh_3)_2Cl_2$, CsF, 1,2-dichloroethane, microwave, 4 h, 100 °C; e) $Pd(dppp)Cl_2$, DMF, CsF, microwave, 1 h, 100 °C; f) Trifluoroacetic anhydride, 1,2-dichloroethane, microwave, 5–15 h, 100 °C.

In order to obtain a DCV-substituted derivative (**4**), dioxolane **11** was prepared via microwave assisted Suzuki-type cross-coupling reaction of boronic acid ester **10** (Chapter 4) with bis-brominated trimer **7b** in a yield of 68% (Scheme 2).

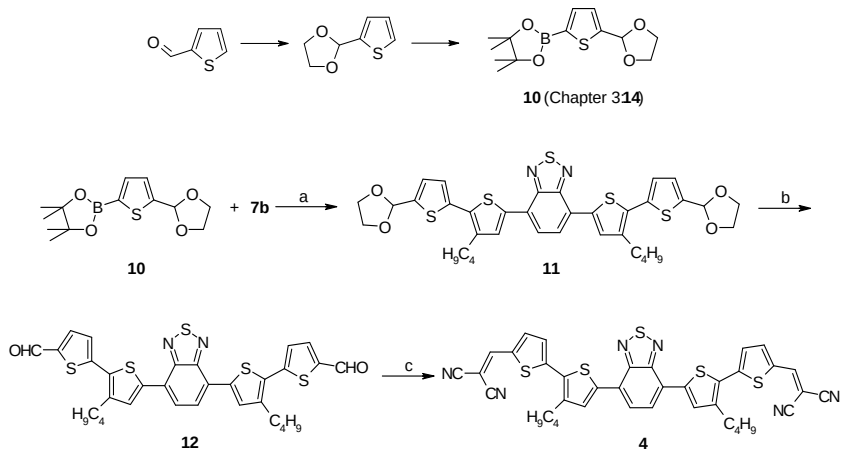

Scheme 2: a) $Pd_2dba_3{\cdot}CHCl_3$, $HP(^tBu)_3BF_4$, THF/water (4:1), potassium phosphate, 100 °C, 1 h, microwave, 68%; b) p-toluenesulfonic acid, THF/water, rt, 18 h, 92%; c) malonitrile, piperidine, 1,2-DCE, rt, 1 d, 76%.

Deprotection of dioxolane **11** in THF and water under acidic conditions, using a catalytic amount of p-toluenesulfonic acid, afforded bis-aldehyde **12** in 92% yield. The obtained aldehyde was further reacted with malonitrile and piperidine in dichloroethane to give title compound **4** as deep red powder in a yield of 76%.

4.3 Physical Properties

Physical and optical properties were investigated to deduce structure-property relations of the novel BTDA oligomers and to determine their suitability for photovoltaic applications.

4.3.1 Steady-State Spectroscopy

Electronic absorption spectra of title compounds **1**-**4** in solution (dichloromethane) and of thin films (30 nm) are presented in Figure 4 and corresponding data are summarized in Table 1.

The UV-vis spectrum of ethyl-substituted derivative **1** showed a longest wavelength absorption maximum at 430 nm, which is blue-shifted by about 80 nm when compared to pentamers **2** and **3**. The hypsochromic shift indicates a twist of the aromatic system, due to strong sterical hindrance in **1**, caused by the BTDA moiety and its adjacent ethyl-substituted thiophene rings. By attaching the terminal acceptor groups, the molar extinction coefficients of the resulting target oligomers were increased by almost a factor of two (e.g. **3**: λ_{max} = 509 nm, ε = 50300 L mol^{-1} cm^{-1}; **9**: λ_{max} = 505 nm, ε = 25400 L mol^{-1} cm^{-1}) in comparison to the

parent oligomers. This effect can be assigned to *1*. the extension of the conjugated π-system and *2*. the enforced quinoidal character of the conjugated system, due to the terminal electron withdrawing TFA groups. The alkyl side chains in BTDA-oligomer **2** increase the donor character of the thiophene rings by hyperconjugation, resulting in a more distinct alternation of electron-rich and electron-deficient moieties in the conjugated system. Thus, derivative **2** showed a longest wavelength absorption at 518 nm, which is red-shifted by 9 nm when compared to the non-alkylated counterpart **3**.

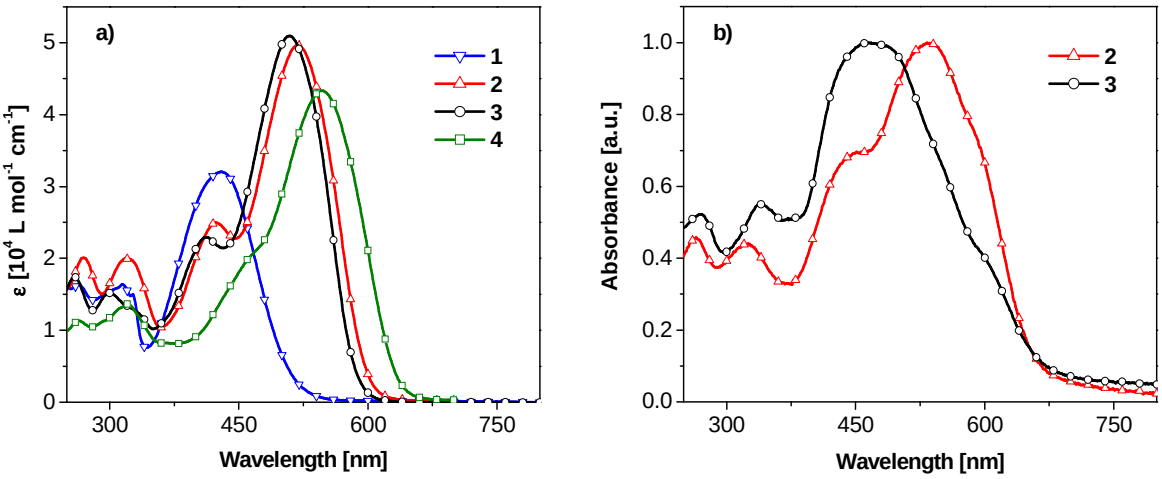

Figure 4: Absorption spectra of BTDA-oligomers **1**-**4** in a) solution b) solid state, 30 nm thin film prepared by vacuum evaporation.

The lowest energy absorption of DCV-derivative **4** is bathochromically shifted by 29 nm, when compared to corresponding TFA compound **2**, while the extinction coefficient is slightly lowered (**2**: 49500 L mol^{-1} cm^{-1}; **4**: 43300 L mol^{-1} cm^{-1}). The observed red-shift is ascribed to the extended π-system of the DCV groups and the stronger electron withdrawing force of which, when compared to the TFA moieties in **2**.

Table 1: UV-vis data of BTDA derivatives **1**-**4** in dichloromethane solution ([c] = 10^{-5} mol L^{-1}) and solid state, 30 nm thin film prepared by vacuum evaporation.

Compound	λ_{abs} (nm)	ε [a] (L mol^{-1} cm^{-1})	λ_{Onset} (nm)	E_g^{opt} (eV)	λ_{abs}^{solid} (nm)
1	315, 430	32000	508	2.44	-
2	320, 423 (sh), 518	49500	597	2.08	534
3	411 (sh), 509	50300	590	2.10	466
4	468 (sh), 547	43300	635	1.95	-

[a] The molar extinction coefficient values are given for the longest wavelength absorption band.

Figure 4b depicts the normalized solid-state UV-vis absorption spectra of **2** and **3** deposited by vacuum evaporation as 30 nm thin films on a quartz plate. Due to the strong hypsochromic shift in solution, no thin films or OSCs were prepared of compound **1**. On account of insufficient solubility, only a small sample of DCV derivative **4** was synthesized for analytical purpose and no thin films or OSCs were prepared of the compound.

In the solid state, derivative **3** showed a broad longest wavelength absorption with a maximum at 466 nm, which is 43 nm blue-shifted when compared to the absorption in solution. The hypsochromic shift in the film is presumably caused by the formation of H-type aggregates, while the broadening indicates the partial formation of J-type aggregates. The solid state spectrum of **2** showed a broad absorption band and a bathochromic shift of 15 nm, when compared to the absorption in solution, which is probably caused by π-stacking of the molecules in the film.

According to semi-empirical calculations (AM1, ZINDO/S), the dominant transition in representative title compound **3** has no intramolecular charge transfer (CT) characteristic. The HOMO is delocalized completely over the entire conjugated backbone, while the LUMO is mainly concentrated on the BTDA moiety and its adjacent thiophene units (Figure 5).

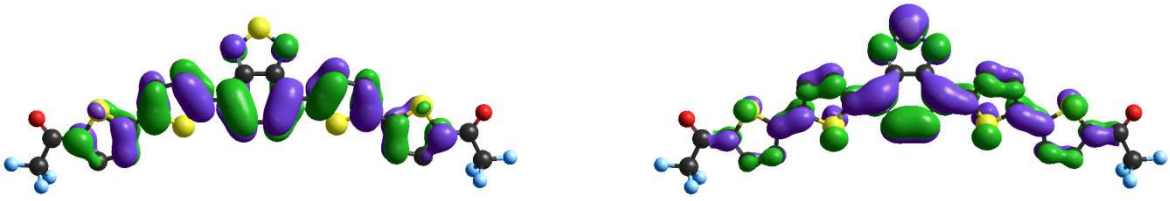

HOMO **LUMO**

Figure 5: Representative electron density distribution of the frontier orbitals in BTDA **2** obtained from semi-empirical AM1 calculations (carbon atoms in black, fluorine in light blue, nitrogen in blue, sulfur in yellow and hydrogen atoms are omitted for clarity reasons).

4.3.2 Electrochemical Studies

Cyclic voltammograms of title compounds **1** – **4** in dilute dichloromethane solution are depicted in Figure 6, and the corresponding electrochemical data, HOMO and LUMO energy levels are collected in Table 2.

In cyclic voltammetry measurements, the studied compounds **1**-**4** each showed two reversible one electron oxidation waves (Figure 6, Table 2). Due to the twist of the thiophene rings adjacent to the BTDA moiety and the resulting weakened conjugation, the electronic

influence of the BTDA acceptor on the neighboring bithiophene units in compound **1** is strongly reduced. Thus, in contrast to BTDA derivatives **2** and **3**, the first oxidation wave in **1** is shifted to higher potential and is therefore observed very close to the second oxidation wave.

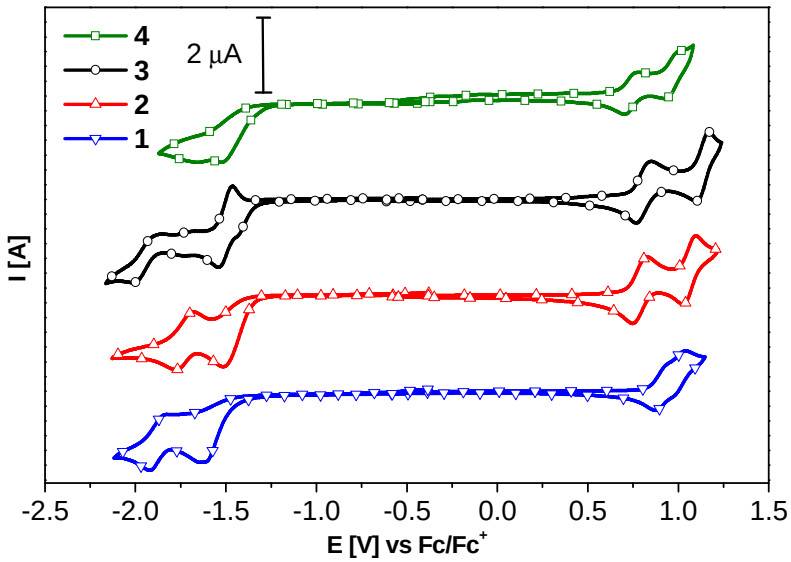

Figure 6: Electrochemical characterization of BTDA derivatives **1 – 4** (**1**-**3**: 1×10^{-3} mol·L^{-1}, **4**: saturated, < 10^{-4} mol·L^{-1}) in dichloromethane-$TBAPF_6$ (0.1M), scan speed 100 mV/s, potentials *vs.* Fc/Fc^+. The oxidation curve of **4** was mathematically enlarged for better visibility by a factor of 5.

In the cathodic potential regime, compound **1** and **2** showed each one irreversible and a reversible reduction wave, corresponding to the reduction of the central BTDA and the terminal TFA moieties, respectively. Compounds **3** displayed a reversible wave corresponding to the reduction of the BTDA unit and one quasi-reversible reduction wave for the terminal acceptor groups. For DCV-derivative **4**, we observed one irreversible reduction wave. A second reduction potential could not be clearly distinguished.

Table 2: Summarized cyclovoltammetry data of BTDA derivatives **1 – 4** (DCM, HOMO/LUMO vs. Fc/Fc^+_{vac} = 5.1 eV).

Compound	$E°_{ox1}$ (V)	$E°_{ox2}$ (V)	$E°_{red1}$ (V)	$E°_{red2}$ (V)	HOMO (eV)	LUMO (eV)	ΔE^{CV} (eV)
1	0.91	1.00	-1.57	-1.88	-5.94	-3.64	2.30
3	0.79	1.06	-1.46	-1.73	-5.82	-3.74	2.08
2	0.81	1.14	-1.50	-1.93	-5.84	-3.73	2.11
4	0.74	0.98	-1.45	-	-5.75	-3.77	1.98

The HOMO and LUMO energy values of these dyes, determined from electrochemical measurements, are suitable for the application in OSCs (Table 2). When comparing DCV compound **4** with parent compound DCV5T, the introduction of the BTDA unit resulted in a

lowering of the HOMO energy level by 0.43 eV, while the LUMO energy level was lowered by only 0.33 eV, leading to a broadening of the band gap by 0.1 eV.

4.3.3 Thermal Properties

Thermal stability of the compounds was investigated by thermogravimetric analysis (TGA) and differential scanning calorimetry (DSC). The onset of the decomposition temperatures (T_d) in TGA were at about 355 °C for **1** and 367 °C for **2** and **3**, respectively (Figure 7). DCV compound **4** was not analyzed by TGA.

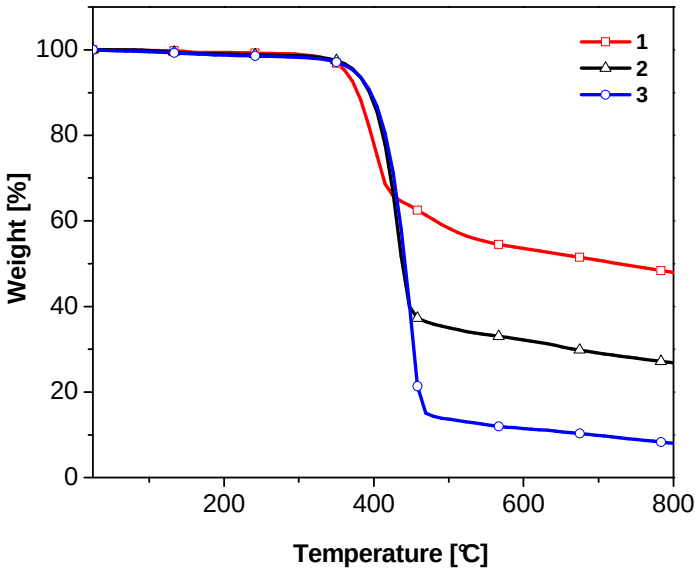

Figure 7: TGA thermograms of compounds **1**-**3** measured under N_2. Conditions: N_2 flow, 50 mL/min; heating rate, 10 °C/min.

Figure 8 depicts DSC curves of title compounds **2**-**4**. For TFA-based compound **2** and **3** a melting point of 190 and 262 °C, respectively, was observed. No exothermic peak was found, and thus no decomposition occurred within the measuring range up to 400 °C. DCV compound **4**, however, showed a melting point at 300 °C and an exothermic peak at around 350 °C, which is assigned to the decomposition of the compound, as proven by subsequent NMR analysis of the sample.

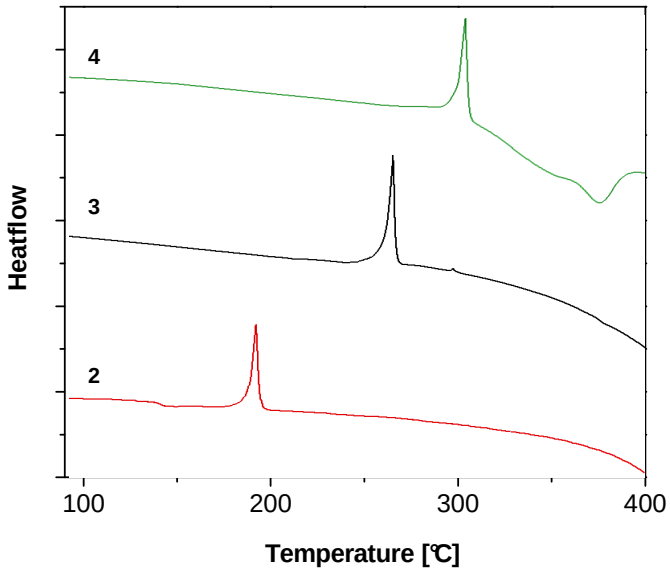

Figure 8: DSC curves of BTDA-compounds **2** (red), **3** (black) and **4** (green). Due to its strong hypsochromic shift in absorption (unsuitable for solar cells), **1** was not investigated by DSC.

Both, TGA and DSC measurements indicate, that TFA compounds **2** and **3** have good thermal stability, and conclusively, very high sublimation yields were found while processing these materials by vacuum deposition technique.

4.4 Photovoltaic Performance

Figure 9 shows the current density-voltage (*J-V*) characteristics of planar heterojunction (PHJ) solar cells comprising the cell structure: ITO/C_{60} (15 nm)/**2**-**3**/BPAPF (5 nm)/BPAPF:NDP9 (30 nm 9wt%)/BPAPF:NDP9 (10 nm 18wt%)/p-ZnPc (10 nm 4wt%)/Au (50 nm). The corresponding solar cell data are summarized in Table 3.

Table 3: Characteristic solar cell data of flat heterojunction solar cells of TFA-derivatives **2** and **3**.

Compound	V_{OC} (mV)	J_{SC} (mA cm^{-2})	*FF*	η (%)
2 (6 nm)	1.17	4.04	0.33	1.56
3 (6 nm)	1.10	4.38	0.30	1.45
3 (10 nm)	1.07	4.01	0.26	1.12

The cells showed clear rectification behavior in the dark. The device based on compound **2** gave an excellent open circuit voltage (V_{OC}) of 1.17 V and a shortcut current density (J_{SC}) of 4.04 mA cm^{-2}. In combination with a fill factor (*FF*) value of 0.33, the device gave an overall

power conversion efficiency (PCE) of 1.56% under AM 1.5G conditions. With compound **3** as donor and a similar layer sequence, we observed an equally high V_{OC} of 1.10 V, a J_{SC} of 4.38 mA cm^{-2}, a *FF* value of 0.30, leading to an overall PCE of 1.45%. Increasing the layer thickness to 10 nm in the case of BTDA **3**, resulted in a lowered PCE of 1.12%, due to a reduced J_{SC} (4.01 mA cm^{-2}), V_{OC} (1.07 V) and *FF* (0.26) value.

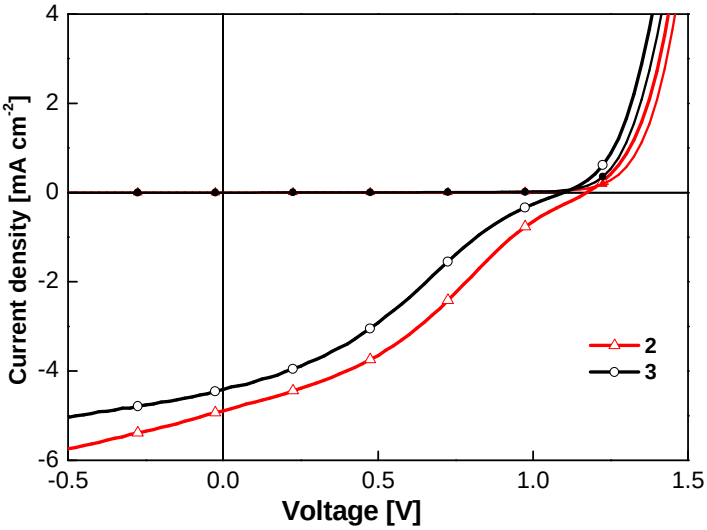

Figure 9: *J-V* characteristics of PHJ solar cells using BTDA-containing compounds **2** and **3** as donor under AM 1.5G white light illumination at 100 mW cm^{-2}.

Due to the low lying HOMO energy level of the BTDA-comprising donors, the V_{OC} obtained for both compounds is very high. However, the S-shape of the *J-V* curve results in a low *FF* value of about 30%. The reason for this S-shape is, that the HOMO of the BTDA derivatives (~-5.8 eV) lies deeper than the HOMO of the hole transporter (BPAPF/NDP9). Therefore, hole injection from the hole transport layer (HTL) into the donor faces an energetic barrier, resulting in a low slope of the *J-V* curve around V_{OC}. However, the S-shape caused by the HOMO misalignment is not the only reason for the low *FF*. We also observe a lack of saturation of photocurrent with reverse bias which indicates significant recombination losses around 0 V. Such behavior may have two reasons: Either it is connected with low carrier mobilities (slow escape of holes from the Coulomb attraction of the electron on C_{60}) or with an insufficient HOMO and/or LUMO offset between the donor and C_{60}.

In summary: Novel oligothiophenes **1**, **2** and **3** comprising BTDA as core and TFA as terminal acceptor units were prepared and characterized, and the materials showed interesting optical and electrochemical properties. Vacuum-processed planar “small molecule” organic solar cells

have been assembled and PCEs as high as 1.56% were obtained. Due to the low lying HOMO energies of these compounds, very high V_{OC} values in the range of 1.2 V were observed. Further improvement of the *FF* and the device efficiency should be possible by using suitable hole-transporting materials.

4.5 Experimental Section

General remarks:

NMR spectra were recorded on a *Bruker AMX 500* (^{1}H NMR: 500 MHz, ^{13}C NMR: 125 MHz) or an *Avance 400* spectrometer (^{1}H NMR: 400 MHz, ^{13}C NMR: 100 MHz), unless mentioned otherwise at 25 °C. Chemical shift values (δ) are expressed in parts per million using residual solvent protons (^{1}H NMR, δ_H = 7.26 for $CDCl_3$, δ_H = 5.32 for CD_2Cl_2, δ_H = 5.93 for CD_2Cl_4; ^{13}C NMR, δ_C = 77.0 for $CDCl_3$, δ_C = 53.8 for CD_2Cl_2, δ_C = 74.2 for CD_2Cl_4) as internal standard. The splitting patterns are designated as follows: s (singulet), d (doublet), t (triplet) and m (multiplet). The assignments are Ar-H (H-atoms of aromatic systems) and Th-H (H-atoms of thiophene rings). Melting points were determined using a *Büchi B-545* apparatus and were not corrected. Elemental analyses were performed on an *Elementar Vario EL* (University of Ulm) and a *Carlo Erba 1104* (University of Stuttgart). Thin layer chromatography was carried out on aluminum plates, pre-coated with silica gel, *Merck Si60* F_{254}. Preparative column chromatography was performed on glass columns packed with silica gel, *Merck Silica 60*, particle size 40 – 43 µm. CI and EI mass spectra were recorded on a *Finnigan MAT SSQ-7000* or a *Varian Saturn 2000* GC-MS, MALDI-TOF on a *Bruker Daltonics Reflex III*. UV/Vis absorption spectra were recorded in 1 cm cuvettes with *Merck* Uvasol grade solvents on a *Perkin Elmer Lambda 19* spectrometer. Cyclic voltammetry experiments were performed with a computer-controlled *Autolab PGSTAT30* potentiostat in a three-electrode single-compartment cell with a platinum working electrode, a platinum wire counter electrode, and an Ag/AgCl reference electrode. All potentials were internally referenced to the ferrocene / ferrocenium couple. Tetrahydrofurane (*Merck*) was dried under reflux over sodium/benzophenone (*Merck*) and dichloromethane (*Merck*) over calcium hydride (*Merck*). All synthetic steps were carried out under argon atmosphere. *N*-Bromo succinimide (NBS), NaOH and K_2CO_3 were purchased from *Merck*, $Pd(PPh_3)_2Cl_2$, trifurylphosphine (TFP) and *n*BuLi (1.6 mol/L in hexane) from *Acro*s, tri-*n*-butyltin chloride and tri-*n*-methyltin chloride from *Aldrich*. Thermogravimetric analysis (TGA) was

conducted on a *Mettler Toledo* TGA/SDTA851^e instrument with a heating rate of 10 ^oC/min under a nitrogen at a flow rate of 50 cm^3/min.

Vacuum-processed solar cells: N9,9-bis(4-[di-(p-biphenyl)aminophenyl])fluorine (BPAPF) and zinc phthalocyanine (ZnPc), doped with proprietary compounds NDP2 or NDP9 of *Novaled GmbH* (Dresden) were used as p-doped hole transport layers. Doping concentrations of BPAPF and ZnPc were 2-5 wt%. C_{60} and ZnPc have been provided by *Alfa Aesar* and Di-NPB by *Sensient Imaging Technologies*. Except the oligothiophenes, all materials were cleaned at least twice by thermal gradient sublimation before evaporation. The organic layers and metal contacts were thermally deposited in an ultra high vacuum system ("UFO", *Bestec GmbH*) at 10^{-8} to 10^{-7} mbar through shadow masks onto semitransparent indium tin oxide (ITO) coated glass substrates (*Thin Film Devices Inc.*, sheet resistance < 30 Ω / sq) without breaking the vacuum. Ceramic or graphite crucibles were used as sublimation sources (*Creaphys GmbH*, Reinhardtsgrimma), temperatures were set by a *Eurotherm* controller and film thicknesses were determined by quartz crystal monitors (*Leybold Inficon Inc.*). Substrates were cleaned using detergent, acetone, and ethanol. The active area of the cells had an average size of 4-7 mm^2. *J-V* characteristics were measured using a Source Measurement Unit 236 SMU (*Keithley*) in an N_2-filled glovebox without exposing the samples to air. Illumination was provided by a sun simulator SOL 1200 (*Hoehnle*) with an intensity of 127 mW cm^{-2}, which was calibrated using an outdoor reference cell provided by the *Fraunhofer Institute for Solar Energy Systems* (Freiburg). External quantum efficiency (EQE) spectra were recorded using a homemade setup based on a xenon lamp (*ILC-Technologies*) and a grating monochromator. Calibration was done using a *Newport Corporation* powermeter or a *Hamamatsu Photonics* photo diode. Organic films for spectral analysis were vapor deposited onto quartz substrates under ultra high vacuum with deposition rates of about 0.1 Å s^{-1}. A commercial *Shimadzu* UV-2101/3101 spectrophotometer was used for absorption measurements. Luminescence spectra were recorded using a *Spex* FluoroMAX with separated monochromators for excitation and luminescence light.

Synthesis:

Tributyl-(3,4-diethyl-thien-2-yl)-stannane (**5a**). Under argon atmosphere, 3,4-diethylthiophene (40.0 g, 285 mmol) was dissolved in dried THF (400 ml). The solution was cooled down

to -10 °C using an ice/sodium chloride bath and then *n*-BuLi (178 ml, 285 mmol, 1.6M solution in *n*-hexane) was added dropwise under vigorous stirring. The internal temperature was maintained at -10 °C for 30 min, then was slowly brings to ambient temperature for a period of 90 min. The reaction mixture was further cool down to -10 °C and tri-*n*-butyltin chloride (77.4 ml, 92.8 g, 285 mmol) was added dropwise. The reaction mixture was slowly warm to room temperature and stirred for 12 h. After diluting the reaction mixture with dethyl ether at 0 ^{o}C, was added cold aqueous saturated $NaHCO_3$ solution under vigorous stirring. The organic phase was separated, and the water phase was extracted with diethyl ether (2 × 100 mL). The combined organic extracts were dried ($MgSO_4$) and filtered, and then the solvent was removed by rotary evaporation. The crude product was purified by distillation under high vacuum (148 ^{o}C, 4 × 10^{-3} mbar) to yield **5a** (106.8 g, 249 mmol, 87%) as a colorless viscous liquid. **^{1}H NMR** ($CDCl_3$, δ ppm) 7.21 (s, 1H, Th-H), 2.59 (dq, ^{3}J = 7.45 Hz, ^{4}J = 0.96 Hz, 2H, CH_2), 2.57 (q, ^{3}J = 7.53 Hz, 2H, CH_2), 1.61-1.5 (m, 6H, CH_2), 1.34 (m, 6H, CH_2), 1.30 (t, ^{3}J = 7.47 Hz, 3H, CH_3), 1.12-1.06 (m, 9H, CH_2), 0.90 (t, ^{3}J = 7.3 Hz, 9H, CH_3). **^{13}C NMR** ($CDCl_3$, δ ppm) 150.7, 144.6, 131.6, 125.6, 29.1, 27.3, 24.5, 21.9, 16.2, 14.1, 13.6, 10.8. **MS** (EI): m/z = 430 (M^+, 2%), 373 (M^+ - C_4H_9, 100%). **Elemental analysis:** $C_{20}H_{38}SSn$: calc. C, 55.96; H, 8.92; S, 7.47%; found C, 55.71; H, 8.82; S, 7.27%.

4,7-Bis(3,4-diethylthien-2-yl)benzo[*c*][1,2,5]thiadiazole (**6a**). 4,7-Dibromo-benzothiadiazole **4** (1.0 g, 3.40 mmol, 1 eq.), palladium(II)bis(triphenylphosphine) dichloride (0.2 mmol, 6 mol%) and tributyl(3,4-diethylthiophen-2-yl)stannane (3.65 g, 8.50 mmol, 2.5 eq.) were dissolved in freshly dried THF (50 ml). The reaction mixture was heated to reflux and stirred for 48 h. The progress was monitored by TLC (silica, DCM:*n*-hexane = 1 : 1). After cooling to ambient temperature, the reaction mixture was extracted with DCM (150 ml). The organic phase was then washed with saturated aqueous solution of NH_4Cl and finally with water. After drying with Na_2SO_4, the solvent was removed under reduced pressure and the product was isolated by column chromatography (SiO_2, DCM:*n*-hexane = 1 : 1) to obtain **6a** (970 mg, 2.35 mmol, 69%) as yellow crystals. **M.p.:** 117-118 °C. **^{1}H NMR** ($CDCl_3$, 400 MHz) δ ppm: 7.65 (s, 2H, Ar-H), 7.13 (t, 2H, *J* = 1.0Hz, Th-H), 2.71 (dq, 4H, *J* = 7.48 Hz, *J* = 1.1 Hz, CH_2), 2.64 (q, 4H, *J* = 7.45 Hz, CH_2), 1.37 (t, 6H, *J* = 7.46 Hz, CH_3), 1.30 (t, 6H, *J* = 7.54 Hz, CH_3). **^{13}C NMR** ($CDCl_3$, 100 MHz) δ ppm: 154.4, 144.2, 141.7, 132.5, 129.9, 128.1, 120.5, 22.3, 21.0, 15.0, 13.7. **MS** (CI): *m/z* 413 ($[M]^+$, 100). **Elemental analysis:** $C_{22}H_{24}N_2S_3$: calc. C, 64.04; H, 5.86; N, 6.79%; found: C, 64.20; H, 5.84; N, 6.78%.

4,7-Bis(5-bromo-3,4-diethylthien-2-yl)benzo[*c*][1,2,5]thiadiazole (**7a**). Benzo[*c*][1,2,5]-thiadiazole **6a** (199 mg, 0.48 mmol, 1 eq.) was dissolved in chloroform (30 ml). The solution was stirred at room temperature and NBS (182 mg, 1.02 mmol, 2.12 eq.) was slowly added. Stirring was continued for 48 h under argon atmosphere, after which the reaction mixture was extracted with DCM. The organic phase was then washed with water, dried over Na_2SO_4. After removal of the solvent by rotary evaporator the compound was purified by column chromatography (SiO_2, DCM:*n*-hexane = 1:1) to yield **7a** (180 mg, 0.32 mmol) as yellow-orange crystals in 65% yield. **M.p.:** 111-112 °C. **^{1}H NMR** ($CDCl_3$, 400 MHz) δ ppm: 7.63 (s, 2H, Ar-H), 2.70 (q, 4H, *J* = 7.58 Hz, CH_2), 2.66 (q, 4H, *J* = 7.51 Hz, CH_2), 1.25 (t, 6H, *J* = 7.56 Hz, CH_3), 1.12 (t, 6H, *J* = 7.54 Hz, CH_3). **^{13}C NMR** ($CDCl_3$, 100 MHz) δ ppm: 154.1, 143.0, 141.8, 132.5, 129.7, 127.3, 111.0, 21.9, 21.7, 15.4, 14.1. **MS** (CI): *m/z* 567.9 ($[M]^+$, 100). **Elemental analysis:** $C_{22}H_{22}Br_2N_2S_3$: calc. C, 46.32; H, 3.89; N, 4.91%; found: C, 46.60; H, 4.00; N, 4.91%.

4,7-Bis(3,4-diethyl-2,2'-bithien-5-yl)benzo[*c*][1,2,5]thiadiazole (**8a**). BTDA derivative **7a** (296 mg, 0.52 mmol, 1 eq.) was dissolved in 1,2-dichloroethane (50 ml). $Pd(PPh_3)_2Cl_2$ (36 mg, 52 µmol, 10 mol-%) and 2-(tributylstannyl)-thiophene (484 mg, 0.41 ml, 1.3 mmol, 2.5 eq.) were added and the mixture was irradiated by microwave in a closed vessel for 4 h at 100 °C. After extracting the orange mixture with DCM, the organic layer was washed with water, dried over Na_2SO_4 and the solvent was removed under reduced pressure. After column chromatography (SiO_2, DCM:n-hexane = 1:1) product **8a** (230 mg, 0.40 mmol) was obtained as orange-red powder in 77% yield. **M.p.:** 142-144 °C. **^{1}H NMR** ($CDCl_3$, 400 MHz) δ ppm: 7.71 (s, 2H, Ar-H), 7.34 (dd, 2H, *J* = 5.16 Hz, *J* = 1.17 Hz, Th-H), 7.22 (dd, 2H, *J* = 3.59 Hz, *J* = 1.17 Hz, Th-H), 7.09 (dd, 2H, *J* = 5.15 Hz, *J* = 3.59 Hz, Th-H), 2.86 (q, 4H, *J* = 7.53 Hz, CH_2), 2.71 (q, 4H, *J* = 7.53 Hz, CH_2), 1.29 (t, 6H, *J* = 7.54 Hz, CH_3), 1.14 (t, 6H, *J* = 7.53 Hz, CH_3). **^{13}C NMR** ($CDCl_3$, 100 MHz) δ ppm: 154.2, 143.1, 140.8, 136.1, 132.1, 131.6, 129.9, 127.6, 127.3, 126.2, 125.5, 21.3, 21.1, 15.5, 15.4. **MS** (CI): *m/z* 576.0 ($[M]^+$, 100). **Elemental analysis:** $C_{30}H_{28}N_2S_5$: calc. C, 62.46; H, 4.89; N, 4.86%; found: C, 62.66; H, 4.99; N, 4.89%.

1,1'-(5',5''-(Benzo[*c*][1,2,5]thiadiazole-4,7-diyl)bis(3',4'-diethyl-2,2'-bithien-5',5-diyl))bis(2,2,2-trifluoroethanone) (**1**). Pentamer **8a** (107 mg, 0.19 mmol, 1 eq.) was dissolved in 1,2-dichloroethane (4 ml) at around 60 °C. Trifluoroacetic anhydride (2.92 g, 13.91 mmol, 75 eq.) was added and the resulting mixture irradiated under microwave conditions in a closed

vessel for 8 h at 100 °C. After extracting the deep orange solution with DCM, the organic layer was washed with water, dried over Na_2SO_4. The organic solvent was removed under reduced pressure. Title compound **1** (86 mg, 0.11 mmol) was isolated by column chromatography (SiO_2, DCM:n-hexane, 1:1) as orange powder in 60% yield. **M.p.:** 138-140 °C. **^{1}H NMR** ($CDCl_3$, 400 MHz) δ ppm: 7.94-7.91 (m, 2H, Th-H), 7.75 (s, 2H, Ar-H), 7.33 (d, 2H, *J* = 4.24 Hz, Th-H), 2.97 (q, 4H, *J* = 7.52 Hz, CH_2), 2.72 (q, 4H, *J* = 7.51 Hz, CH_2), 1.34 (t, 6H, *J* = 7.55 Hz, CH_3), 1.15 (t, 6H, *J* = 7.54 Hz, CH_3). **^{13}C NMR** ($CDCl_3$, 100 MHz) δ ppm: 154.0, 144.3, 143.9, 134.8, 134.5, 130.7, 130.0, 127.4, 127.0, 21.4, 21.2, 15.4, 14.9. **MS** (MALDI-TOF): *m/z* 768.2 $[M]^+$ (calc. for $C_{34}H_{26}F_6N_2O_2S_5$: 768.1). **Elemental analysis:** $C_{34}H_{26}F_6N_2O_2S_5$: calc. C, 53.11; H, 3.41; N, 3.64%; found: C, 53.16; H, 3.70; N, 3.57%.

4,7-Bis-(4-butyl-thien-2-yl)-benzo[*c*][1,2,5]thiadiazole (**6b**). 4,7-dibromobenzo[*c*][1,2,5]thiadiazole (768 mg, 2.67 mmol, 1.0 eq.), tributyl-(4-butyl-thiophen-2-yl)-stannane (2.87 g, 6.68 mmol, 2.5 eq.) and $Pd(PPh_3)_2Cl_2$ (188 mg, 0.27 mmol, 10 mol%) were dissolved in 1,2-dichloroethane (30 ml). CsF(1.62 g, 10.7 mmol, 4.0 eq.) was added and the resulting mixture heated to 110 °C under microwave irradiation. Only the desired product was observed by TLC (silica, DCM:n-hexane = 1:1) after irradiating for 3.5 h. The mixture was extracted with DCM, and the organic layer washed with saturated aqueous solution of NH_4Cl and then with water. After drying the organic phase with Na_2SO_4, the solvent was removed under reduced pressure and purified by column chromatography (SiO_2, DCM:n-hexane = 1:1) to yield **6b** (451 mg, 1.1 mmol) as yellow crystals in 41% yield. **M.p.:** 77 - 78 °C. **^{1}H NMR** ($CDCl_3$, 400 MHz) δ ppm: 7.97 (d, 2H, *J* = 1.37 Hz, Th-H), 7.79 (s, 2H, Ar-H), 7.03 (d, 2H, *J* = 1.16 Hz, Th-H), 2.71 (t, 4H, *J* = 7.78 Hz, CH_2), 1.76-1.66 (m, 4H, CH_2), 1.48-1.40 (m, 4H, CH_2), 0.98 (t, 6H, *J* = 7.36 Hz, CH_3). **^{13}C NMR** ($CDCl_3$, 100 MHz) δ ppm: 152.5, 144.2, 138.9, 128.9, 125.9, 125.4, 121.4, 32.6, 30.3, 22.4, 13.9. **MS** (CI): *m/z* 413 ($[M]^+$, 100). **Elemental analysis:** $C_{22}H_{24}N_2S_3$: calc. C, 64.04; H, 5.86; N, 6.79%; found: C, 64.23; H, 5.96; N, 6.53%.

4,7-Bis-(5-bromo-4-butyl-thien-2-yl)-benzo[*c*][1,2,5]thiadiazole (**7b**). NBS (403 mg, 2.27 mmol, 2.05 eq.) was dissolved in chloroform (35 ml) and the solution was added drop wise at 0 °C to a stirred solution of benzothiadiazole **6b** (456 mg, 1.11 mmol, 1 eq.) in chloroform (35 ml). The cooling bath was removed and the mixture was stirred at room temperature for 2 h under argon atmosphere. The reaction mixture was extracted with DCM, washed with water, dried over Na_2SO_4. The solvent was removed by rotary evaporator and then purified by

column chromatography (SiO_2, DCM:n-hexane = 1:1) followed by recrystallization from n-hexane afforded **7b** (450 mg, 0.79 mmol) as yellow-orange solid in 71% yield. **M.p.:** 114-115 °C. **^{1}H NMR** ($CDCl_3$, 400 MHz) δ ppm: 7.77 (s, 2H, Th-H), 7.73 (s, 2H, Ar-H), 2.65 (t, 4H, CH_2), 1.72-1.61 (m, 4H, *J* = 7.59 Hz, CH_2), 1.49-1.38 (m, 4H, CH_2), 0.98 (t, 6H, *J* = 7.34 Hz, CH_3). **^{13}C NMR** ($CDCl_3$, 100 MHz) δ ppm: 152.2, 143.0, 138.5, 128.1, 125.3, 124.8, 111.6, 31.9, 29.4, 22.4, 13.9. **MS** (CI): *m/z* 567.9 ([M]$^+$, 100). **Elemental analysis:** $C_{22}H_{22}Br_2N_2S_3$: calc. C, 46.32; H, 3.89; N, 4.91%; found: C, 46.26; H, 3.82; N, 4.88%.

4,7-Bis-(3-butyl-[2,2']bithien-5-yl)-benzo[*c*][1,2,5]thiadiazole (**8b**). Benzothiadiazole **7b** (190 mg, 0.33 mmol, 1.0 eq.), 2-(tributylstannyl)-thiophene (0.264 ml, 0.83 mmol, 2.5 eq.) and $Pd(PPh_3)_2Cl_2$ (23 mg, 0.03 mmol, 10mol%) were dissolved in 1,2-dichloroethane (25 ml). CsF (304 mg, 2.00 mmol, 6.0 eq.) was added and the mixture was irradiated by microwave for 4 h at 100 °C. After extracting the deep red solution with DCM, the organic phase was washed with water, dried over Na_2SO_4. The solvent was removed under reduced pressure and then passed through a short SiO_2 column (DCM:n-hexane = 1:1). The crude product was further purified by recrystallization from n-hexane to obtain **8b** (127 mg, 0.22 mmol) as deep red powder in 66% yield. **M.p.:** 108 - 111 °C. **^{1}H NMR** ($CDCl_3$, 400 MHz) δ ppm: 7.99 (s, 2H, Th-H), 7.83 (s, 2H, Ar-H), 7.35 (dd, 2H, *J* = 5.16 Hz, *J* = 1.16 Hz, Th-H), 7.24 (dd, 2H, *J* = 3.60 Hz, *J* = 1.17 Hz, Th-H), 7.11 (dd, 2H, *J* = 5.15 Hz, *J* = 3.60 Hz, Th-H), 2.85 (t, 4H, *J* = 7.79 Hz, CH_2), 1.79-1.68 (m, 4H, CH_2), 1.53-1.41 (m, 4H, CH_2), 0.97 (t, 6H, *J* = 7.35 Hz, CH_3). **^{13}C NMR** ($CDCl_3$, 100 MHz) δ ppm: 152.5, 140.4, 136.9, 136.0, 132.3, 130.5, 127.4, 126.0, 125.5, 125.4, 125.2, 32.8, 29.2, 22.7, 13.9. **MS** (CI): *m/z* 576.1 ([M]$^+$, 100). **Elemental analysis:** $C_{30}H_{28}N_2S_5$: calc. C, 62.46; H, 4.89; N, 4.86%; found: C, 62.52; H, 4.97; N, 4.82%.

1-(3'-Butyl-5'-(7-[3-butyl-5'-(2,2,2-trifluoro-acetyl)-[2,2']bithienyl-5-yl]-benzo[*c*][1,2,5]-thiadiazol-4-yl)-[2,2']bithien-5-yl)-2,2,2-trifluoro-ethanone (**2**). Pentamer **8b** (127 mg, 0.22 mmol, 1 eq.) was dissolved in 1,2-dichloroethane (20 ml) at around 60 °C and after cooling down to room temperature, trifluoroacetic anhydride (4.62 g, 22 mmol, 100 eq.) was added. The resulting mixture was irradiated by microwave for 5 h at 100 °C. The solvent was then removed under reduced pressure and the product isolated by column chromatography (SiO_2, gradiential eluention from DCM:n-hexane = 7:3 to pure DCM). Further recrystallization from n-hexane using a Soxhlet apparatus afforded title compound **3** (116 mg, 0.15 mmol) as deep red powder in 69% yield. **M.p.** (DSC): 190 °C. **^{1}H NMR** ($CDCl_3$, 400 MHz) δ ppm: 7.99 (s, 2H, Th-H),

7.92 (m, 2H, Th-H), 7.86 (s, 2H, Ar-H), 7.35 (d, 2H, *J* = 4.21 Hz, Th-H), 2.91 (t, 4H, *J* = 7.7 Hz, CH_2), 1.82-1.70 (m, 4H, CH_2), 1.57-1.45 (m, 4H, CH_2), 1.01 (t, 6H, *J* = 7.35 Hz, CH_3). **^{13}C NMR** ($CDCl_3$, 100 MHz) δ ppm: 152.2, 149.1, 143.9, 139.5, 136.9, 134.6, 131.1, 131.0, 126.7, 125.5, 125.3, 32.3, 29.8, 22.7, 14.0. **MS** (MALDI-TOF): *m/z* 768.2 $[M]^+$ (calc. for $C_{34}H_{26}F_6N_2O_2S_5$: 768.1). **Elemental analysis:** $C_{34}H_{26}F_6N_2O_2S_5$: calc. C, 53.11; H, 3.41; N, 3.64%; found: C, 53.26; H,3.53; N, 3.60%.

4,7-Bis-[2,2']bithien-5-yl-benzo[*c*][1,2,5]thiadiazole (**9**). 4,7-dibromobenzo[*c*][1,2,5]thiadiazole (208 mg, 0.71 mmol), [2,2']Bithiophenyl-5-yl-tributyl-stannane (743 mg, 1.63 mmol, 2.3 eq.), CsF (593 mg, 3.90 mmol, 5.5 eq.) and Pd(dppp)Cl_2 (50 mg, 0.07 mmol, 10mol%) were dissolved in dry DMF (30 ml) under argon atmosphere. The reaction mixture was irradiated in a closed vessel by microwave for 3 h at 100 °C. The resulting deep red solution was then extracted with DCM and washed with water. The organic phase was dried over Na_2SO_4 and removed by rotary evaporator. Column chromatography (SiO_2, 1. DCM, 2. DCM:n-hexane = 1:1) and successive recrystallization from ethanol afforded the desired product **9** (201 mg, 0.43 mmol) as deep red powder in a yield of 61%. **M.p.:** 189-191 °C. **^{1}H NMR** (CD_2Cl_4, 500 MHz, 100 °C) δ ppm: 8.00 (d, 2H, *J* = 3.89 Hz, Th-H), 7.80 (s, 2H, Ar-H), 7.25 (dd, 2H, *J* = 3.58 Hz, *J* = 1.1 Hz, Th-H), 7.24 – 7.21 (m, 4H, Th-H), 7.05 (dd, 2H, *J* = 5.11 Hz, *J* = 3.59 Hz, Th-H). **^{13}C NMR** (CD_2Cl_4, 125 MHz, 100 °C) δ ppm: 152.8, 139.1, 138.5, 137.4, 128.6, 128.1, 126.0, 125.4, 125.1, 124.9, 124.4. **MS** (CI): *m/z* 464.0 ($[M]^+$, 100). **Elemental analysis:** $C_{22}H_{12}N_2S_5$: calc. C, 56.87; H, 2.60; N, 6.03%; found: C, 56.81; H, 2.82; N, 5.74%.

2,2,2-Trifluoro-1-(5'-(7-[5'-(2,2,2-trifluoro-acetyl)-[2,2']bithienyl-5-yl]-benzo[*c*][1,2,5]-thiadiazol-4-yl)-[2,2']bithien-5-yl)-ethanone (**3**). Pentamer **9** (143 mg, 0.31 mmol) was dissolved in 1,2-dichloroethane (18 ml) at ca. 60 °C. Then trifluoroacetic anhydride (4.3 ml, 30.8 mmol, 100 eq.) was added and the resulting mixture heated in a closed vessel to 110 °C under microwave conditions. Only the desired product was observed by TLC (DCM:n-hexane = 7:3) after irradiating for 15 h. The solvent was removed under reduced pressure and the insoluble solid was then adsorbed on flash silica gel before subjecting to column chromatography (SiO_2, DCM:n-hexane = 7:3). Title compound **3** (135 mg, 0.20 mmol) was obtained as deep red powder in 67% yield. **M.p.** (DSC): 262 °C. **^{1}H NMR** (CD_2Cl_4, 500 MHz, 100 °C) δ ppm: 8.08 (d, 2H, J = 4.0 Hz, Th-H), 7.90 (s, 2H, Ar-H), 7.86 - 7.84 (m, 2H, Th-H), 7.48 (d, 2H, J = 3.98 Hz, Th-H), 7.36 (d, 2H, J = 4.16 Hz, Th-H). **^{13}C NMR** (CD_2Cl_4, 125 MHz, 100 °C) δ

ppm: 152.5, 149.9, 142.0, 137.6, 137.5, 137.1, 134.7, 129.2, 128.0, 126.1, 126.0, 125.5. **MS** (CI): *m/z* 656.1 ([M]$^+$, 100). **Elemental analysis:** $C_{26}H_{10}F_6N_2O_2S_5$: calc. C, 47.55; H, 1.53; N, 4.27%; found: C, 47.27; H, 1.69; N, 4.09%.

4,7-Bis-(3-butyl-5'-[1,3]dioxolan-2-yl-[2,2']bithienyl-5-yl)-benzo[1,2,5]thiadiazole (**11**). Bis-brominated trimer **7b** (50 mg, 0.09 mmol), boronic ester **10** (59 mg, 0.21 mmol, 2.4 eq.), $Pd_2dba_3{\cdot}CHCl_3$ (3.6 mg, 4 µmol, 4 mol-%) and $HP(^tBu)_3BF_4$ (2 mg, 10 µmol, 8 mol-%) were dissolved in dry THF (5 ml). Aqueous solution of potassium phosphate (2 mol L^{-1}, 1 ml) was added and the mixture heated to 100 °C under microwave conditions. TLC (DCM : n-hexane = 1 : 1) showed complete turnover after 1 h of irradiation. The reaction mixture was extracted with DCM and water. The organic layer was dried over sodium sulfate and removed of the solvent under reduced pressure. Column chromatography (silica, DCM : triethylamine = 98 : 2) afforded the desired product as violet powder in a raw yield of 68% (43 mg, 0.06 mmol). The material was used without further purification in the subsequent reaction. **^{1}H NMR** ([D_2]DCM, 400 MHz) δ ppm: 7.95 (s, 2H, Th-H), 7.78 (s, 2H, Ar-H) , 7.35 (d, 2H, Th-H), 7.10 (d, 2H, Th-H), 6.06 (s, 2H, ^{t}C-H), 4.23-4.05 (m, 8H, -O-CH_2), 2.86-2.78 (m, 4H, Th-CH_2-), 1.77-1.65 (m, 4H, CH_2) , 1.52-1.40 (m, 4H, CH_2), 0.96 (t, 6H, CH_3).

5',5''-(Benzo[c][1,2,5]thiadiazole-4,7-diyl)bis(3'-butyl-2,2'-bithiophene-5-carbaldehyde) (**12**). Bis-dioxolane **11** (79 mg, 0.11 mmol) was dissolved in THF (40 ml) and a catalytic amount of p-toluenesulfonic acid (10 mg). Water (4 ml) was added and the mixture stirred for 1 d at ambient temperature. THF was removed under reduced pressure and the residue extracted with DCM and water. The organic phase was dried over sodium sulfate and removed of the solvent. Column chromatography (silica, DCM) afforded the product as deep red-violet powder in a yield of 92% (65 mg, 0.10 mmol). The product was pure enough to be used in the subsequent reaction. **^{1}H NMR** ($CDCl_3$, 400 MHz) δ ppm: 9.91 (s, 2H, OHC), 8.00 (s, 2H, Th-H), 7.87 (s, 2H, Ar-H), 7.75 (d, 2H, Th-H), 7.35 (d, 2H, Th-H), 2.91 (t, 4H, CH_2), 1.81-1.70 (m, 4H, CH_2), 1.55-1.44 (m, 4H, CH_2), 0.99 (t, 6H, CH_3). **^{13}C NMR** ($CDCl_3$, 100 MHz) δ ppm: 182.6, 152.3, 146.0, 142.9, 142.4, 138.8, 136.8, 126.2, 125.5, 125.4, 32.4, 29.6, 22.7, 13.9.

3,3'-(5',5''-(Benzo[c][1,2,5]thiadiazole-4,7-diyl)bis(3'-methyl-2,2'-bithiophene-5',5-diyl))bis(2-isocyanoacrylonitrile) (**4**). Bis-aldehyde **11** (55 mg, 0.09 mmol) was dissolved in 1,2-dichloroethane (5 ml) and malonitrile (115 mg, 1.8 mmol, 20 eq.) was added at room

temperature. Finally piperidine was added and the resulting mixture heated to 100 °C under microwave conditions. After 1 h of irradiation, TLC (silica, DCM) showed complete turnover. The mixture was extracted with DCM and water. Then the organic phase was dried over sodium sulfate and removed of the solvent. Column chromatography (silica, DCM) yielded product **4** as deep violet powder in a yield of 76% (48 mg, 0.07 mmol). **M.p.** (DSC): 300 °C. **^{1}H NMR** ([D_2]TCE, 500 MHz, 100 °C) δ ppm: 8.01 (s, 2H, Th-H), 7.90 (s, 2H, Ar-H), 7.76 (s, 2H, Vinyl-H), 7.73 (d, 2H, Th-H), 7.38 (d, 2H, Th-H), 2.92 (t, 4H, CH_2), 1.82-1.72 (m, 4H, CH_2), 1.55-1.47 (m, 4H, CH_2), 1.00 (t, 6H, CH_3). **^{13}C NMR** ([D_2]TCE, 125 MHz, 100 °C): n/a (insufficient solubility). **MS** (MALDI-TOF): *m/z* 728.1 $[M]^+$ (calc. for $C_{38}H_{28}N_6S_5$: 728.1). **Elemental analysis:** $C_{38}H_{28}N_6S_5$: calc. C, 62.61; H, 3.87; N, 11.53%; found: C, 62.64; H, 4.08; N, 11.24%.

4.6 References

[1] E. Bundgaard, F. C. Krebs, *Sol. Energy Mater. Sol. Cells* **2007**, *91*, 954.
[2] A. P. Kulkarni, Y. Zhu, S. A. Jenekhe, *Macromolecules* **2008**, *41*, 339.
[3] G. E. Gunbas, A. Durmus, L. Toppare, *Adv. Mater.* **2008**, *20*, 691.
[4] P. M. Beaujuge, S. Ellinger, J. R. Reynolds, *Adv. Mater.* **2008**, *20*, 2772.
[5] N. Blouin, A. Michaud, M. Leclerc, *Adv. Mater.* **2007**, *19*, 2295.
[6] J. H. Hou, H. Y. Chen, S. Q. Zhang, G. Li, Y. Yang, *J. Am. Chem. Soc.* **2008**, *130*, 16144.
[7] S. H. Park, A. Roy, S. Beaupre, S. Cho, N. Coates, J. S. Moon, D. Moses, M. Leclerc, K. Lee, A. J. Heeger, *Nat. Photon.* **2009**, *3*, 297.
[8] C. Kitamura, S. Tanaka, Y. Yamashita, *Chem. Mater.* **1996**, *8*, 570.
[9] H. A. M. Van Mullekom, J. A. J. M. Vekemans, E. W. Meijer, *Chem. Eur. J.* **1998**, *4*, 1235.
[10] C. J. Brabec, C. Winder, N. S. Sariciftci, J. C. Hummelen, A. Dhanabalan, P. A. v. Hal, R. A. J. Janssen, *Adv. Funct. Mater.* **2002**, *12*, 709.
[11] W. C. Chen, W. C. Wu, C. L. Liu, *Polymer* **2006**, *47*, 527.
[12] F. Zhang, K. G. Jespersen, C. Björström, M. Svensson, M. R. Andersson, V. Sundström, K. Magnusson, E. Moons, A. Yartsev, O. Inganäs, *Adv. Funct. Mater.* **2006**, *16*, 667.
[13] W. S. Shin, S. C. Kim, S.-J. Lee, H.-S. Jeon, M.-K. Kim, B. V. K. Naidu, S.-H. Jin, J.-K. Lee, J. W. Lee, Y.-S. Gal, *J. Polym. Sci. A* **2007**, *45*, 1394.
[14] S. Durben, D. Nickel, R. A. Krüger, T. C. Sutherland, T. Baumgartner, *J. Polym. Sci. A* **2008**, *46*, 8179.
[15] J. Lu, F. Liang, N. Drolet, J. Ding, Y. Tao, R. Movileanu, *Chem. Comm.* **2008**, 5315.
[16] M. Jayakannan, P. A. V. Hal, R. A. J. Janssen, *J. Polym. Sci. A* **2002**, *40*, 2360.
[17] M. Melucci, L. Favaretto, C. Bettini, M. Gazzano, N. Camaioni, P. Maccagnani, P. Ostoja, M. Monari, G. Barbarella, *Chem. Eur. J.* **2007**, *13*, 10046.
[18] M. Akhtaruzzaman, M. Tomura, J.-i. Nishida, Y. Yamashita, *J. Org. Chem.* **2004**, *69*, 2953.
[19] S. Song, Y. Jin, S. H. Kim, J. Moon, K. Kim, J. Y. Kim, S. H. Park, K. Lee, H. Suh, *Macromolecules* **2008**, *41*, 7296.
[20] Y. He, X. Wang, J. Zhang, Y. Li, *Macromol. Rapid Commun.* **2009**, *30*, 45.

[21] J. Mei, N. C. Heston, S. V. Vasilyeva, J. R. Reynolds, *Macromolecules* **2009**, *42*, 1482.
[22] J.-L. Wang, Z.-M. Tang, Q. Xiao, Y. Ma, J. Pei, *Org. Lett.* **2009**, *11*, 863.
[23] P. F. Xia, J. Lu, C. H. Kwok, H. Fukutani, M. S. Wong, Y. Tao, *J. Polym. Sci. A* **2009**, *47*, 137.
[24] P. Anant, N. T. Lucas, J. Jacob, *Org. Lett.* **2008**, *10*, 5533.
[25] M. Svensson, F. L. Zhang, S. C. Veenstra, W. J. H. Verhees, J. C. Hummelen, J. M. Kroon, O. Inganas, M. R. Andersson, *Adv. Mater.* **2003**, *15*, 988.
[26] Q. M. Zhou, Q. Hou, L. P. Zheng, X. Y. Deng, G. Yu, Y. Cao, *Appl. Phys. Lett.* **2004**, *84*, 1653.
[27] A. J. Moulé, A. Tsami, T. W. Bünnagel, M. Forster, N. M. Kronenberg, M. Scharber, M. Koppe, M. Morana, C. J. Brabec, K. Meerholz, U. Scherf, *Chem. Mater.* **2008**, *20*, 4045.
[28] J. K. Lee, W. L. Ma, C. J. Brabec, J. Yuen, J. S. Moon, J. Y. Kim, K. Lee, G. C. Bazan, A. J. Heeger, *J. Am. Chem. Soc.* **2008**, *130*, 3619.
[29] X. Chen, G. L. Schulz, X. Han, Z. Zhou, S. Holdcroft, *J. Phys. Chem. C* **2009**, *113*, 8505.
[30] M. Helgesen, S. A. Gevorgyan, F. C. Krebs, R. A. J. Janssen, *Chem. Mater.* **2009**, *21*, 4669.
[31] J. Hou, H. Y. Chen, S. Zhang, Y. Yang, *J. Phys. Chem. C* **2009**, *113*, 21202.
[32] J. Y. Kim, Y. Qin, D. M. Stevens, V. Kalihari, M. A. Hillmyer, C. D. Frisbie, *J. Phys. Chem. C* **2009**, *113*, 21928.
[33] Q. Li, C. Du, F. Li, Y. Zhou, M. Fahlman, Z. Bo, F. Zhang, *Chem. Mater.* **2009**, *21*, 5327.
[34] F. Liang, J. Lu, J. Ding, R. Movileanu, Y. Tao, *Macromolecules* **2009**, *42*, 6107.
[35] E. Wang, M. Wang, L. Wang, C. Duan, J. Zhang, W. Cai, C. He, H. Wu, Y. Cao, *Macromolecules* **2009**, *42*, 4410.
[36] S. Wen, J. Pei, Y. Zhou, P. Li, L. Xue, Y. Li, B. Xu, W. Tian, *Macromolecules* **2009**, *42*, 4977.
[37] W. Yue, Y. Zhao, S. Shao, H. Tian, Z. Xie, Y. Geng, F. Wang, *J. Mater. Chem.* **2009**, *19*, 2199.
[38] W. Yue, Y. Zhao, D. Song, H. Tian, Z. Xie, D. Yan, Y. Geng, F. Wang, *Macromolecules* **2009**, *42*, 6510.
[39] J. Kim, S. H. Kim, I. H. Jung, E. Jeong, Y. Xia, S. Cho, I. W. Hwang, K. Lee, H. Suh, H. K. Shim, H. Y. Woo, *J. Mater. Chem.* **2010**, *20*, 1577.
[40] J. Kim, S. H. Park, S. Cho, Y. Jin, I. Kim, J. S. Lee, J. H. Kim, H. Y. Woo, K. Lee, H. Suh, *Polymer* **2010**, *51*, 390.
[41] W. Y. Lee, K. F. Cheng, T. F. Wang, W. C. Chen, F. Y. Tsai, *Thin Solid Films* **2010**, *518*, 2119.
[42] H. Zhou, L. Yang, S. Xiao, S. Liu, W. You, *Macromolecules* **2010**, *43*, 811.
[43] P. Sonar, S. P. Singh, S. Sudhakar, A. Dodabalapur, A. Sellinger, *Chem. Mater.* **2008**, *20*, 3184.
[44] J. A. Kong, E. Lim, K. K. Lee, S. Lee, S. H. Kim, *Sol. Energy Mater. Sol. Cells* **2010**, *doi:10.1016/j.solmat.2010.06.016*.
[45] K. Schulze, B. Maennig, K. Leo, Y. Tomita, C. May, J. Hüpkes, E. Brier, E. Reinold, P. Bäuerle, *App. Phys. Lett.* **2007**, *91*, 073521.
[46] K. Schulze, C. Uhrich, R. Schüppel, K. Leo, M. Pfeiffer, E. Brier, E. Reinold, P. Bäuerle, *Adv. Mater.* **2006**, *18*, 2872.
[47] C. Uhrich, R. Schüppel, A. Petrich, M. Pfeiffer, K. Leo, E. Brier, P. Kilickiran, P. Bäuerle, *Adv. Funct. Mater.* **2007**, *17*, 2991.
[48] R. Schüppel, K. Schmidt, C. Uhrich, K. Schulze, D. Wynands, J. L. Brédas, E. Brier, E. Reinold, H.-B. Bu, *Phys. Rev. B* **2008**, *77*, 085311.

[49] F. Würthner, S. Yao, T. Debaerdemaeker, R. Wortmann, *J. Am. Chem. Soc.* **2002**, *124*, 9431.
[50] F. F. Mancilha, B. A. D. Neto, A. S. Lopes, P. F. J. Moreira, F. H. Quina, R. S. Goncalves, J. Dupont, *Eur. J. Org. Chem.* **2006**, 4924.
[51] J. Krömer, P. Bäuerle, *Tetrahedron* **2001**, *57*, 3785.
[52] T. Pinault, F. Chérioux, Bruno Therrien, G. Süss-Fink, *Heteroatom. Chem.* **2004**, *15*, 121.

Chapter 5

Benzothiadiazole and Thiadiazolo pyridine as Terminal Acceptors in A-D-A-type Oligothiophenes

Abstract

Novel A-D-A-type oligothiophenes incorporating benzothiadiazole (BTDA) or thiadiazolo pyridine (TDAPy) as terminal acceptor groups have been developed for vacuum and solution processed "small molecule" solar cells (SMSC). Vacuum-processed planar heterojunction devices based on TDAPy showed a high open circuit voltage (V_{OC}) of 1.0 V, a short-circuit current density (J_{SC}) of 4.7 mA cm^{-2}, and a fill factor (*FF*) of 0.67, resulting in a power conversion efficiency (PCE) of 3.15% under AM1.5G conditions. Solution processed devices based on BTDA produced a V_{OC} of 0.93 V, a J_{SC} of 4.4 mA cm^{-2}, a *FF* of 0.37, and hence a PCE of 1.56% under standard reporting conditions.

5.1 Introduction

Introducing a thienothiadiazole (TTDA), thienopyrazine (TP) or benzothiadiazole (BTDA) moiety as an additional electron acceptor into the core of DCV5T[1-5]-analogous structures resulted in all cases in a lowering of the solar cell efficiency (Chapter 4 and 5). The electron deficient core unit in an A-D-A-D-A-type oligothiophene could lead to an undesired concentration of the LUMO electron density at the center of the molecules, thus constituting a hole trap in the thin films and resulting in the observed modest device performances.

However, the BTDA unit could still be of interest to replace the terminal DCV-groups in the DCVnT-series, due to its excellent thermal stability, high absorption coefficient, suitable HOMO and LUMO energy levels, and strong intermolecular π-π interactions, leading to ordered morphologies in the solid state (Chapter 5).[6-16] Less explored in the field of organic photovoltaics is the BTDA-analogous thiadiazolo[3,4-*c*]pyridine (TDAPy), which has due to its pyridine-based structure a stronger electron withdrawing force than the BTDA unit. In 2008, Leclerc and co-workers reported a low band gap polymer, PCDTPT, comprising TDAPy and carbazole units for use in solution-processed bulk heterojunction (BHJ) solar cells (Figure 1).[17]

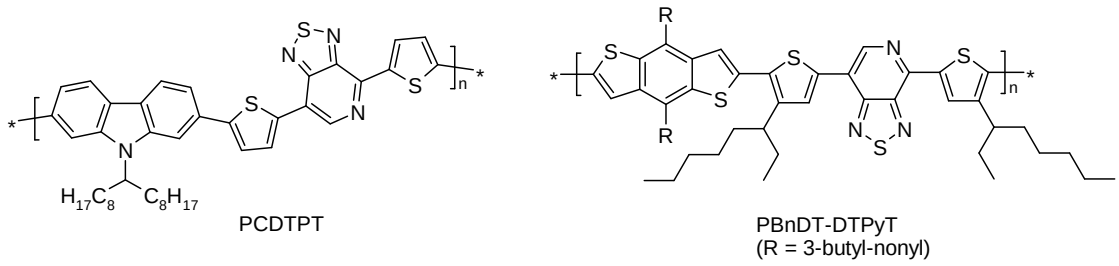

Figure 1: Thiadiazolo pyridine-based polymer for solution-processed BHJSC.[17]

In comparison to the corresponding BTDA polymer, the pyridine moiety decreased both, HOMO and LUMO energy levels, resulting in a low band gap of 1.73 eV. A BHJ solar cell gave a moderate PCE of 0.7%. Very recently, You *et. al.* assembled highly efficient solution-processed solar cells based on TDAPy-comprising polymers.[18] Polymer PBnDT-DTPyT evinced a very high lying LUMO energy level of 3.44 eV (as determined by cyclic voltammetry measurements) and as a consequence, the photovoltaic devices showed a high V_{OC} of 0.85 V and an overall efficiency of 6.3% (Figure 1). Thus, TDAPy could be an interesting building block for oligomers in "small molecule" solar cells (SMSC), because of: *1*. its greater acceptor strength compared to BTDA and *2*. the additional nitrogen at the pyridine of the TDAPy unit, which may lead to better stacking in the solid state, due to stronger intermolecular interactions.

The objective of this study was the synthesis and characterization of novel A-D-A-type oligomers up to the heptamer, comprising an oligothiophene donor as core end-capped with electron accepting BTDA or TDAPy moieties. Depicted in Figure 2 are the corresponding target structures **1**-**4**.

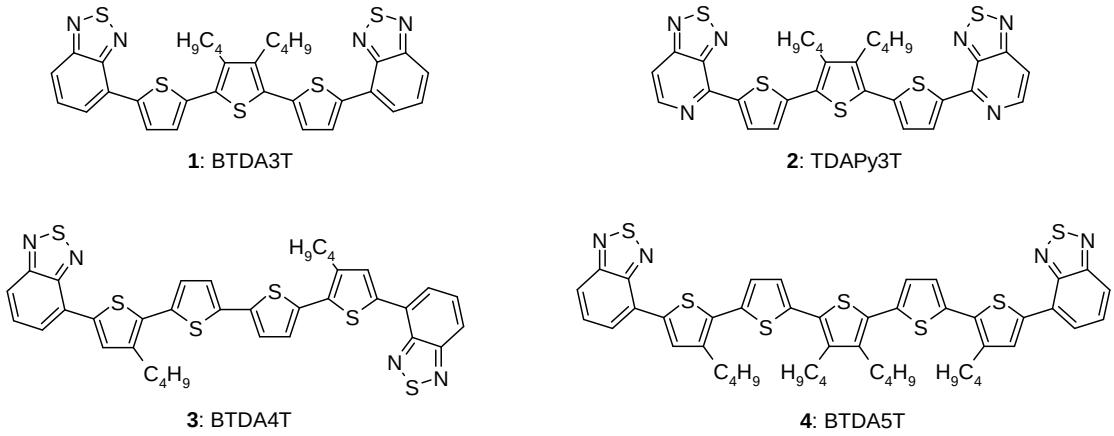

Figure 2: Novel target structures **1**-**4** end-capped with benzothiadiazole or thiadiazole pyridine for oligomer solar cells.

The application of these materials as donor in organic solar cells prepared by vacuum and solution processing is described.

5.2 Synthesis

A-D-A-type terthiophenes **1** and **2** were synthesized according to Scheme 1. Terthiophene **5** was prepared according to literature[19] and reacted with *n*-BuLi and trialkyltin chloride to give bis-stannylated terthiophene **6a** and **6b** in 50 and 77% yield, respectively. Microwave-assisted Pd^0-catalyzed Stille-type coupling reaction of **6a** and 4-bromobenzo[*c*][1,2,5]-thiadiazole **7**[20] afforded BTDA3T **1** in 21% yield.

Thiadiazolo-pyridine-functionalized pentamer **2** was synthesized in analogy to BTDA derivative **1**. In order to improve the yield of the coupling reaction, tributyl stannane **6a** was switched to the corresponding trimethyl derivative **6b**, which is accessible in higher purity by recrystallization from methanol. Thiadiazolo pyridine **8** was obtained in a modest yield of 19% by ring closure reaction of 2-bromopyridine-3,4-diamine[21] with thionyl chloride.[17] During this reaction, the bromine atom is substituted by chlorine, as proven by mass spectra and NMR analysis. Using thionylaniline instead of thionyl chloride did not improve the reaction

yield and resulted in undesired products, as reported for analogue systems.[17] Due to the electron deficiency of the carbon atom near the N-position, compound **8** is highly activated for nucleophilic substitution, rendering it difficult to obtain the product in higher yields. Furthermore, under non-protective atmosphere, the chlorine atom is quickly replaced with a hydroxy group from air moisture.

Microwave-assisted Stille coupling of **6b** and **8** gave title compound TDAPy3T **2** as dark red powder in 48% yield. The unusual good performance of chlorine-based compound **8** in the Stille-type coupling reaction might be due to the fact that, *1.* the nitrogen binds coordinatively to the Pd-center during the catalytic cycle[22] and *2.* an electron deficiency of the chlorine, which facilitates the oxidative addition to palladium. The chlorine atom in **8** is highly activated for hydrolysis at ambient temperature under non-protective atmosphere, which also indicates the electron deficiency of the halide.

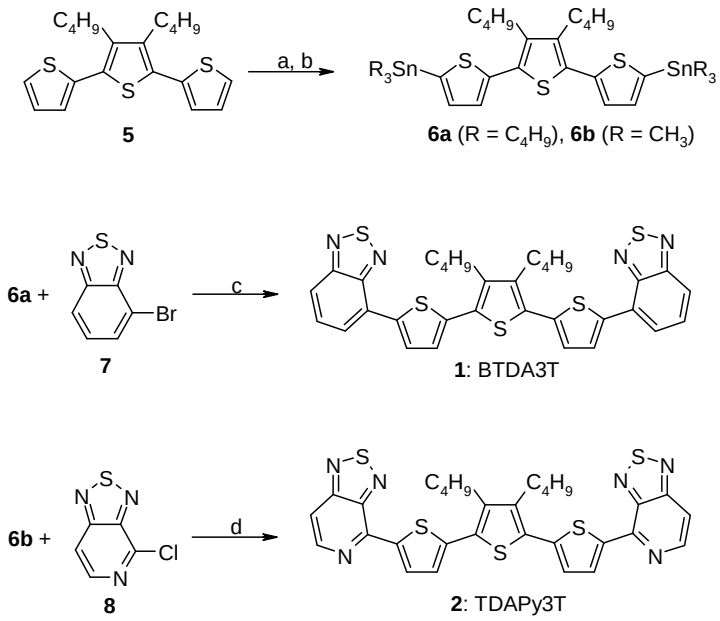

Scheme 3: a) 1. *n*-BuLi, 2. tributyltin chloride, THF, -50 °C to 0 °C, 2 h, 77%; b) 1. *n*-BuLi, 2. trimethyltin chloride, THF, -50 °C to 30 °C, 2 h, 50%; c) CsF, $Pd(PPh_3)_2Cl_2$, 1,2-DCE, DMF, 100 °C, microwave, 4 h, 21%; d) $Pd(PPh_3)_2Cl_2$, DMF, 90 °C, microwave, 2 h, 48%.

Novel BTDA-based quater- and quinquethiophenes **3** and **4** were synthesized according to Scheme 2. A Stille-type coupling reaction of 4-bromobenzo[*c*][1,2,5]thiadiazole **7** and tributyl-(4-butyl-thiophen-2-yl)-stannane[23] afforded **9** in 59% yield. The stannane in this reaction was prepared in analogy to reference [23].

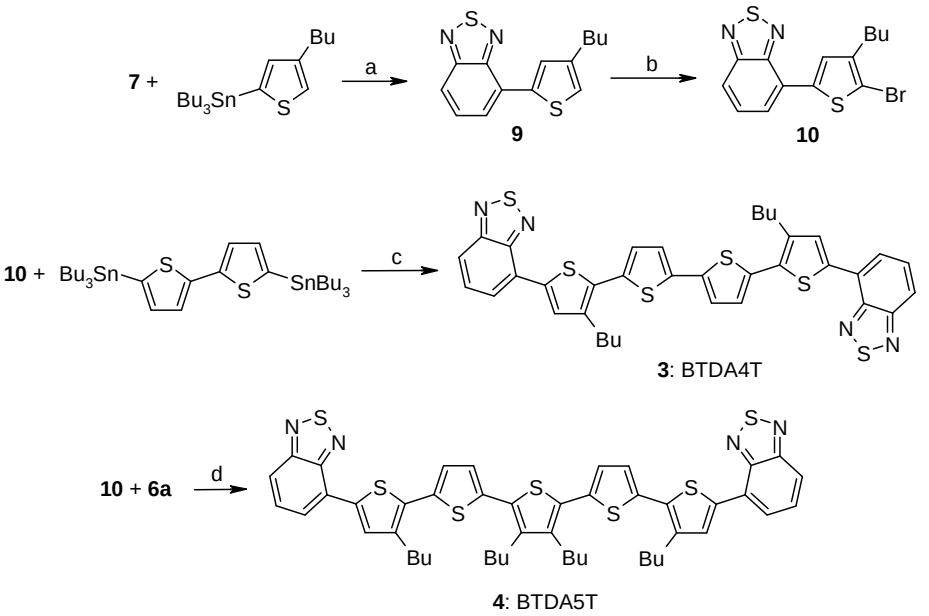

Scheme 4: Synthesis of novel oligothiophenes **3** and **4**. a) $Pd(PPh_3)_2Cl_2$, DMF, 100 °C, microwave, 2 h, 59%; b) NBS, chloroform, 0 °C – r.t., 1 h, 95%; c) CsF, $Pd(PPh_3)_2Cl_2$, 1,2-dichloroethane, 100 °C, microwave, 4 h, 57%; d) CsF, $Pd(PPh_3)_2Cl_2$, 1,2-DCE, 100 °C, microwave, 5 h, 53%.

In the course of synthesizing TDAPy3T **2**, Stille-type cross-coupling reactions of 7-bromo-4-chloro-[1,2,5]thiadiazolo[3,4-c]pyridine[17] **11** with stannylated terthiophene **6a** were carried out (Scheme 3). MALDI-TOF measurements and thin layer chromatography (TLC) revealed qualitative coupling tendencies of bromine and chlorine in **11**, depending on the catalytic system. Application of Stille standard catalyst $Pd(PPh_3)_2Cl_2$ in DMF afforded a product ratio of **A**:**B**:**C** = 2:5:1 (chlorine coupling preferred), while under similar reaction conditions a ratio of **A**:**B**:**C** = 3:1:1 (bromine coupling preferred) was obtained by use of the more active catalyst Pd_2dba_3 with trifurylphosphine (TFP) as ligand in THF. This result is in agreement with the observed good coupling tendency of chloride **8** during the preparation of title compound **2** (Scheme 1).

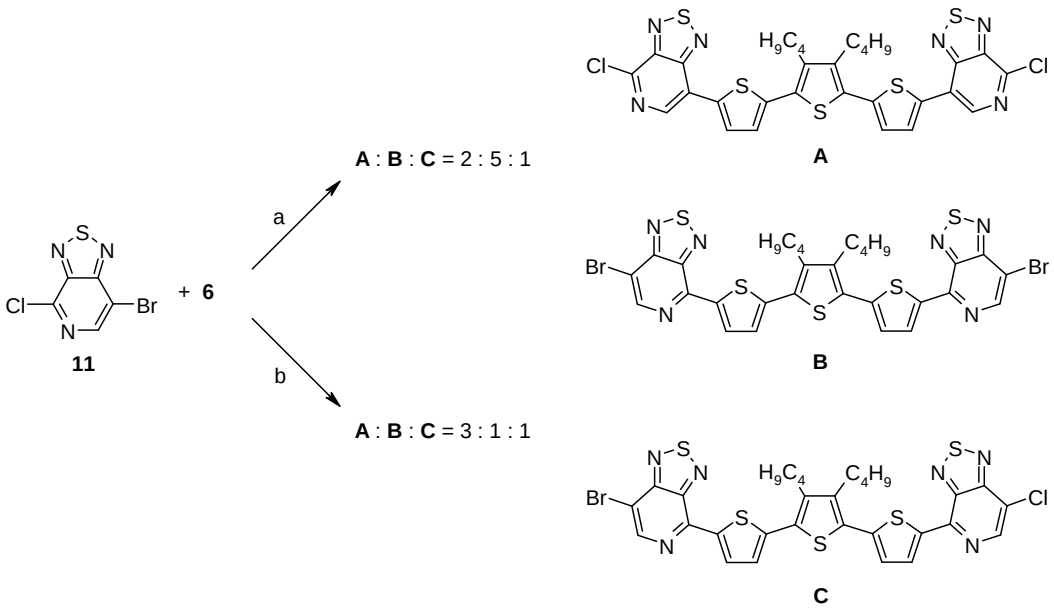

Scheme 3: a) $Pd(PPh_3)_2Cl_2$, DMF, rt, 2 d; b) Pd_2dba_3, TFP, THF, rt, 2 d.

5.3 Physical Properties

Physical and optical properties were investigated to deduce structure-property relations of the novel A-D-A-type oligothiophenes and to determine their suitability for photovoltaic applications.

5.3.1 Steady-State Spectroscopy

Electronic absorption spectra of compounds **1**-**4** in solution (dichloromethane) and of thin films (30 nm) are presented in Figure 3 and corresponding data are summarized in Table 1.

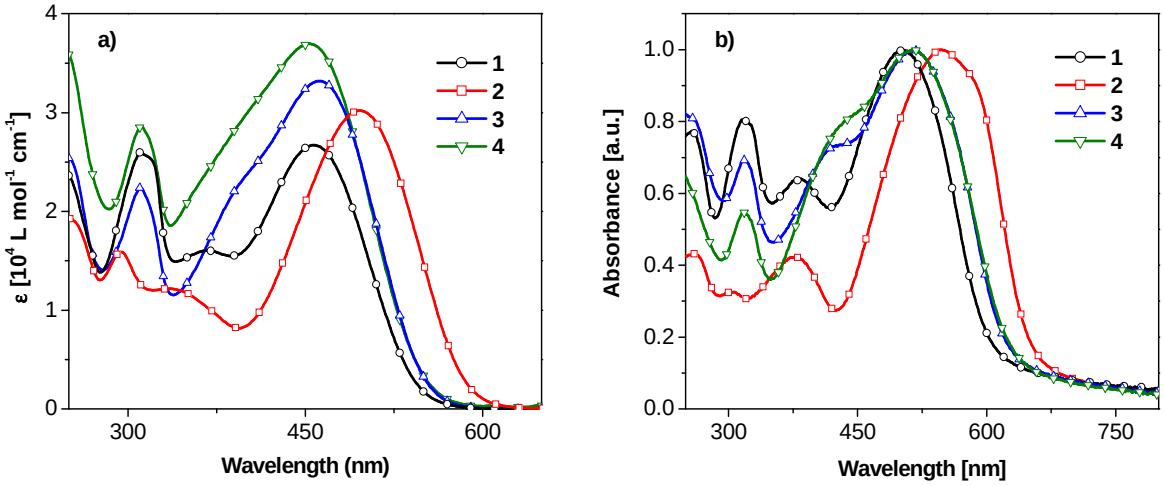

Figure 3: Absorption spectra of title compounds **1**-**4** in a) solution b) solid state, 30 nm thin film prepared by vacuum evaporation.

BTDA derivatives **1**,**3** and **4** showed a longest wavelength absorption maximum at 458, 462 and 454 nm, respectively, which corresponds to a blue-shift of about 50 nm, when compared to the corresponding DCV-derivatives, reported earlier by our group.[3-4] The hypsochromic shift can be assigned to the weaker acceptor strength of the terminal BTDA functionalities compared to the DCV units.

Table 1: UV-vis data of title compounds **1**-**4** in dichloromethane solution ([c] = 10^{-5} M) and solid state, 30 nm thin film prepared by vacuum evaporation.

Compound	λ_{abs} (nm)	ε [a] (L mol^{-1} cm^{-1})	λ_{Onset} (nm)	E_g^{opt} (eV)	λ_{abs}^{solid} (nm)
BTDA3T (**1**)	310, 364 (sh), 458	27000	541	2.29	503
TDAPy3T (**2**)	295, 336 (sh), 496	31000	592	2.09	548
BTDA4T (**3**)	310, 462	32500	548	2.26	516
BTDA5T (**4**)	311, 454	37000	547	2.27	513

[a] The molar extinction coefficient values are given for the longest wavelength absorption band.

With increasing number of thiophene units in BTDA **1** ,**3** and **4**, a significant spectral broadening and raise of the molar absorption was observed, whereas the lowest energy absorption maxima were bathochromically shifted by less than ten nanometers. The broadening mainly occurred towards higher energies, leading to similar onset values of the longest wavelength absorption bands (541 nm, 548 nm and 547 nm, respectively), and thus almost identical band gaps of the three compounds (2.29 eV, 2.26 eV and 2.27 eV, respectively). When comparing quaterthiophene **3** and quinquethiophene **4**, the observed blue-shift of 8 nm despite a larger π-system, is probably caused by steric hindrance of β-butyl groups in compound **4**. TDAPy **2**, however, shows a longest wavelength absorption maximum at 496 nm, which is red-shifted around 40 nm compared to BTDA compounds **1**, **3** and **4** and is in agreement with the increased acceptor strength of the TDAPy moiety. Furthermore, a decrease of about 30-40% of the molar extinction coefficients was observed for the longest wavelength absorption maxima of **1**-**4**, when compared to the DCVnT-series (DCV3T: 48500, DCV4T: 37000, DCV5T: 51500 L mol^{-1} cm^{-1}). The observed multiple absorption bands for the investigated oligomers at higher energies (< 400 nm) can be assigned to the combined transitions of the terminal chromophores and the oligothiophene core.

Compared to the solution spectra, the longest wavelength absorption maxima of compounds **1**-**4** in thin films, prepared by vacuum sublimation, are significantly red-shifted

(Figure 3b). A bathochromic shift of around 50 nm on the low energy band is observed, which is presumably caused by intermolecular π-π stacking and ordering of the molecules in the bulk (Figure 3b). In accordance with the spectral analysis in solution, hardly any shift of the longest wavelength absorption maximum is found for BTDA-based oligomers **1**, **3** and **4**, despite the varying thiophene chain length. The significant broadening of the absorption spectrum of **2** as compared to **1** may indicate better ordering of the molecules in the bulk and is manifested in the behavior of the external quantum efficiency (EQE).

5.3.2 Theoretical calculations

We investigated the influence of the BTDA and TDAPy units on the π-system of compounds **1** and **2**, respectively, and the nature of the electronic transitions by theoretical calculations at a semi-empirical level (Austin Model 1). The most stable conformations show an all-trans arrangement of the aromatic units with average torsion angles around 25° for TDAPy **2** and 31° for BTDA **1** (Figure 4, Table 2).

Table 2: Semi-empirically calculated (AM1) torsion angles along the aromatic units of compound **1** and **2**.

Compound	A-Th	Th-Th	Th-Th	Th-A
BTDA3T (**1**)	37°	24°	25°	38°
TDAPy3T (**2**)	28°	21°	21°	28°

The slightly less twisted conjugated backbone in **2** is ascribed to a reduced sterical hindrance of the thiophene rings adjacent to TDAPy when compared to BTDA. For both compounds the electron density of the HOMO is mainly distributed over the oligothiophene core, whereas the electron density of the LUMO prevails on the terminal acceptor moieties. Furthermore, the HOMO of TDAPy **2** evinces a particularly low electron density at the N-position of the pyridines, which is the only distinctive difference in the calculated isosurfaces.

1

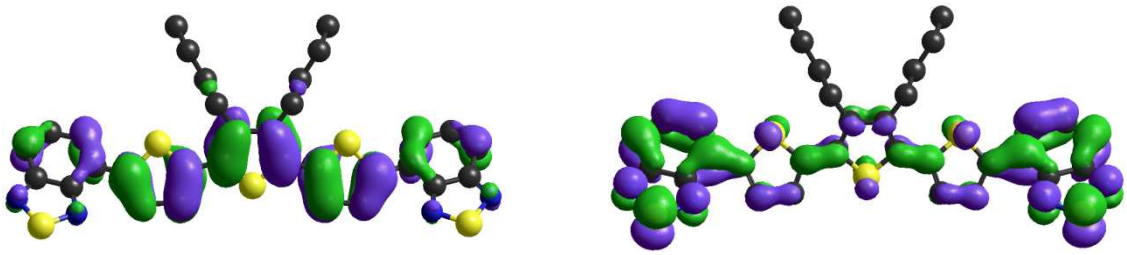

2

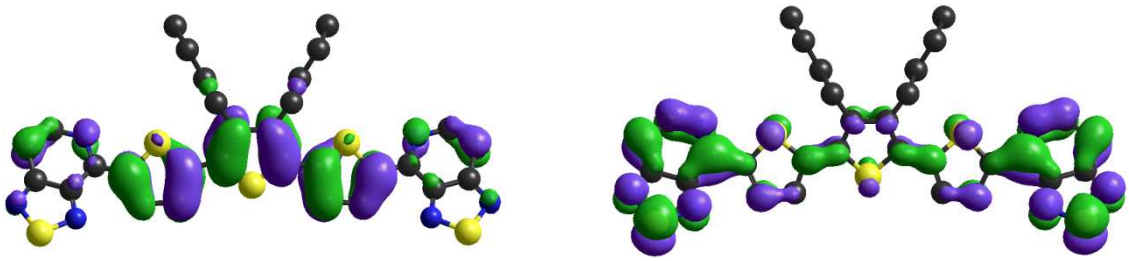

HOMO **LUMO**

Figure 4: Electron density distribution of the frontier orbitals in BTDA **1** and TDAPy **2** obtained from semi-empirical AM1 calculations (carbon atoms in black, nitrogen in blue, sulfur in yellow and hydrogen atoms are omitted for clarity reasons).

Furthermore, the calculated electronic transitions (ZINDO/S) at 566 and 531 nm for TDAPy **2** and BTDA **1**, respectively, exhibit no charge transfer character and correspond well to the empirically determined absorption bands at 548 and 503 nm.

5.3.3 Electrochemical Studies

Cyclic voltammograms of title compounds **1**-**4** in dilute dichloromethane solution are depicted in Figure 5, and the corresponding electrochemical data, HOMO and LUMO energy levels are collected in Table 3.

Table 3: Summarized cyclovoltammetry data of title compounds **1**-**4** (DCM, HOMO/LUMO vs. Fc/Fc^{+}_{vac} = 5.1 eV).

Compound	$E°_{ox1}$ (V)	$E°_{ox2}$ (V)	$E°_{red1}$ (V)	HOMO (eV)	LUMO (eV)	ΔE^{CV} (eV)
BTDA3T (**1**)	0.47	0.84	-1.83	-5.50	-3.34	2.16
TDAPy3T (**2**)	0.63	1.03	-1.56	-5.65	-3.64	2.01
BTDA4T (**3**)	0.34	0.63	-1.85	-5.39	-3.33	2.06
BTDA5T (**4**)	0.31	0.55	-1.83	-5.36	-3.33	2.03

In cyclic voltammetry measurements, the oxidative regime of **3** showed two quasi-reversible and one irreversible wave (Figure 5). Two reversible or quasi-reversible oxidation waves were observed for compounds **1**, **2** and **4**, which can be assigned to the stepwise oxidation of the oligothiophene core and the formation of radical cations and dications, respectively. Furthermore, the investigated compounds showed each a fully reversible $2e^{-}$ reduction wave, which is correlated to the reduction of the terminal acceptors and the formation of independent radical anions.

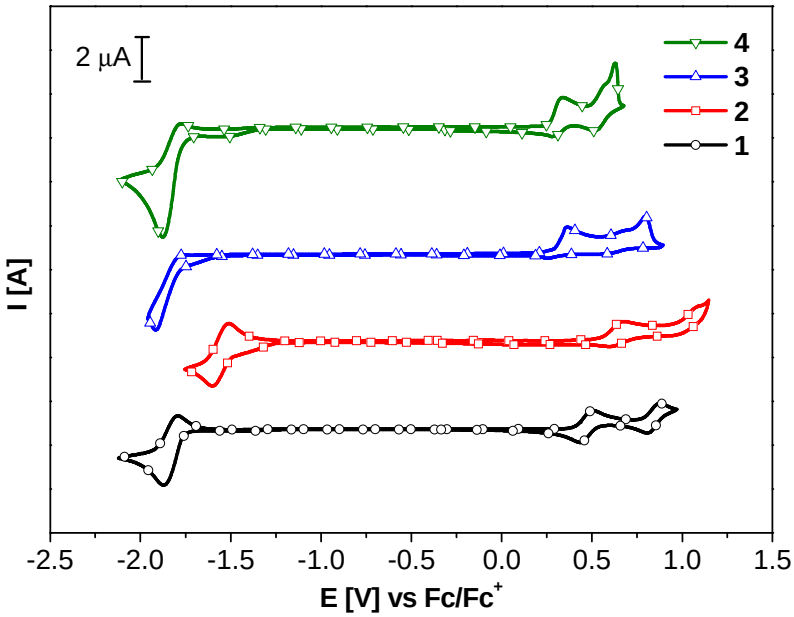

Figure 5: Cyclic voltammograms of title compounds **1**-**4** (1×10-3 mol·L-1) in dichloromethane-$TBAPF_6$ (0.1M), scan speed 100 mV/s, potentials *vs.* Fc/Fc^+.

Reflecting the stronger electron withdrawing nature of the pyridine-based acceptor group, TDAPy **2** showed a first oxidation potential at 0.63 V and a reduction potential at -1.56 V, which is positively shifted by 0.16 V and 0.27 V, respectively, in comparison to analogous BTDA-derivative **1**. The electrochemical band gaps are well supported by the optical band gaps, i.e. the replacement of the BTDA units by the π-electron deficient TDAPy units shows a smaller band gap. Both HOMO and LUMO energy levels are shifted to more positive values when compared to the corresponding DCV-derivatives,[3-5] indicating that BTDA and TDAPy are weaker acceptors than the terminal DCV-groups. We further elucidated, with increasing number of thiophene units, the oxidation potentials of BTDA-based compounds **1**, **3** and **4** were reduced from 0.47 to 0.31 V, resulting in a minor raise of the HOMO energy levels from -5.50 to -5.36 eV. The compounds also show almost equal reduction potentials (**1**: -1.83 V, **2**: -1.85 V, **3**: -1.83 V), thus, the length of the oligothiophene core has no influence on the size of the band gap.

5.3.4 Thermal Properties

Thermal stability of the compounds was investigated by thermogravimetric analysis (TGA) and differential scanning calorimetry (DSC). The onset of the decomposition temperatures (T_d) in TGA were at about 440 °C for compound **3** and **4** (Figure 6). Compound **1** and **2** were not subjected to TGA.

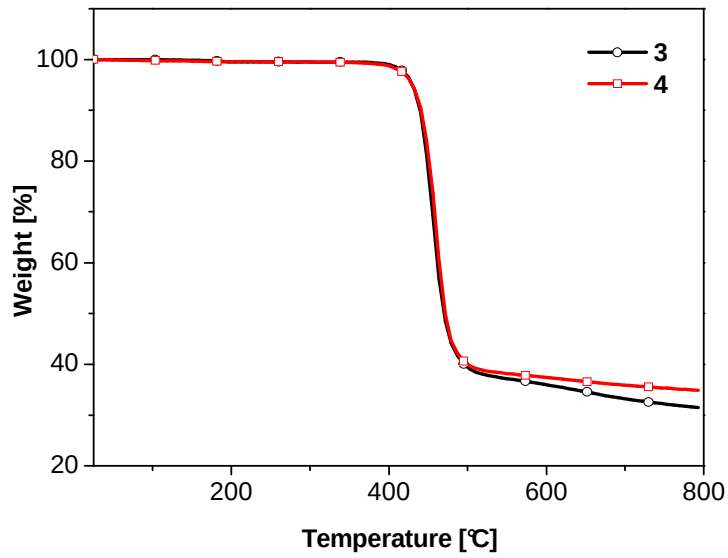

Figure 6: TGA thermograms of compounds **3** and **4** measured under N_2. Conditions: N_2 flow, 50 mL/min; heating rate, 10 ^{o}C/min.

DSC-analysis of title compounds **1**, **3** and **4** were carried out and melting points of 141, 184 and 160 °C, respectively, were observed (Figure 7). The melting point of TDAPy **2** was determined by a *Büchi B-545* apparatus as 167-169 °C. No exothermic peaks, and hence no sign of decomposition was found in the DSC measurements within the temperature range up to 400 °C.

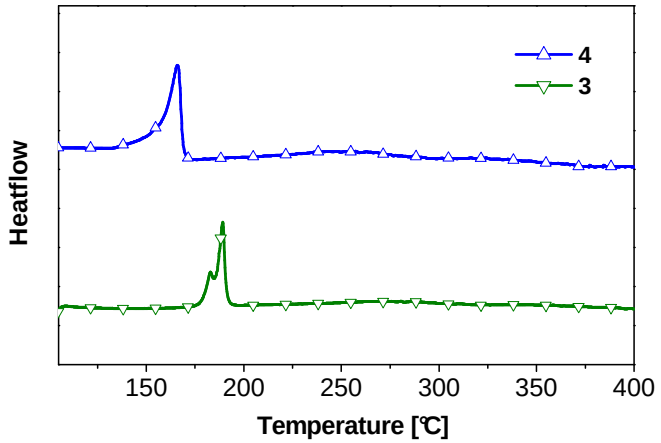

Figure 7: Representative DSC curves of BTDA **3** and **4**.

BTDA **3** evinced a distinct shoulder during the melting process, which could be due to a solid state phase transition.

These results indicate good thermal stability of the investigated compounds, and conclusively, excellent sublimation yields were found while processing the materials by vacuum deposition technique.

5.4 Photovoltaic Performance

5.4.1 Vacuum-processed Solar Cells

Figure 8a shows the mismatch corrected current density-voltage (*J-V*) characteristics of representative m-i-p type planar heterojunction (PHJ) and bulk heterojunction (BHJ) solar cells. The PHJ layer structure is: ITO/C_{60} (15 nm)/donor (10 nm)/Di-NPB (5 nm)/Di-NPB:NDP9 (53 nm 5wt%)/NDP9 (1 nm)/Au (50 nm). Characterictic solar cell data are summarized in Table 4. The cells were prepared by keeping the substrate at room temperature and all cells were measured with an aperture mask of 2.76 mm^2. A clear rectification behaviour is observed in the dark.

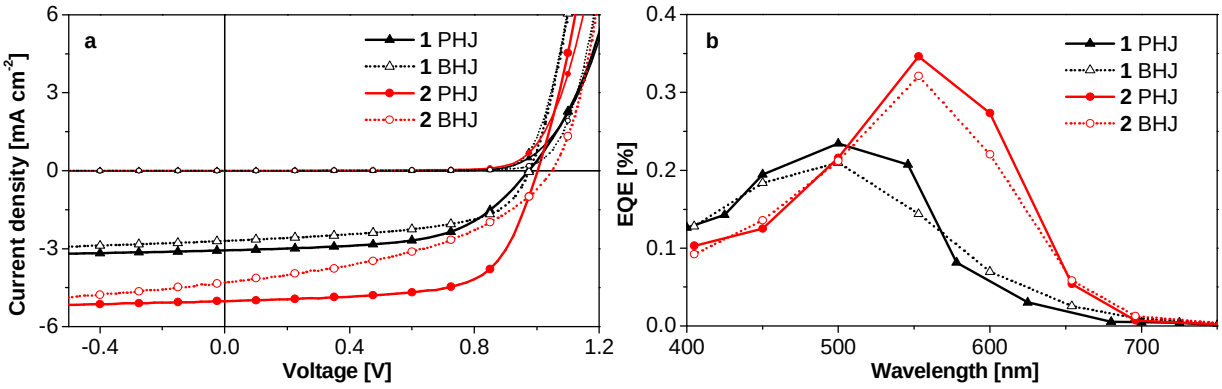

Figure 8: a) *J-V* characteristics of m-i-p type PHJ and BHJ solar cells using BTDA **1** and TDAPy **2** as donors under AM 1.5G white light illumination at 100 mW cm^{-2}. b) EQE spectra of the corresponding PHJ and BHJ solar cells of **1** and **2**.

The PHJ-device based on compound **1** gave an open circuit voltage V_{OC} of 0.98V, a short circuit current density (J_{SC}) of 3.1 mA cm^{-2}, and a fill factor (*FF*) of 0.57, leading to a PCE of 1.73% under simulated solar illumination in AM1.5 conditions. In contrast, devices based on TDAPy **2** delivered a superior performance with a V_{OC} of 1.00 V, a J_{SC} of 4.7 mA cm^{-2}, and a *FF* of 0.67, thus improving the PCE to 3.15%. The excellent *FF* obtained with **2** could be due to better stacking in the thin film, caused by intermolecular H-bonding interactions via the nitrogen atom of the pyridine ring. Reducing the layer thickness of the investigated compounds to 6 nm resulted in only slightly changed values in the device performances.

Table 4: Characteristic solar cell data of oligomers **1**-**4** as donor and C_{60} as acceptor in vacuum-processed planar and bulk heterojunction m-i-p-type solar cells. The blend layers in BHJ devices comprised a mixture ratio of donor:C_{60} of 2:1 (w/w).

Compound	Architecture	Layer (nm)	V_{OC} (mV)	J_{SC} (mA cm^{-2})	*FF*	η (%)
BTDA3T **1**	PHJ	6	0.96	3.0	0.63	1.81
BTDA3T **1**	PHJ	10	0.98	3.1	0.57	1.73
BTDA3T **1**	BHJ, 90 °C[a]	20	0.98	2.7	0.57	1.50
TDAPy3T **2**	PHJ	6	1.01	3.9	0.73	2.88
TDAPy3T **2**	PHJ	10	1.00	4.7	0.67	3.15
TDAPy3T **2**	BHJ, 70 °C[a]	20	1.05	4.5	0.46	2.17
TDAPy3T **2**	BHJ, 90 °C[a]	20	1.05	4.3	0.43	1.94
BTDA4T **3**	PHJ	6	0.78	3.5	0.58	1.58
BTDA4T **3**	PHJ	10	0.79	3.8	0.56	1.68
BTDA5T **4**	PHJ	6	0.73	3.5	0.61	1.56
BTDA5T **4**	PHJ	10	0.74	3.6	0.60	1.60

[a] Temperature of the substrate during the layer deposition.

BHJ solar cells were prepared using a blend layer of oligomers **1** or **2** and C_{60} with the layer sequence: ITO/C_{60} (15 nm)/donor:C_{60} ((20 nm, 2:1)/BPAPF (5 nm)/ BPAPF:NDP9 (50 nm, ~10wt%)/NPD9 (1 nm)/Au (50 nm)**.** The blend layer was deposited at a substrate temperature of 90 ^{o}C. In comparison to the PHJ solar cells described above, an additional layer of C_{60} was used to stabilize the contact to the ITO. The decrease of the efficiency to 1.5% in the case of the BTDA **1**-based BHJ device as compared to the PHJ cell is due to a decrease in the shortcut current density (J_{SC}). On the other hand, devices prepared with TDAPy **2** showed a large decrease of the efficiency to 1.99% due to lower J_{SC} and *FF* values. Although the poorer performance of the BHJ device for **2** is not clearly understood at this stage, the lower *FF* value of 0.43 could be an indication for a different organization of the molecules in the blended films. This is further corroborated by the slight decrease of the J_{SC} value. Furthermore, when applying a lower substrate temperature of 70 °C during the layer deposition, a slightly higher *FF* value of 0.46 was observed. This indicates, that the organized alignment of the molecules could be lost due to thermal rearrangement at higher temperatures.

Figure 8b shows the EQE measurements of the dyes in PHJ and BHJ solar cells. In the optimized PHJ solar cells, both compounds **1** and **2** display reasonable EQE values with a maximum of 23% at 500 nm and 35% at 550 nm, respectively. The EQE maxima are in good agreement with the thin film absorption spectrum. The J_{SC} values calculated by integration of the EQE

curves with the AM1.5 spectrum are close to the experimental values, indicating minor spectral mismatch. The higher J_{SC} for the device with **2** compared to the device based on **1** is reflected in the higher EQE values in the red wavelength region.

J-V curves of PHJ solar cells comprising BTDA **3** and **4** as 10 nm thin films with the same layer sequence as described above, are shown in Figure 9, and Table 4 summarizes the corresponding solar cell data.

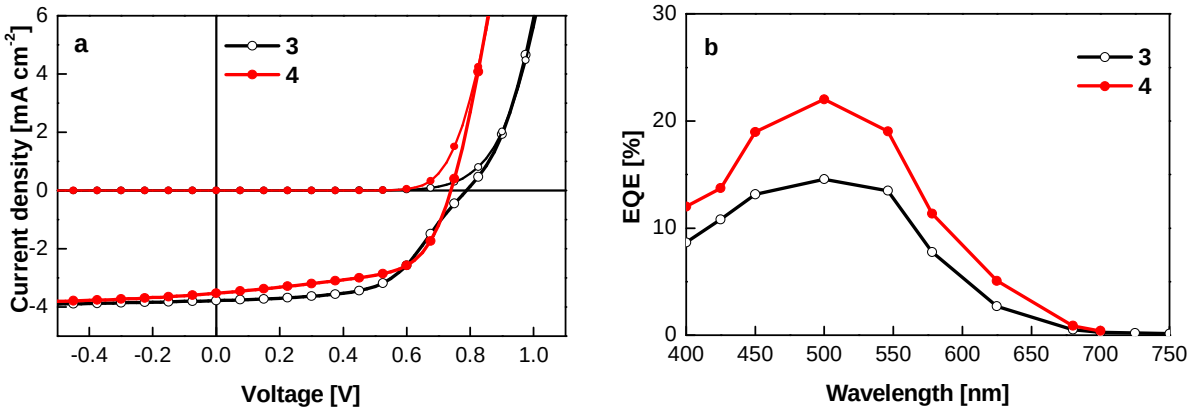

Figure 9: a) *J-V* characteristics of PHJ solar cells using 10 nm thin films of BTDA **3** or **4** as donors and fullerene C_{60} as acceptor under AM 1.5G white light illumination at 100 mW cm^{-2}. b) EQE spectra of the corresponding PHJ solar cells of **3** and **4**.

Applied as 10 nm thin films in a PHJ solar cells, we observed for BTDA **3** an open circuit voltage (V_{OC}) of 0.79 V, a shortcut current density (J_{SC}) of 3.8 mA cm^{-2}, a fill factor (*FF*) of 0.56, and hence an efficiency of 1.68%. The slight S-shape in the *J-V* curve hints at an energetic barrier between the different transporting layers. In a similar configuration, BTDA **4** showed a slightly lower V_{OC} of 0.74 V, a shortcut current density (J_{SC}) of 3.6 mA cm^{-2}, a fill factor value of 0.60, and an overall PCE of 1.60%. Both compounds, BTDA **3** and **4** gave reasonable EQE values according to their absorption spectra with a maximum of 15% and 22%, respectively, at 500 nm.

To conclude, very high V_{OC} values of ~1.0 V and reasonable fill factors (*FF*) around 0.6 were observed for compounds **1**-**4**, which are in the same range as reported values for corresponding DCV-substituted derivatives. In general, the solar cell performance of the investigated devices comprising BTDA compounds **1**, **3** and **4**, dropped with increasing length of the oligothiophene backbone, which is presumably due to better packing of the shorter oligothiophenes in the bulk. TDAPy-based terthiophene **2** showed outstanding cell

characteristics with high efficiencies, probably due to strong intermolecular interactions, causing well defined packing in the solid state.

5.4.2 Solution-processed Solar Cells

We further prepared bulk heterojunction solar cells (BHJSCs) applying BTDA-based dyes **3** and **4** by solution processing. *J-V* characteristics of these devices were measured with 100 mW cm^{-2} simulated solar light under AM1.5G conditions and are depicted in Figure 9. The characteristic solar cell data are collected in Table 5.

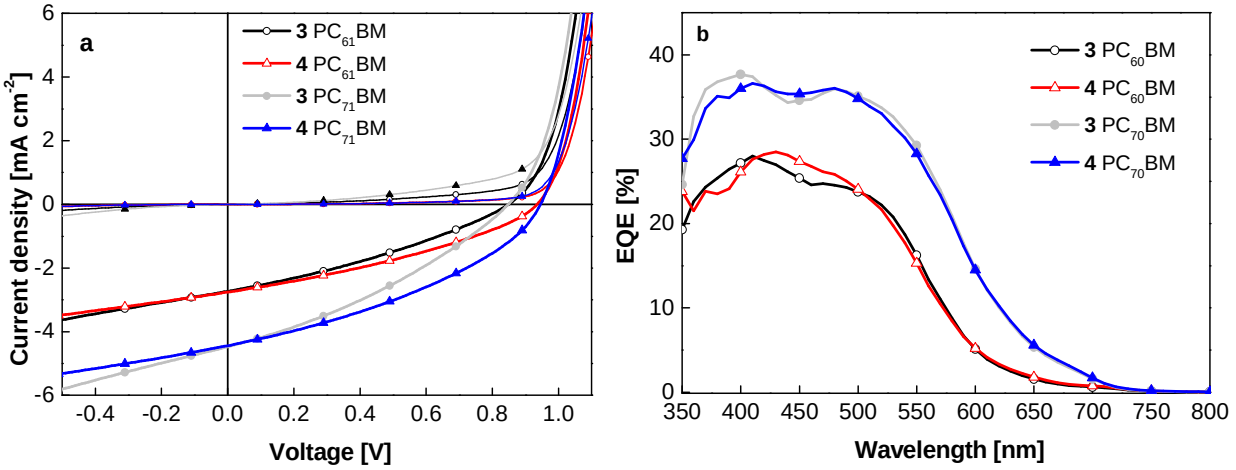

Figure 10: a) *J-V*-characteristics of solution-processed bulk heterojunction solar cells with BTDA **3** (black) and **4** (red) as donor and $PC_{61}BM$ and $PC_{70}BM$ as acceptor in a blend ratio of 1:2 (w/w). b) EQE spectra of the corresponding BHJ solar cells of **3** and **4**.

The active layers were spin-coated from chlorobenzene solutions of **3**/**4** as donor and soluble fullerene derivatives [6.6]-phenyl-C_{61}-butyric acid methyl ester ($PC_{61}BM$) or [6.6]-phenyl-C_{71}-butyric acid methyl ester ($PC_{71}BM$) as acceptor in a ratio of 1:2. The optimized thicknesses of the active layer were between 60 and 70 nm. The layer sequence used was: ITO/PEDOT:PSS (60 nm)/**donor**:PCBM (60-70 nm, 1:2 (w/w))/LiF (1 nm)/Al (100 nm).

In BHJ solar cells using $PC_{61}BM$ as the acceptor, BTDA **3** and **4** showed reasonable performance with PCEs of 0.7% and 0.9%, respectively. Higher efficiencies of 1.3% and 1.6% were observed with $PC_{71}BM$ as the acceptor. The increase of efficiency of around 80% is attributed to the absorption properties of $PC_{71}BM$, which strongly contributes to the photocurrent density in the visible region, when compared to $PC_{61}BM$.

Table 5: Solar cell data of solution-processed bulk heterojunction devices containing **3** and **4** as donor and PCBM as acceptor in a blend ratio of 1:2 (w/w)

Compound	Acceptor	EQE_{max}@wavelength (nm)	V_{OC} (mV)	J_{SC} (mA cm^{-2})	*FF*	η (%)
BTDA4T **3**	$PC_{61}BM$	0.28@400 0.25@480	0.85	2.73	0.32	0.74
BTDA4T **3**	$PC_{71}BM$	0.38@400 0.36@480	0.85	4.47	0.33	1.25
BTDA5T **4**	$PC_{61}BM$	0.28@430	0.93	2.76	0.35	0.90
BTDA5T **4**	$PC_{71}BM$	0.37@410 0.36@480	0.93	4.44	0.37	1.56

Both compounds showed almost identical EQE spectra, resulting in very similar photo currents (J_{SC}). However, cells with BTDA **4** showed a higher open circuit voltage (V_{OC} = 0.93 V) than those using BTDA **3** (V_{OC} = 0.85 V). Furthermore, the fill factor values of **4** were slightly higher, when compared to **3**, which was probably due to the difference of molecular packing in the solid state or a higher charge carrier mobility caused by the larger π-system of **4**.

When comparing solution- and vacuum-processed devices containing compounds **3** and **4** with fullerene C_{60} and $PC_{61}BM$, respectively, as the acceptor, vacuum-processing resulted in significantly higher PCEs (**3**: 1.68% vs. 0.74%; **4**: 1.60% vs. 0.90%). While V_{OC} is slightly higher in the case of solution-processed cells (**3**: 0.79 V vs. 0.85 V; **4**: 0.74 V vs. 0.93 V), both current density (J_{SC}) and fill factor values (*FF*) are about 30% higher for vacuum-processed devices. This behavior is probably due to a better morphology in the thin film of vacuum-processed solar cells, leading to higher charge carrier mobilities.

In summary: Novel oligothiophenes **1**-**4** end-capped with BTDA and TDAPy acceptor units were successfully synthesized, and materials with interesting optical and electrochemical properties were obtained. Vacuum-processed small molecule organic solar cells have been assembled and PCEs as high as 3.15% were achieved. High V_{OC} in the range of 1.0 V and high *FF* values up to 0.67 V were observed for these compounds, which are among the highest values reported for small molecule-based organic solar cells. Furthermore, solution-processed "small molecule" solar cells have been assembled of BTDA-based dyes **3**/**4** and efficiencies of up to 1.6% have been achieved.

5.5 Experimental Section

General remarks:

NMR spectra were recorded on a *Bruker AMX 500* (^{1}H NMR: 500 MHz, ^{13}C NMR: 125 MHz) or an *Avance 400* spectrometer (^{1}H NMR: 400 MHz, ^{13}C NMR: 100 MHz), unless mentioned otherwise at 25 °C. Chemical shift values (δ) are expressed in parts per million using residual solvent protons (^{1}H NMR, δ_H = 7.26 for $CDCl_3$, δ_H = 5.32 for [D_2]DCM, δ_H = 5.91 for [D_2]TCE and δ_H = 3.57 for [D_8]THF; ^{13}C NMR, δ_C = 77.0 for $CDCl_3$, δ_C = 53.8 for [D_2]DCM, δ_C = 74.2 for [D_2]TCE and δ_C = 67.2 for [D_8]THF) as internal standard. The splitting patterns are designated as follows: s (singulet), d (doublet), t (triplet) and m (multiplet). The assignments are Ar-H (H-atoms of aromatic systems) and Th-H (H-atoms of thiophene rings). Melting points were determined using a *Büchi B-545* apparatus and were not corrected. Elemental analyses were performed on an *Elementar Vario EL* (University of Ulm) and a *Carlo Erba 1104* (University of Stuttgart). Thin layer chromatography was carried out on aluminum plates, pre-coated with silica gel, *Merck Si60* F_{254}. Preparative column chromatography was performed on glass columns packed with silica gel, *Merck Silica 60*, particle size 40 − 43 µm. CI and EI mass spectra were recorded on a *Finnigan MAT SSQ-7000* or a *Varian Saturn 2000* GC-MS, MALDI-TOF on a *Bruker Daltonics Reflex III*. UV/Vis absorption spectra were recorded in 1 cm cuvettes with *Merck* Uvasol grade solvents on a *Perkin Elmer Lambda 19* spectrometer. Cyclic voltammetry experiments were performed with a computer-controlled *EG&G PAR 273* potentiostat in a three-electrode single-compartment cell with a platinum working electrode, a platinum wire counter electrode, and an Ag/AgCl reference electrode. All potentials were internally referenced to the ferrocene / ferrocenium couple. Tetrahydrofurane (*Merck*) was dried under reflux over sodium/benzophenone (*Merck*) and dichloromethane (*Merck*) over calcium hydride (*Merck*). All synthetic steps were carried out under argon atmosphere. *N*-Bromo succinimide (NBS), NaOH and K_2CO_3 were purchased from *Merck*, $Pd(PPh_3)_2Cl_2$, trifurylphosphine (TFP) and *n*BuLi (1.6 mol/L in hexane) from *Acro*s, tri-*n*-butyltin chloride and tri-*n*-methyltin chloride from *Aldrich*.

Vacuum-processed solar cells: N,N′-di(naphthalen-1-yl)-N,N′-diphenyl-benzidine (Di-NPB) and zinc phthalocyanine (ZnPc), doped with proprietary compounds NDP2 or NDP9 of *Novaled GmbH* (Dresden) were used as p-doped hole transport layers. Doping concentrations of Di-NPB

and ZnPc were 2-5 wt%. C_{60} and ZnPc have been provided by *Alfa Aesar* and Di-NPB by *Sensient Imaging Technologies*. Except the oligothiophenes, all materials were cleaned at least twice by thermal gradient sublimation before evaporation. The organic layers and metal contacts were thermally deposited in an ultra high vacuum system ("UFO", *Bestec GmbH*) at 10^{-8} to 10^{-7} mbar through shadow masks onto semitransparent indium tin oxide (ITO) coated glass substrates (*Thin Film Devices Inc.*, sheet resistance < 30 Ω / sq) without breaking the vacuum. Ceramic or graphite crucibles were used as sublimation sources (*Creaphys GmbH*, Reinhardtsgrimma), temperatures were set by a *Eurotherm* controller and film thicknesses were determined by quartz crystal monitors (*Leybold Inficon Inc.*). Substrates were cleaned using detergent, acetone, and ethanol. The active area of the cells had an average size of 4-7 mm^2. *J-V* characteristics were measured using a Source Measurement Unit 236 SMU (*Keithley*) in an N_2-filled glovebox without exposing the samples to air. Illumination was provided by a sun simulator SOL 1200 (*Hoehnle*) with an intensity of 127 mW cm^{-2}, which was calibrated using an outdoor reference cell provided by the *Fraunhofer Institute for Solar Energy Systems* (Freiburg). External quantum efficiency (EQE) spectra were recorded using a homemade setup based on a xenon lamp (*ILC-Technologies*) and a grating monochromator. Calibration was done using a *Newport Corporation* powermeter or a *Hamamatsu Photonics* photo diode. Organic films for spectral analysis were vapor deposited onto quartz substrates under ultra high vacuum with deposition rates of about 0.1 Å s^{-1}. A commercial *Shimadzu* UV-2101/3101 spectrophotometer was used for absorption measurements. Luminescence spectra were recorded using a *Spex* FluoroMAX with separated monochromators for excitation and luminescence light.

Solution-processed solar cells: Devices were made by spin coating poly-(ethylenedioxythiophene):poly(styrene sulfonate) (PEDOT:PSS, ca. 60 nm) (*Clevios*, VP Al4083) onto pre-cleaned, patterned indium tin oxide (ITO) substrates (14 Ω / sq) (*Naranjo Substrates*). The photoactive layer was deposited by spin coating a chlorobenzene solution containing 8 mg mL^{-1} of the donor compound and 16 mg mL^{-1} PCBM. The counter electrode, consisting of LiF (1 nm) and Al (100 nm), was deposited by vacuum evaporation at ca. $3 \cdot 10^{-7}$ mbar. The active area of the cells was 0.091 cm^2. *J-V* characteristics were measured under ca. 100 mW cm^{-2} white light from a tungsten-halogen lamp filtered by a *Schott* GG385 UV and a *Hoya* LB120 daylight filter, using a *Keithley* 2400 source meter. Short-circuit currents under AM1.5G conditions were estimated from the spectral response and convolution with the solar spectrum. The

spectral response was measured under simulated 1 sun operation conditions using bias light from a 532 nm solid state laser (*Edmund Optics*). Monochromatic light from a 50 W tungsten halogen lamp (*Philips Focusline*) in combination with a Cornerstone 130 monochromator (*Oriel*) was modulated with a mechanical chopper. The response was recorded as the voltage over a 50 Ω resistance, using a SR830 lock-in amplifier (*Stanford Research Systems*). A calibrated silicon cell was used as reference. The device was kept behind a quartz window in a nitrogen filled container. The thickness of the active layers in the photovoltaic devices was measured on a *Veeco* Dektak150 profilometer.

Synthesis:

5,5''-Bis(tributylstannyl)-3',4'-dibutyl-2,2':5'2''-terthiophene (**6a**). 3',4'-Dibutyl-2,2':5'2''-terthiophene (1.00 g, 2.77 mmol, 1.0 eq.) was dissolved under argon atmosphere in dry THF (20 mL). A solution of *n*-BuLi in *n*-hexane (2.5M, 6.93 mmol, 2.50 eq.) was added drop wise at -50 °C. Stirring was then continued for 30 minutes at around -25 °C. The solution was stirred for another hour at 0 °C and then again cooled down to -15 °C. Tributyltin chloride (1.92 mL, 7.07 mmol, 2.55 eq.) was added, the cooling bath removed and the reaction mixture was stirred over night at ambient temperature. The crude product was washed with water and extracted with dichloromethane, dried over Na_2SO_4. The solvents were removed under reduced pressure and the crude product (2.00 g, 2.13 mmol) was obtained as yellow-brown oil in a yield of 77% as confirmed by ^{1}H-NMR and was used without further purification. **^{1}H NMR** ($CDCl_3$, 400 MHz) δ ppm: 7.25 (d, *J* = 3.34 Hz, 2H, Th-H), 7.10 (d, *J* = 3.34 Hz, 2H, Th-H), 2.77-2.67 (m, 4H, Th-CH_2), 1.65-1.26 (m, 32H, CH_2), 1.16-1.09 (m, 12H, CH_2), 0.95 (t, *J* = 7.25 Hz, 6H, CH_3), 0.91 (t, *J* = 7.30 Hz, 18H, CH_3). **MS** (MALDI-TOF): *m/z* 932.4 $[M]^+$ (calc. for $C_{44}H_{76}S_3Sn_2$: 940.3).

5,5''-Bis(trimethlstannyl)-3',4'-dibutyl-2,2':5'2''-terthiophene (**6b**). 3',4'-Dibutyl-2,2':5'2''-terthiophene (177 mg, 0.49 mmol, 1.00 eq.) was dissolved under argon atmosphere in dry THF (2 mL) and TMEDA (0.16 mL, 1.08 mmol, 2.20 eq.) was added. At -50 °C a solution of *n*BuLi in *n*-hexane (1.6M, 0.718 mL, 1.15 mmol, 2.34 eq.) was added drop wise. The cooling bath was removed and stirring was continued for 30 minutes. The reaction mixture was then heated to 30 °C for another 20 minutes, after which it was again cooled below -50 °C. A solution of trimethyltin chloride (229 mg, 1.15 mmol, 2.34 eq.) in THF (1.5 mL) was added, the cooling

bath removed and the mixture stirred over night at room temperature. The mixture was then poured into ice cold aq. NH_4Cl solution (25 mL) and extracted with diethyl ether. The organic phase was dried over Na_2SO_4 and concentrated in vacuum. Recrystallization from methanol afforded the desired compound (160 mg, 0.23 mmol, 48%) as yellow solid. The product was used in subsequent syntheses without further purification. **^{1}H NMR** ($CDCl_3$, 400 MHz) δ ppm: 7.24 (d, *J* = 3.39 Hz, 2H, Th-H), 7.13 (d, *J* = 3.39 Hz, 2H, Th-H), 2.75-2.67 (m, 4H, Th-CH_2), 1.61-1.54 (m, 4H, CH_2), 1.50-1.39 (m, 4H, CH_2), 0.96 (t, *J* = 7.27 Hz, 6H, CH_3), 0.39 (s, 18H, Sn-CH_3).

5,5''-Di(benzo[*c*][1,2,5]thiadiazol-4-yl)-3',4'-dibutyl-2,2':5'2''-terthiophene (**1**, BTDA3T). Stannylated terthiophene **6a** (362 mg, 0.39 mmol, 1.0 eq.), 4-bromobenzo[*c*][1,2,5]thiadiazole (290 mg, 1.35 mmol, 3.5 eq.), CsF (351 mg, 2.31 mmol, 6.0 eq.) and $Pd(PPh_3)_2Cl_2$ (27 mg, 40 µmol, 0.1 eq.) were dissolved in DMF (5 mL) and 1,2-dichloroethane (2 mL) under argon atmosphere. The mixture was irradiated by microwave for 4 h at 100 °C. The formed dark red, gel like mixture was further extracted with dichloromethane and water. The organic layer was dried over Na_2SO_4 and the solvent was removed by rotary evaporation. Title compound **1** (50 mg, 0.08 mmol) was purified by column chromatography (SiO_2, gradient eluent from DCM:*n*-hexane (7:3) → pure DCM) as red-brown powder in a yield of 21%. **M.p.** (DSC): 141 °C. **^{1}H NMR** (CD_2Cl_2, 400 MHz) δ ppm: 8.12 (d, 2H, *J* = 3.85 Hz, Th-H), 7.92 (dd, 2H, J = 0.88 Hz, J = 8.67 Hz, Ar-H), 7.88 (dd, 2H, J = 0.90 Hz, J = 7.06 Hz, Ar-H), 7.65 (dd, 2H, J = 7.09 Hz, J = 8.67 Hz, Ar-H), 7.28 (d, 2H, J = 3.90 Hz, Th-H), 2.85 (t, 4H, Th-CH_2-), 1.68-1.59 (m, 4H, CH_2), 1.56-1.46 (m, 4H, CH_2), 1.01 (t, 6H, *J* = 7.28 Hz, -CH_3). **^{13}C NMR** (CD_2Cl_2, 100 MHz) δ ppm: 155.63, 140.96, 138.89, 137.65, 131.99, 130.12, 129.68, 128.34, 127.09, 126.46, 124.97, 120.03, 32.85, 28.05, 23.10, 13.71. **MS** (MALDI-TOF): *m/z* 628.4 $[M]^+$ (calc. for $C_{32}H_{28}N_4S_5$: 628.1). **Elemental analysis:** $C_{32}H_{28}N_4S_5$: calc. C, 61.11; H, 4.49; N, 8.91%; found: C, 60.88; H, 4.50; N, 8.85%.

4-Chloro-[1,2,5]thiadiazolo[3,4-*c*]pyridine (**7**). 2-Bromopyridine-3,4-diamine (285 mg, 1.52 mmol) was dissolved in thionyl chloride (8.3 mL, 13.5 g, 0.11 mol) and the mixture was refluxed for 5 h. Excess thionyl chloride was distilled off under reduced pressure and the crude product was neutralized carefully with saturated solution of aq. $NaHCO_3$. The crude product was washed with water and extracted with dichloromethane, dried over Na_2SO_4. The solvent was removed by rotary evaporator. Recrystallization from methanol furnished the product (50 mg, 0.29 mmol, 19%) as orange-brown needles. **M.p.:** 109-112 °C. **^{1}H NMR** (DMSO-d_6, 400 MHz) δ ppm: 8.44 (d, *J* = 6.16 Hz, 1H, Ar-H), 8.10 (d, *J* = 6.16 Hz, 1H, Ar-H). **MS** (EI): m/z = 171

([M]$^+$, 100), 136 (50). (Due to air and moisture sensitivity, the material was fully decomposed before ^{13}C NMR and elemental analysis were measured).

5,5''-Di([1,2,5]thiadiazolo[3,4-c]pyridin-4-yl)-3',4'-dibutyl-2,2':5'2''-terthiophene (**2**, TDAPy3T). Bis-stannylated terthiophene **6b** (120 mg, 0.17 mmol, 1.0 eq.), thiadiazolo-pyridine **7** (63 mg, 0.37 mmol, 2.1 eq.) and $Pd(PPh_3)_2Cl_2$ (6.14 mg, 8.74 µmol, 5 mol-%) were dissolved in DMF (2 mL) under argon atmosphere. The mixture was heated under microwave conditions for 2 h at 90 °C. After washed with water and extraction with DCM, the organic phase was dried over Na_2SO_4 and concentrated in vacuum. The desired product (53 mg, 0.08 mmol) was purified by gradient column chromatography (SiO_2: DCM:ethyl acetate (97:3) → pure DCM) as deep red powder in a yield of 48%. **M.p.:** 167-169 °C. **^{1}H NMR** ($CDCl_3$, 400 MHz) δ ppm: 8.70 (d, 2H, *J* = 4.01 Hz, Ar-H), 8.54 (d, 2H, *J* = 6.21 Hz, Ar-H), 7.72 (d, 2H, *J* = 6.18 Hz, Ar-H), 7.34 (d, 2H, *J* = 4.03 Hz, Ar-H), 2.88 (t, 4H, Th-CH_2-), 1.70 (m, 4H, CH_2), 1.57-1.48 (m, 4H, CH_2), 1.00 (t, 6H, *J* = 7.28 Hz, CH_3). **^{13}C NMR** ($CDCl_3$, 100 MHz) δ ppm: 157.77, 148.42, 148.06, 144.93, 141.63, 141.46, 140.94, 133.10, 130.85, 127.40, 112.85, 32.68, 28.17, 23.03, 13.90. **MS** (HR MS, Ion Polarity: Positive): *m/z* 630.0814 [M+H]$^+$ (calc. for $C_{30}H_{27}N_6S_5$: 630.0817). **Elemental analysis:** $C_{14}H_{14}N_2S_2$: calc. C, 57.11; H: 4.15; N: 13.32; S: 25.41; found: C: 57.05; H: 4.31; N: 13.26; S: 25.28.

4-(4-Butylthiophen-2-yl)benzo[c][1,2,5]thiadiazole (**9**). 4-Bromobenzo[*c*][1,2,5]thiadiazole (813 mg, 3.78 mmol, 1.00 eq.) and tributyl(4-butylthiophen-2-yl)stannane (1.62 g, 3.78 mmol, 1.00 eq.) were dissolved in dry DMF (22 mL). $Pd(PPh_3)_2Cl_2$ (133 mg, 189 µmol, 0.05 eq.) was added and the reaction mixture was irradiated under microwave conditions for two hours at 100 °C. The resulting dark-orange solution was diluted with diethyl ether (200 mL) and washed with water (3 x 200 mL) to remove DMF. The organic layer was dried over sodium sulfate and removed of the solvent under reduced pressure. Column chromatography (silica, *n*-hexane : DCM = 6 : 4) furnished the desired product (610 mg, 2.22 mmol) as yellow oil in 59% yield. **^{1}H NMR** ($CDCl_3$, 400 MHz) δ ppm: 7.98 (d, *J* = 1.41 Hz, 1H, Th-H), 7.90 (dd, *J* = 8.78 Hz, *J* = 0.98 Hz, 1H, Ar-H), 7.82 (dd, *J* = 7.10 Hz, *J* = 0.97 Hz, 1H, Ar-H), 7.60 (dd, *J* = 8.71 Hz, *J* = 7.10 Hz, 1H, Ar-H), 7.04 (dd, *J* = 2.25 Hz, *J* = 0.97 Hz, 1H, Th-H), 2.71 (t, *J* = 7.40 Hz, 2H, Th-CH_2-), 1.74-1.65 (m, 2H, -CH_2), 1.45-1.34 (m, 2H, -CH_2), 0.96 (t, *J* = 7.34 Hz, 3H, CH_3). **^{13}C NMR** ($CDCl_3$, 100 MHz) δ ppm: 144.49, 144.23, 138.83, 130.47, 129.56, 129.35, 127.83, 125.16, 121.50, 119.83, 32.60,

30.29, 22.37, 13.88. **MS** (CI): *m/z* 274.0 ($[M]^+$, 100). **Elemental analysis:** $C_{14}H_{14}N_2S_2$: calc. C, 61.28; H, 5.14; N, 10.21%; found: C, 61.16; H, 5.24; N, 10.27%.

4-(5-Bromo-4-butylthiophen-2-yl)benzo[c][1,2,5]thiadiazole (**10**). NBS (402 mg, 2.26 mmol, 1.05 eq.) dissolved in chloroform (64 mL), was added drop wise to a ice cooled solution of benzothiadiazole compound 8 (590 mg, 2.15 mmol, 1.00 eq.) in chloroform (64 mL). After complete addition, the cooling bath was removed and the mixture was stirred at room temperature for 30 minutes. After extraction with DCM and water, the organic layer was dried over sodium sulfate and removed of the solvent. Column chromatography (silica, DCM : *n*-hexane = 1 : 1) afforded the product (720 mg, 2.04 mmol) as yellow powder in a yield of 95%. **M.p.:** 51-52 °C**.** **^{1}H NMR** ($CDCl_3$, 400 MHz) δ ppm: 7.91 (dd, *J* = 8.76 Hz, *J* = 0.96 Hz, 1H, Ar-H), 7.77 (s, 1H, Th-H), 7.73 (dd, *J* = 7.11 Hz, *J* = 0.96 Hz, 1H, Ar-H), 7.58 (dd, *J* = 8.77 Hz, *J* = 7.10 Hz, 1H, Ar-H), 2.65 (t, *J* = 7.64 Hz, 2H, -CH_2), 1.72-1.61 (m, 2H, -CH_2), 1.48-1.37 (m, 2H, CH_2), 0.97 (t, *J* = 7.31 Hz, 3H, CH_3). **^{13}C NMR** ($CDCl_3$, 100 MHz) δ ppm: 155.46, 151.88, 142.95, 138.54, 129.55, 128.41, 126.93, 124.68, 120.20, 111.40, 31.93, 29.42, 22.39, 13.93. **MS** (MALDI-TOF): *m/z* 352.0 $[M]^+$ (calc. for $C_{14}H_{13}BrN_2S_2$: 352.0). **Elemental analysis:** $C_{14}H_{13}BrN_2S_2$: calc. C, 47.59; H, 3.71; N, 7.93%; found: C, 47.54; H, 3.68; N, 7.88%.

5,5'''-Di(benzo[c][1,2,5]thiadiazol-4-yl)-3,3'''-dibutyl-2,2':5'2'':5''2'''-quaterthiophene (**3**, BTDA4T). 5,5'-bis(tributylstannyl)-2,2'-bithiophene (280 mg, 0.38 mmol, 1.0 eq.), benzothiadiazole 9 (332 mg, 0.94 mmol, 2.5 eq.), cesium fluoride (343 mg, 2.26 mmol, 6.0) and $Pd(PPh_3)_2Cl_2$ (26 mg, 40 µmol, 0.1 eq.) were dissolved under argon atmosphere in 1,2-dichloroethane (21 mL). The mixture was irradiated by microwave for 4 h at 100 °C. The resulting dark red solution was further extracted with DCM and water. The organic layer was dried over sodium sulfate and removed of the solvent under reduced pressure. The title compound (152 mg, 0.21 mmol) was isolated by column chromatography (silica, DCM : n-hexane = 7 : 3) as dark red-brown powder in a yield of 57%. **M.p.** (DSC): 184 °C. **^{1}H NMR** ($CDCl_3$, 400 MHz) δ ppm: 8.00 (s, 2H, Th-H), 7.92 (dd, *J* = 8.76 Hz, *J* = 0.77 Hz, 2H, Ar-H), 7.83 (dd, *J* = 7.08 Hz, *J* = 0.82 Hz, 2H, Ar-H), 7.62 (dd, *J* = 8.70 Hz, *J* = 7.14 Hz, 2H, Ar-H), 7.20 (d, *J* = 3.84 Hz, 2H, Th-H), 7.17 (d, *J* = 3.81 Hz, 2H, Th-H), 2.90 (t, *J* = 7.73 Hz, 4H, Th-CH_2-), 1.81-1.71 (m, 4H, CH_2), 1.55-1.45 (m, 4H, CH_2), 1.00 (t, *J* = 7.32 Hz, 6H, CH_3). **^{13}C NMR** ($CDCl_3$, 100 MHz) δ ppm: 161.65, 155.58, 152.10, 140.64, 137.02, 132.13, 129.62, 126.73, 125.00, 124.09, 120.03, 32.74, 29.38, 22.73, 13.99. **MS** (MALDI-TOF): *m/z* 710.3 $[M]^+$ (calc. for $C_{36}H_{30}N_4S_6$: 710.1).

Elemental analysis: $C_{36}H_{30}N_4S_6$: calc. C, 60.81; H, 4.25; N, 7.88%; found: C, 60.93; H, 4.25; N, 7.81%.

5,5''''-Di(benzo[c][1,2,5]thiadiazol-4-yl)-3,3'',3'''',4''-tetrabutyl-2,2':5'2'':5''2''':5''':2''''-quaterthiophene (**4**, BTDA5T). Stannylated terthiophene 6a (284 mg, 0.30 mmol, 1.0 eq.), benzothiadiazole 9 (267 mg, 0.76 mmol, 2.5 eq.), cesium fluoride (276 mg, 1.82 mmol, 6.0 eq.) and $Pd(PPh_3)_2Cl_2$ (21 mg, 30 µmol, 0.1 eq.) were dissolved under argon atmosphere in 1,2-dichloroethane (21 mL). The mixture was heated under microwave conditions for 5 h at 100 °C. The formed dark red, gel like mixture was further extracted with DCM and water. The organic layer was dried over sodium sulfate and the solvent was removed by rotary evaporation. The product (144 mg, 0.16 mmol) was isolated by column chromatography (silica, n-hexane : DCM = 7 : 3) as red-brown powder in 53% yield. **M.p.** (DSC): 160 °C. **^{1}H NMR** ([D2]TCE, 500 MHz, 100 °C) δ ppm: 7.90 (s, 2H, Th-H), 7.83 (dd, *J* = 8.71 Hz, *J* = 0.84 Hz, 2H, Ar-H), 7.77 (dd, *J* = 7.07 Hz, *J* = 0.84 Hz, 2H, Ar-H), 7.56 (dd, *J* = 8.73 Hz, *J* = 7.14 Hz, 2H, Ar-H), 7.15 (d, *J* = 3.83 Hz, 2H, Th-H), 7.09 (d, *J* = 3.81 Hz, 2H, Th-H), 2.82 (t, *J* = 7.73 Hz, 4H, Th-CH_2-), 2.70 (t, *J* = 8.47 Hz, 4H, Th-CH_2-), 1.73-1.63 (m, 4H, CH_2), 1.48-1.36 (m, 4H, CH_2), 0.92 (dt, *J* = 7.39 Hz, *J* = 4.04 Hz, 12H, CH_3). **^{13}C NMR** ([D2]TCE, 125 MHz, 100 °C) δ ppm: 155.07, 151.62, 140.11, 140.06, 136.26, 135.81, 135.20, 131.94, 130.72, 129.47, 129.28, 126.62, 125.96, 125.63, 124.69, 119.60, 53.47, 32.48, 32.43, 29.12, 22.77, 22.48, 13.81, 13.69. **MS** (MALDI-TOF): *m/z* 904.4 $[M]^+$ (calc. for $C_{48}H_{48}N_4S_7$: 904.2). **Elemental analysis:** $C_{34}H_{32}N_2S_3$: calc. C, 63.68; H, 5.34; N, 6.19%; found: C, 63.74; H, 5.33; N, 6.09%.

5.6 References

[1] K. Schulze, B. Maennig, K. Leo, Y. Tomita, C. May, J. Hüpkes, E. Brier, E. Reinold, P. Bäuerle, *App. Phys. Lett.* **2007**, *91*, 073521.

[2] K. Schulze, C. Uhrich, R. Schüppel, K. Leo, M. Pfeiffer, E. Brier, E. Reinold, P. Bäuerle, *Adv. Mater.* **2006**, *18*, 2872.

[3] C. Uhrich, R. Schüppel, A. Petrich, M. Pfeiffer, K. Leo, E. Brier, P. Kilickiran, P. Bäuerle, *Adv. Funct. Mater.* **2007**, *17*, 2991.

[4] R. Schüppel, K. Schmidt, C. Uhrich, K. Schulze, D. Wynands, J. L. Brédas, E. Brier, E. Reinold, H.-B. Bu, *Phys. Rev. B* **2008**, *77*, 085311.

[5] R. Schüppel, C. Uhrich, M. Pfeiffer, K. Leo, E. Brier, E. Reinold, P. Baeuerle, *ChemPhysChem* **2007**, *8*, 1497.

[6] M. Jayakannan, P. A. V. Hal, R. A. J. Janssen, *J. Polym. Sci. A* **2002**, *40*, 2360.

[7] M. Melucci, L. Favaretto, C. Bettini, M. Gazzano, N. Camaioni, P. Maccagnani, P. Ostoja, M. Monari, G. Barbarella, *Chem. Eur. J.* **2007**, *13*, 10046.
[8] H. A. M. Van Mullekom, J. A. J. M. Vekemans, E. W. Meijer, *Chem. Eur. J.* **1998**, *4*, 1235.
[9] M. Akhtaruzzaman, M. Tomura, J.-i. Nishida, Y. Yamashita, *J. Org. Chem.* **2004**, *69*, 2953.
[10] J. Lu, F. Liang, N. Drolet, J. Ding, Y. Tao, R. Movileanu, *Chem. Comm.* **2008**, 5315.
[11] S. Song, Y. Jin, S. H. Kim, J. Moon, K. Kim, J. Y. Kim, S. H. Park, K. Lee, H. Suh, *Macromolecules* **2008**, *41*, 7296.
[12] Y. He, X. Wang, J. Zhang, Y. Li, *Macromol. Rapid Commun.* **2009**, *30*, 45.
[13] J. Mei, N. C. Heston, S. V. Vasilyeva, J. R. Reynolds, *Macromolecules* **2009**, *42*, 1482.
[14] J.-L. Wang, Z.-M. Tang, Q. Xiao, Y. Ma, J. Pei, *Org. Lett.* **2009**, *11*, 863.
[15] P. F. Xia, J. Lu, C. H. Kwok, H. Fukutani, M. S. Wong, Y. Tao, *J. Polym. Sci. A* **2009**, *47*, 137.
[16] P. Anant, N. T. Lucas, J. Jacob, *Org. Lett.* **2008**, *10*, 5533.
[17] N. Blouin, A. Michaud, D. Gendron, S. Wakim, E. Blair, R. Neagu-Plesu, M. Belletete, G. Durocher, Y. Tao, M. Leclerc, *J. Am. Chem. Soc.* **2008**, *130*, 732.
[18] H. Zhou, L. Yang, S. C. Price, K. J. Knight, W. You, *Angew. Chem.* **2010**, *DOI : 10.1002/ange.201003357*.
[19] E. Reinold, A. Vogt, P. Bäuerle, *(pending)* **2010**.
[20] K. Pilgram, M. Zupan, R. Skiles, *J. Heterocycl. Chem.* **1970**, *7*, 629.
[21] K.-Y. Jung, K.-H. Lee, *J. Ind. Eng. Chem.* **1997**, *3*, 46.
[22] L. Ackermann, R. Vicente, A. R. Kapdi, *Angew. Chem. Int. Ed.* **2009**, *48*, 9792.
[23] Q. Hou, Q. Zhou, Y. Zhang, W. Yang, R. Yang, Y. Cao, *Macromolecules* **2004**, *37*, 6299.

Summary

The objective of this thesis was to develop novel donor-acceptor substituted low band gap oligothiophenes and to adjust molecular properties for the application in “small molecule” organic solar cells (Figure 1). We intended to deduce structure-property relations in order to develop new materials with optimized UV-vis absorption, HOMO-LUMO energy levels, volatility and long term stability for the envisaged objective.

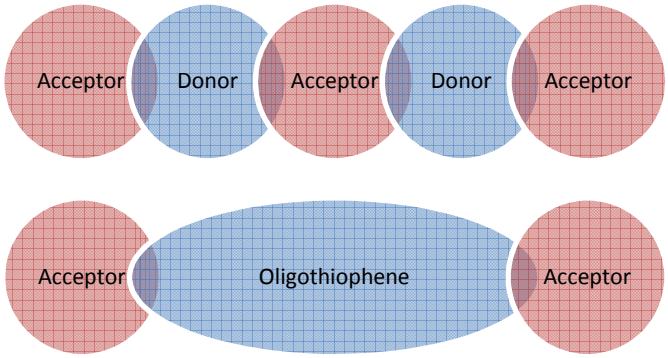

Figure 1: Donor-acceptor functionalized oligomers as red/NIR absorbers for “small molecule” solar cells (SMSC).

First (Chapter 3), we introduced heterocyclic thienothiadiazole (TTDA) and thienopyrazine (TP) as an additional acceptor into the core of reported quinquethiophene DCV5T[1-5], in order to achieve an A-D-A-D-A-type push-pull system with absorption down to the near IR region (Figure 2).

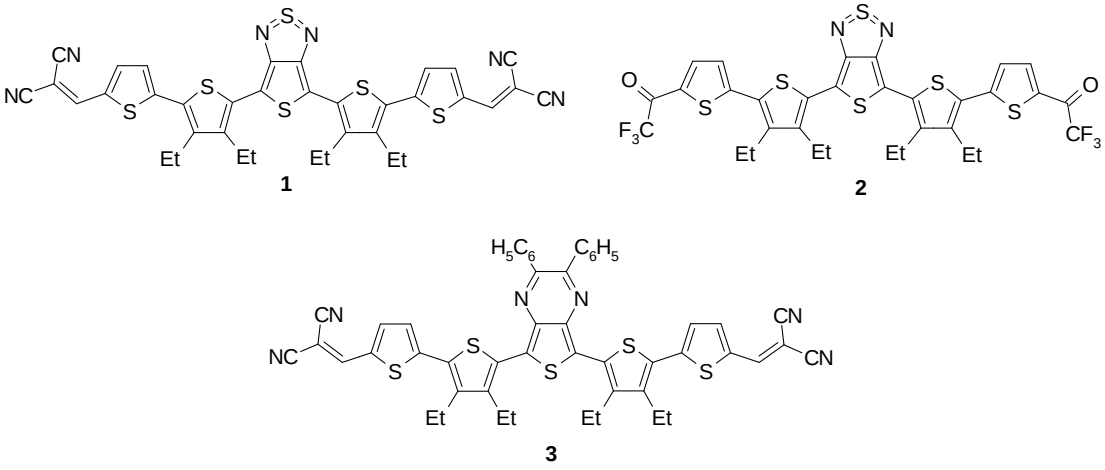

Figure 2: Novel oligothiophenes based on DCV5T, comprising thienothiadiazole or thienopyrazine as core and dicyanovinyl (DCV) or trifluoroacetyl (TFA) as terminal acceptor units.

While preparing thin films by vacuum deposition technique of DCV-derivative **1**, the sublimation yield was very low, due to thermal degradation. To improve the stability and

volatility of the compound, the dicyanovinyl-groups (DCV) were replaced in pentamer **2** with trifluoroacetyl (TFA) units. By incorporating the building-block thienopyrazine in oligomer **3**, we intended to investigate an alternate core acceptor with reduced electron withdrawing force when compared to TTDA.

The obtained oligomers showed narrow band gaps down to 1.2 eV in thin films with a bathochromic shift of more than 200 nm when compared to parent compound DCV5T. The red-shift in absorption is ascribed to the TTDA/TP core moiety, which leads to a pronounced donor-acceptor alternation and increases the quinoid character of the conjugated system. Substitution of the terminal dicyanovinyl groups with trifluoroacetyl moieties increased both, thermal stability and volatility of the compound, resulting in a significantly higher sublimation yield of **2** as compared to **1** during vacuum deposition of thin films. TP-derivative **3** showed a red-shift in absorption of only 113 nm when compared to DCV5T, which indicates the lower electron withdrawing force of the TP unit compared to TTDA. Furthermore, photoinduced degradation of **3** was observed when exposed to oxygen and a mechanism was proposed.

Photovoltaic devices based on these materials in vacuum processed m-i-p-type solar cells showed efficiencies as high as 1.1%. A low fill factor value of the assembled cells indicates, that thienothiadiazole and thienopyrazine may act as a hole trap, resulting possibly in a reduced charge carrier mobility.

In our next project (Chapter 4), we used benzothiadiazole (BTDA) as novel building block, to further investigate the influence of the electron accepting core moiety on the molecular properties of A-D-A-D-A-type oligothiophenes (Figure 3).

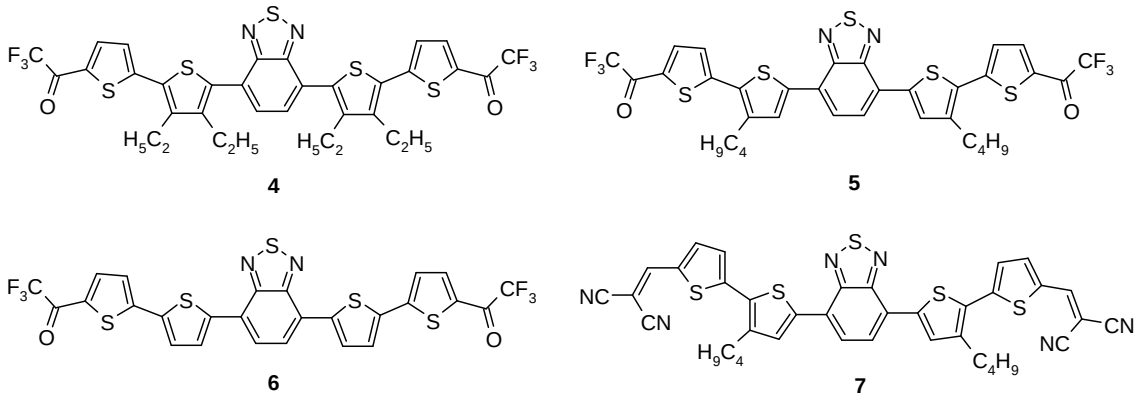

Figure 3: DCV5T-analogous pentamers comprising BTDA as core and DCV or TFA as terminal acceptors.

Compound **4** evinced strong sterical hindrance between the BTDA and its adjacent ethyl-

substituted thiophene rings. As a result, a twist of the aromatic system and with it a drastic hypsochromic shift in the absorption (λ_{max} = 430 nm) was observed. Therefore, the alkylation pattern was adapted in compounds **5**-**7** in order to prevent the sterical hindrance. Despite the alkyle chains, compound **7** showed very low solubility and only a small sample for analytical purpose was prepared. BTDA oligomers **5** and **6** showed high extinction coefficients (> 50000 L mol^{-1} cm^{-1} in dichloromethane solution) with absorption down to ~650 nm in thin films. Excellent thermal stability was observed during processing the materials by vacuum deposition technique. M-i-p-type organic solar cells have been assembled and power conversion efficiencies (PCE) as high as 1.56% with very high open-circuit voltage (V_{OC}) in the range of 1.2 V were achieved.

Introducing a TTDA, TP or BTDA moiety into the core of DCV5T-analogous structures resulted in all cases in a lowering of the solar cell efficiency (Chapter 3 and 4). We assume, the core acceptor constitutes an exciton hole trap in the intrinsic layer of photovoltaic devices. Therefore, novel terminal acceptor moieties were investigated to replace the DCV-groups in the DCVnT-series (Chapter 5). BTDA and thiadiazolo pyridine (TDAPy) were introduced as novel end-capping units in a series of A-D-A-type oligothiophenes. (Figure 4). Due to the electron deficient pyridine of the TDAPy unit, we expected as compared to BTDA a red-shift in absorption and strong intermolecular interactions, resulting in a well defined morphology in the solid state.

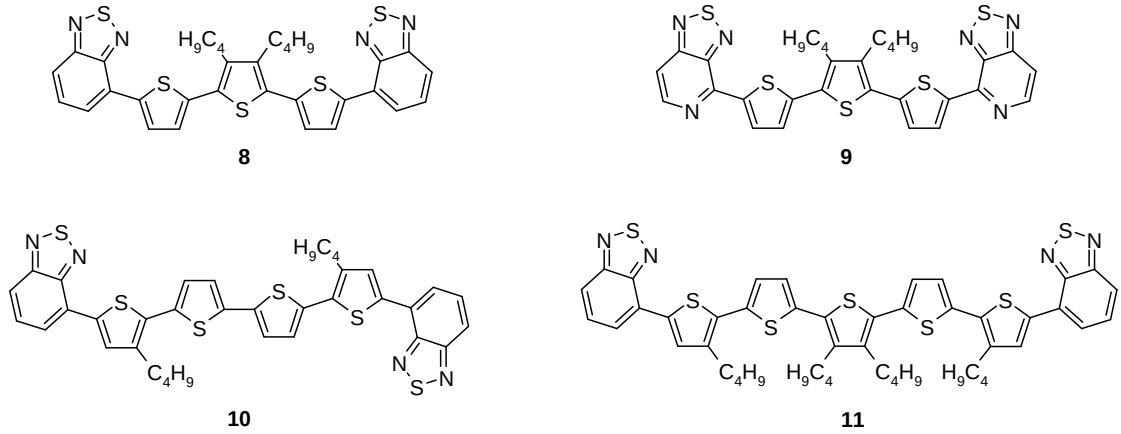

Figure 4: A-D-A-series of oligothiophenes end-capped with BTDA or thiadiazolo pyridine (TDAPy).

The obtained oligomers showed excellent thermal stability and in the case of TDAPy-based compound **9,** absorption in thin films extending down to over 650 nm. Vacuum-processed organic solar cells comprising **9** as donor have been assembled and PCEs up to 3.15% were

achieved. High V_{OC} in the range of 1.0 V and high *FF* values as high as 0.67 V were observed for these compounds, which are among the highest values reported for small molecule-based organic solar cells. Furthermore, solution processed “small molecule” solar cells have been assembled of BTDA-based dyes **10** and **11** and promising efficiencies of up to 1.6% have been achieved.

To conclude: By introducing various donor and acceptor functions (TTDA, TP, BTDA, TDAPy, TFA, DCV) into oligothiophenes, tailored low band gap materials with intriguing properties meeting the requirements for application in “small molecule” organic solar cells were successfully developed and photovoltaic devices with record efficiencies as high as 3.15% were achieved. In the course, we established interesting structure-property relations and in the field of “small molecule” solar cells, a novel, promising acceptor unit – thiadiazolo pyridine (TDAPy) – was introduced. We expect that further careful improvement of these materials and devices will result in even higher efficiencies in future photovoltaic cells.

Zusammenfassung

Ziel dieser Arbeit war es, neue Donor-Akzeptor substituierte Verbindungen mit schmaler Bandlücke auf Basis von Oligothiophenen zu entwickeln und die molekularen Eigenschaften, wie energetische Lage von HOMO/LUMO, UV/Vis Absorption, Langzeitstabilität und Sublimierbarkeit, entsprechend den Anforderungen für organische Solarzellen zu optimieren (Abbildung 1).

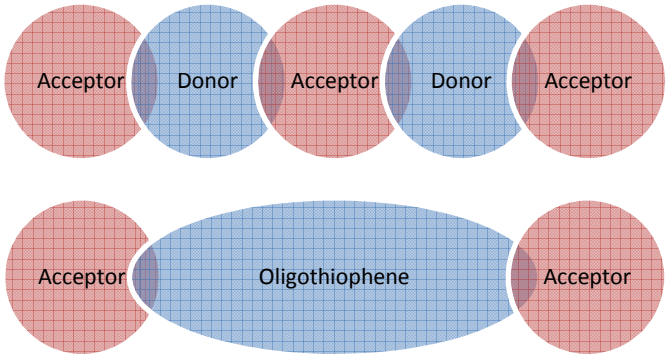

Abbildung 1: Donor-Akzeptor funktionalisierte Oligomere als Rot/NIR-Absorber für oligomer-basierte, organische Solarzellen.

Zunächst führten wir die Heterozyklen Thienothiadiazol (TTDA) bzw. Thienopyrazin (TP) als zusätzliche Kern-Akzeptor-Einheit in das literaturbekannt Quinquethiophen DCV5T[1-5] ein (Kapitel 3), um ein Donor-Akzeptor System mit Absorption bis in den nahen Infrarot-Bereich zu erreichen (Abbildung 2).

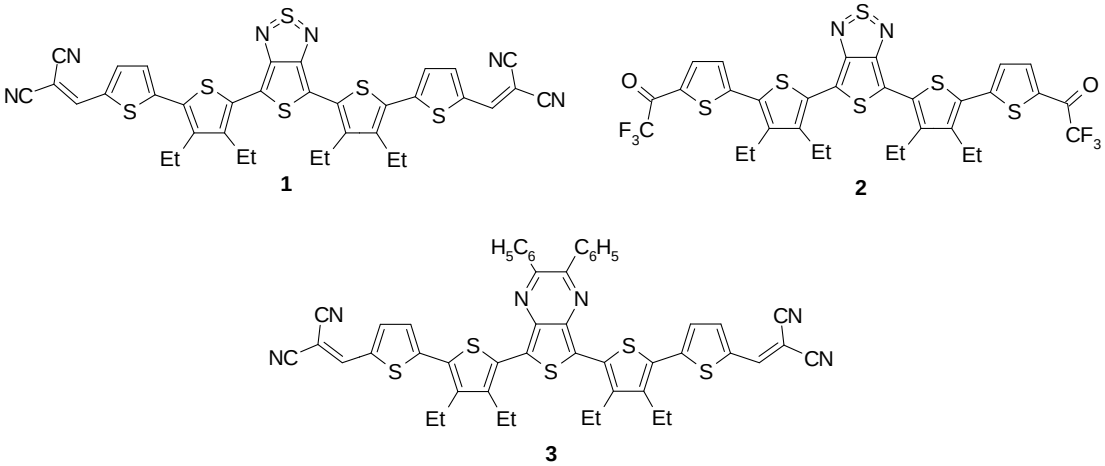

Abbildung 2: Auf DCV5T-basierende, neuartige Oligothiophene mit Thienothiadiazol bzw. Thienopyrazin als Kern- und Dicyanovinyl (DCV) bzw. Trifluoroacetyl (TFA) als endständige Akzeptor-Gruppen.

Für DCV-Verbindung **1** wurde bei der Herstellung von Dünnfilmen durch Sublimation nur eine geringe Ausbeute erzielt, da sich das Material während des Prozesses thermisch

zersetzte. Um dessen Stabilität und Volatilität zu erhöhen, wurden die DCV-Gruppen in Pentamer **2** durch Trifluoroacetyl-Einheiten (TFA) ersetzt. Um einen alternativen Kern-Akzeptor mit geringerem Elektronenzug als TTDA zu untersuchen, wurde in Oligomer **3** das Thienopyrazin eingesetzt.

Die erhaltenen Verbindungen wiesen im Dünnfilm eine schmale Bandlücke von nur 1.2 eV auf und zeigten im Vergleich zu DCV5T eine bathochrome Verschiebung der Absorption von über 200 nm. Die Rotverschiebung wurde dem Einfluss der zentralen TTDA- bzw. TP-Einheiten zugeschrieben, die zu einem ausgeprägten Wechseln zwischen Donor und Akzeptor führen und gleichzeitig den chinoiden Charakter des konjugierten Systems erhöhen. Substitution der endständigen Dicyanovinyl-Gruppen durch Trifuoroacetyl-Einheiten erhöhte die thermische Stabilität und Volatilität von Verbindung **2** und führte im Vergleich zu DCV-Verbindung **1** zu deutlich höheren Sublimationsausbeuten während der Herstellung von Dünnfilmen. TP-Derivat **3** zeigte eine Rotverschiebung von nur 113 nm gegenüber DCV5T, was auf den schwächeren Elektronenzug der TP-Einheit im Vergleich zum TTDA zurückzuführen ist. Weiterhin wurde für diese Verbindung eine lichtinduzierte Zersetzungsreaktion beobachtet, für die ein erklärender Mechanismus vorgeschlagen wurde.

M-i-p Solarzellen auf Basis der neuen Materialien zeigten eine Effizienz von bis zu 1.1%. Der niedrige Füllfaktor dieser Zellen deutet darauf hin, dass TTDA und TP als Lochfalle wirken könnte, was zu einer verringerten Ladungsträgermobilität führt.

In unserem nächsten Projekt (Kapitel 4) setzen wir Benzothiadiazol (BTDA) als neuen zentralen Akzeptor-Baustein ein und untersuchten dessen Einfluss auf die molekularen Eigenschaften der A-D-A-D-A-Oligothiophene (Abbildung 3).

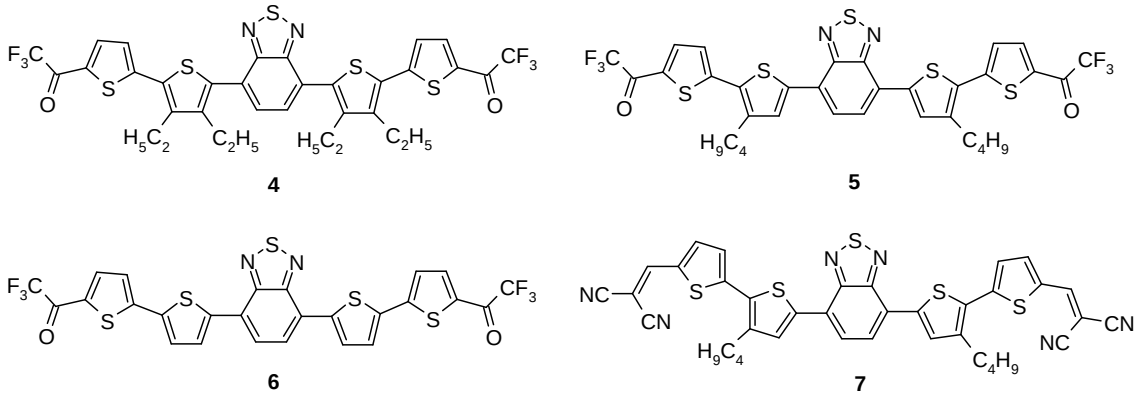

Abbildung 3: DCV5T-analoge Pentamere mit BTDA als Kern- und DCV oder TFA als endständige Akzeptor-Gruppen.

In Verbindung **4** liegt eine starke sterische Hinderung zwischen der BTDA-Einheit und den benachbarten Thiophenringen vor. Dies resultierte in einer Verdrillung des aromatischen Systems und führte zu einer starken hypsochromen Verschiebung der Absorption (λ_{max} = 430 nm). Das Alkylierungsmuster wurde entsprechend in den Verbindungen **5**-**7** angepasst, um die sterische Hinderung zu vermeiden. Trotz der Alkylketten zeigte DCV-Derivat **7** jedoch eine sehr geringe Löslichkeit, so dass nur eine analytische Probe hergestellt wurde. Die BTDA-Verbindungen **5** und **6** zeigten hohe Extinktionskoeffizienten (> 50000 L mol^{-1} cm^{-1} in Dichlormethan gelöst) mit Absorption über ~650 nm im Dünnfilm. Des Weiteren wurde herausragende thermische Stabilität von BTDA **5** und **6** während der Verarbeitung durch Vakuum-Verdampfung festgestellt. Organische M-i-p Solarzellen zeigten eine Effizienz von bis zu 1.56% bei sehr hohen Offenen-Stromkreis Potenzialen (V_{OC}) im Bereich von 1.2 V.

Die Einführung von TTDA, TP und BTDA als zusätzliche Kern-Einheit von DCV5T-analogen Strukturen resultiere in allen Beispielen in einer erniedrigten Solarzelleneffizienz (Kapitel 3 und 4). Wir nehmen an, der Kern-Akzeptor stellt in der aktiven Solarzellenschicht eine Lochfalle für Excitonen dar. Daher wurde im Weiteren nach neuen, endständigen Akzeptor-Bausteinen gesucht, um die DCV-Gruppen in der DCVnT-Serie zu ersetzen (Kapitel 5). BTDA und Thiadiazolo Pyridin (TDAPy) wurden in einer neuen Oligothiophen-Serie des Musters A-D-A als neuartige terminale Akzeptoren eingesetzt (Abbildung 4). Auf Grund des Elektronenmangels der Pyridin-basierten TDAPy-Einheit erwarteten wir gegenüber BTDA eine Rotverschiebung in der Absorption und starke intermolekulare Wechselwirkungen, die zu geordneten Strukturen im festen Zustand führen sollten.

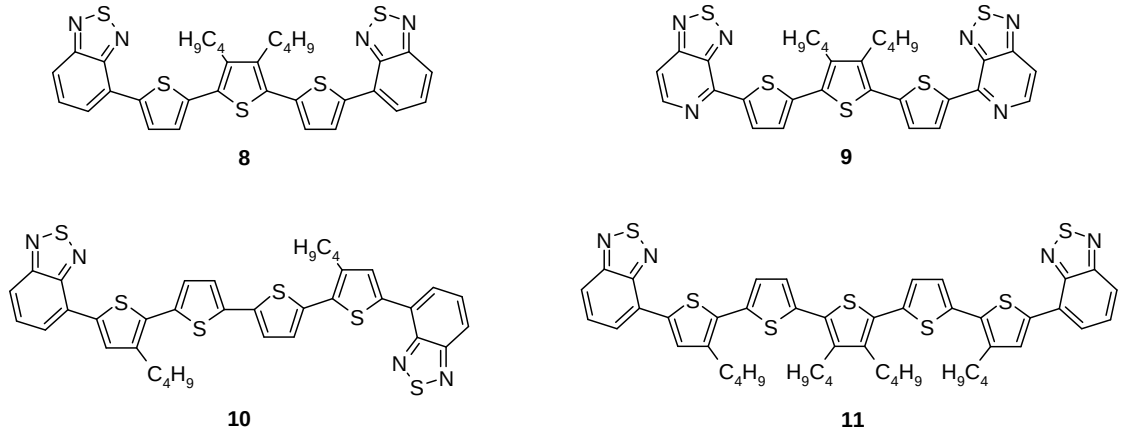

Abbildung 4: A-D-A-Reihe von Oligothiophenen mit BTDA oder Thiadiazolo Pyridin (TDAPy) als neuartige endständige Akzeptor-Gruppen.

Die erhaltenen Oligomere zeigten eine herausragende thermische Stabilität und im Fall von TDAPy-Verbindung **9**, eine Absorption im Dünnfilm bis über 650 nm. Durch Vakuum-Verdampfung hergestellte organische Solarzellen mit **9** als Donor, zeigten Effizienzen von bis zu 3.15%. Hohe Offene-Stromkreis Potenziale (V_{OC}) im Bereich von 1.0 V und Füllfaktoren (*FF*) bis zu 0.67 wurden festgestellt, was derzeit zu den höchsten Werten im Bereich der Oligomer-basierenden organischen Solarzellen zählt. Weiterhin wurden mit den Farbstoffen **10** und **11** Solarzellen aus Lösung hergestellt und vielversprechende Effizienzen von bis zu 1.6% wurden dabei erreicht.

Zusammengefasst: Durch Einführung unterschiedlicher Donor- und Akzeptor-Funktionen (TTDA, TP, BTDA, TDAPy, TFA, DCV) in Oligothiophene wurden maßgeschneidert Materialien mit schmaler Bandlücke und anderen faszinierenden Eigenschaften für die Anwendung in Organischen Solarzellen hergestellt und dabei Rekord-Effizienzen von bis zu 3.15% erzielt. Im Zuge dessen gewannen wir Einblick in interessante Struktur-Eigenschaftsbeziehungen, und eine auf dem Gebiet der Oligomer-Solarzellen völlig neuartige, vielversprechende Akzeptor-Einheit – Thiadiazolo Pyridin (TDAPy) – wurde eingeführt. Wir gehen davon aus, dass durch weitere Verbesserung dieser Materialien und Zellen noch höhere Effizienzen bei zukünftigen Solarzellen möglich sind

References – Literaturverzeichnis

[1] K. Schulze, B. Maennig, K. Leo, Y. Tomita, C. May, J. Hüpkes, E. Brier, E. Reinold, P. Bäuerle, *App. Phys. Lett.* **2007**, *91*, 073521.

[2] K. Schulze, C. Uhrich, R. Schüppel, K. Leo, M. Pfeiffer, E. Brier, E. Reinold, P. Bäuerle, *Adv. Mater.* **2006**, *18*, 2872.

[3] C. Uhrich, R. Schüppel, A. Petrich, M. Pfeiffer, K. Leo, E. Brier, P. Kilickiran, P. Bäuerle, *Adv. Funct. Mater.* **2007**, *17*, 2991.

[4] R. Schüppel, K. Schmidt, C. Uhrich, K. Schulze, D. Wynands, J. L. Brédas, E. Brier, E. Reinold, H.-B. Bu, *Phys. Rev. B* **2008**, *77*, 085311.

[5] R. Schüppel, C. Uhrich, M. Pfeiffer, K. Leo, E. Brier, E. Reinold, P. Baeuerle, *ChemPhysChem* **2007**, *8*, 1497.

List of Publications

Sylvia Schmid, Daniel Schühle, Simon Steinberger, Zhang Xin, Volkhard Austel
"Synthesis of 1,2,2a,3-Tetrahydro-1,4,7b-triazacyclopenta[*cd*]indenes"
Syntheis **2005**, *18*, 3107-3118.

Simon Steinberger, Amaresh Mishra, Egon Reinold, Jordan Levichkov, Christian Uhrich, Martin Pfeiffer, and Peter Bäuerle
"Vacuum-processed small molecule solar cells based on terminal acceptor-substituted low-band gap oligothiophenes"
Chem. Comm. **2011**, *47*, 1982-1984.

Simon Steinberger, Amaresh Mishra, Egon Reinold, Christian M. Müller, Christian Uhrich, Martin Pfeiffer, and Peter Bäuerle
"Vacuum-Deposited Organic Solar Cells based on A-D-A-D-A-Type Oligothiophenes"
Org. Lett. **2011**, *13*, 1, 90-93.

Simon Steinberger, Amaresh Mishra, Egon Reinold, Elena Mena-Osteritz, Heiko Müller, Christian Uhrich, Martin Pfeiffer, and Peter Bäuerle
"Synthesis and Characterizations of Red/Near-IR-Absorbing A-D-A-D-A-type Oligothiophenes Containing Thienothiadiazole and Thienopyrazine Central Units"
J. Mater. Chem. DOI:10.1039/C2JM13285K.

Simon Steinberger, Amaresh Mishra, Egon Reinold, Chang-Qi Ma, Florian Rauh, Christian Uhrich, René A. J. Janssen, Martin Pfeiffer, and Peter Bäuerle
"Terminal Benzothiadiazole-Substituted Oligothiophenes for Small Molecule Solar Cells"
Org. Lett. Pending 11/2011

Presentations and Posters

"Oligothiophene-based red/NIR-absorbers for organic solar cells"
KOPO, Blaubeuren, Germany, October 26 th, **2007**

"Oligothiophene-based red/NIR-absorbers for organic solar cells"
Fπ8, Graz, Austria, July 22nd, **2008**

"Oligothiophene-based red/NIR-absorbers for organic solar cells"
KOPO, Blaubeuren, Germany, October 14 th, **2009**

Curriculum Vitae

Simon Steinberger
Born: 23th June 1978 in Ulm
Nationality: German

Marktplatz 5
89134 Blaustein
Germany

Phone: +49 / 8321 / 694 00 81
Mobile: +49 / 176 / 23 88 47 87
E-Mail: simon.steinberger@gmx.net

03/2010 – 10/2011	Self employment in software engineering
04/2007 – 03/2010	PhD studies at the Institute of Organic Chemistry II and Advanced Materials at the University of Ulm (Prof. Dr. Peter Bäuerle) Thesis: Synthesis of Donor-Acceptor Functionalized Low Band Gap Oligothiophenes as Red/NIR-Absorbers for Organic Solar Cells
12/2006 – 4/2007	Travelling in India, Nepal and South-East Asia
4/2006 – 12/2006	Research at the Institute of Organic Chemistry II and Advanced Materials at the University of Ulm (Prof. Dr. Peter Bäuerle) Synthesis of Donor-Acceptor Functionalized Low Band Gap Oligothiophenes as Red/NIR-Absorbers for Organic Solar Cells
11/2005 – 3/2006	Travel and Work in New Zealand
4/2001 – 11/2005	Studies of chemistry at the University of Ulm Degree: Diploma (Grade: 1.2) Diploma thesis at the Institute of Organic Chemistry II (Prof. Dr. Peter Bäuerle) Thesis: Synthese maßgeschneiderter Oligothiophene für organische Solarzellen (Synthesis of Tailored Oligothiophenes for Organic Solar Cells)
10/2003 – 03/2004	Erasmus program at the faculty of Mathematics, Physics and Natural Science (Analytical Chemistry) at the University of L'Aquila, Italy (Prof. Dr. Pietro Mazzeo) Research topic: Effects of Softeners in Polyvinyl Chloride on Human Health
2/2000 – 3/2001	Alternative Service
10/1999 – 2/2000	Studies of chemistry at the University of Ulm
9/1989 – 6/1999	Hans und Sophie Scholl-Gymnasium Ulm Degree: Abitur (Grade: 1.3)